Carnegie Mellon University

CARNEGIE INSTITUTE OF TECHNOLOGY

THESIS

SUBMITTED IN PARTIAL FULFILLMENT OF THE REQUIREMENTS

FOR THE DEGREE OF Doctor of Philosophy

TITLE Sources of Atmospheric Particles in the U.S.

PRESENTED BY Laura Posner

ACCEPTED BY THE DEPARTMENT OF

Chemical Engineering

SPYROS PANDIS	7/24/15
SPYROS PANDIS, ADVISOR	DATE
LORENZ BIEGLER	7/24/15
LORENZ BIEGLER, DEPARTMENT HEAD	DATE

APPROVED BY THE COLLEGE COUNCIL

VIJAYAKUMAR BHAGAVATULA	7/24/15
DEAN	DATE

Sources of atmospheric particles in the U.S.

Submitted in partial fulfillment of the requirements for

the degree of

Doctor of Philosophy

in

Chemical Engineering

Laura N. Posner

B.S., Chemical Engineering, University of Rochester

Carnegie Mellon University
Pittsburgh, PA

August, 2015

Acknowledgements

Thank you to my adviser, Spyros Pandis, for opening my mind to the world of air quality, sharing his genius on the subject, and taking the time to read through and offer constructive criticism of my work. He has helped me grow from a fledgling researcher to a much more independent thinker. To all of my committee members, thank you for taking the time to read my proposal and thesis documents, listen to my talks, and help me improve my research. I am grateful to Peter Adams for his research guidance and making me feel welcome from my very first introduction to CAPS. Thank you to Neil Donahue for many engaging chats at departmental happy hours and CAPS barbeques. I would like to thank Ryan Sullivan for always asking challenging, insightful questions and taking my word that the model is reliable despite near-zero concentrations over Canada. Last but certainly not least, I am grateful to Lynn Walker for recognizing and convincing me during adviser selection that I belonged with the Center for Atmospheric Particle Studies (CAPS) hippies on the B-level of Doherty Hall.

I thank every member of CAPS for maintaining such a positive, collaborative vibe in our research group. I would like to thank Allen Robinson for sharing his wisdom and advice to help me improve my biomass burning research. Thank you to my friend and CAPS colleague Melissa Day for her consistent emotional and intellectual support, sharing her infectious sense of adventure, co-commiseration over Fortran77 errors for which Google can only locate an unanswered post from 1993, and many intense yet respectful political discussions even though we are on the same extreme side of the political spectrum. To Ben

Murphy I express my gratitude for continuously helping me with PMCAMx, and both he and CAPS colleague Erica Trump use their positive attitudes to encourage me to persevere in research and personal life. I am very grateful to Jinhyok Heo, Pablo García, and Marguerite Marks for their help in maintaining and troubleshooting the servers on which I run my simulations. Equally important is that Marguerite and I share a love of animals, fostering, and talking about animals and fostering. I am indebted to Andrea Paciga for always making me laugh, listening, and never giving up on me during tough times. I would also like to thank Nivedita Kumar for her support and friendship, Elina Karnezi for brightening my days with jokes and cute animal photos, and Wayne Chuang for his never-ending support, willingness to help, and our wonderful Chipotle dates. To my industry mentor Lisa Gable, former Society of Women Engineers (SWE) adviser Suzie Laurich-McIntyre, and undergraduate adviser Ben Ebenhack and his wife MJ, I express my gratitude for their friendship, support, and insight on achieving my professional goals.

I would not have made it here without the love, encouragement and support of my mother and father, brother Matthew, Aunts Janis, Carolyn, and Karen, Uncle Fred, cousins Irv and Amy, and the elder generation of my family who have passed on. Thank you to my girlfriend Sarah Beth, my ever-supportive friend Kayla, my best friend Lori and her family for always believing in me. Thank you to my friends Janice and Jason Hinkledire for their support, friendship, and letting me spend time with their adorable senior pups. I am very lucky to be surrounded by so many loving and supportive people.

Additionally, I am grateful to the wonderful staff and volunteers at the Animal Rescue League for their friendship, free weekly dog cuddles, summer kitten rentals, and, most importantly, introducing me to my feline companion Renny. I thank Renny for ignoring me before my qualifier and proposal (and probably my defense) and then, immediately after they finished, admitting the anxiety it caused her by running around making silly noises in between begging for as many pets as I can give. I also thank Renny for helping to rear my foster kittens into upstanding cats with her no-kitten-nonsense iron paw. Lastly, I would like to thank my therapist, Karen Cristman, for her constant support as she helped me navigate chronic depression and the stresses of graduate school. I have talked with many students about depression they have experienced for the first time due to the stresses of graduate school and their qualms about seeking professional help. I hope that future students know that depression in the midst of stressful graduate school experiences is common but not something they have to fight through alone.

This research was supported by the EPA STAR program through the National Center for Environmental Research (NCER) and the Joint Fire Science Program (JFSP). No official endorsement should be inferred.

Abstract

The development of effective atmospheric particulate matter (PM) mitigation strategies relies on understanding source contributions to the corresponding PM levels. Most previous work has focused on PM mass concentrations. However, recent health studies suggest that particle number may also contribute to the negative health effects of particles, and particle number concentrations indirectly affect the energy balance of our planet.

In the first part of this work, the aerosol number-focused CTM PMCAMx-UF is used to investigate the sources of particle number concentrations during a photochemically-active period in the Eastern U.S. A new aerosol number emissions inventory is developed for the July 2001 period. With the new emissions as input, PMCAMx-UF reproduces particle number concentrations within 12% of observations in Pittsburgh. Nucleation is predicted to be the dominant source of total number concentrations (>90%). Gasoline vehicles are predicted to contribute 36% to primary particle number concentrations, followed by industrial sources (31%), non-road diesel (18%), on-road diesel (10%), biomass burning (1%), and long-range transport (4%).

The effects of reductions in diesel PM emissions are investigated in the second part of this work. A 50% reduction of diesel particulate emissions results as expected in lower (23%) black carbon mass concentrations and similar changes both in magnitude and spatial pattern to the absorption coefficient (27-30%). Contrary to what is expected, an average 1.6% increase of the total particle number concentrations is predicted due to a decrease in the coagulation and condensation

sinks. At the same time, a 1.6% decrease in N_{100} (particles larger than 100 nm) particle concentrations is predicted. Both changes in number concentrations are significantly different from those expected assuming a proportional change. These results suggest that mitigation of large diesel particles and/or particle mass emissions will reduce absorption climate-relevant properties related to black carbon and have health benefits; however the changes could also have the unintended effect of increased ultrafine particle number concentrations. The changes in cloud condensation nuclei (CCN) are predicted to be significantly less than expected assuming a proportional reduction during this photochemically active period.

Next, the mass-focused CTM PMCAMx was used to explore the contribution of biomass burning organic aerosol (bbOA) to organic aerosol (OA) mass concentrations in the continental U.S. for three representative months of the modeling year 2008. PMCAMx uses the volatility basis set (VBS) to track the evolution of semivolatile OA. The simulation-averaged predicted bbOA contribution to OA concentrations is 8% for April, 22% for July, and 10% for September. Locally and on days of maximum biomass burning, bbOA sources can be significant both downwind (21-27% of OA) and near fire (56-90%). Compared to the CTM CAMx, which assumes non-volatile OA, PMCAMx predicts 20% more bbOA on average and estimates that most of the bbOA is secondary (oxidized vapors that condensed) whereas CAMx predicts all primary (emitted directly in the particle phase). Generally PMCAMx predicts less bbOA near fires due to the evaporation of primary OA and more bbOA downwind of fires due to the formation of secondary OA.

Finally, a trajectory model is used to quantify the changes in OA concentrations in a biomass burning plume as it travels and dilutes. The model suggests that in the first few hours the evaporation of primary OA dominates over the production of secondary products and that the OA levels normalized to CO levels decrease despite the secondary production. Sensitivity studies are performed for parameters that affect OA concentrations (e.g. OH concentration, aging rate), and the results are analyzed to determine which scenarios lead to net loss, increase, or no significant changes of OA concentrations.

Table of contents

List of tables

List of figures and illustrations

Chapter 1. Introduction

Atmospheric aerosols are an important area of research due to their negative effects on human health and influence on climate change. Exposure to elevated concentrations of particulate matter less than 2.5 μm in diameter ($PM_{2.5}$) has been linked to increased risk of cardiovascular disease and mortality (Pope et al., 2009; Lelieveld et al., 2013). Studies highlighted in the review by Delfino et al. (2005) indicate a possible link between exposure to ultrafine particles (particles less than 100 nm in diameter) and cardiovascular disease in humans. In addition, a review by Janssen et al. (2012) suggests that exposure to the $PM_{2.5}$ component black carbon (BC) in the short and long term may be associated with increased risk of cardiopulmonary disease.

Atmospheric particulate matter plays a significant role in the earth's climate by directly reflecting or absorbing sunlight and affecting the formation and properties of clouds. Since ultrafine particles typically dominate aerosol number concentrations, they can greatly contribute to the number of cloud condensation nuclei (CCN) through growth by condensation (Pierce and Adams, 2009). CCN affect the albedo (reflectance) of a cloud, with greater numbers increasing the cloud's albedo (Seinfeld and Pandis, 2006). Some aerosol components (such as organic matter) and aerosol precursors (e.g., sulfur dioxide) reflect sunlight and have a negative (cooling) effect on the radiative balance of the earth (IPCC, 2013). BC, however, strongly absorbs sunlight and therefore has a positive (warming) effect on the global radiative balance (Bond et al., 2013). The net effect of the absorbance and reflectance of sunlight by aerosols and the secondary effects of

aerosol size and composition changes on cloud properties remain the most uncertain factors in the global radiative balance (IPCC, 2013).

Quantification of the contributions of different sources (nucleation, biomass burning, diesel engines, gasoline automobiles, etc.) to particle concentrations is essential to developing effective mitigation strategies. Chemical transport models (CTMs) can be used to investigate the contribution of these sources to particle concentrations and to then explore the effects of control strategies. CTMs such as PMCAMx simulate the emission, advection, diffusion, wet and dry deposition, chemistry, and aerosol processes that affect pollutant concentrations (Gaydos et al., 2007).

Previous work investigating nucleation as a source of ultrafine particles used a simplified representation of emissions in the three-dimensional CTM PMCAMx-UF (Jung et al., 2010). Accurate source apportionment of atmospheric particle emission sources in a CTM, however, requires careful consideration of the characteristics of modeled emissions and their effects on atmospheric aerosol processes. This work investigates the contributions of different sources to atmospheric particles, first focusing on particle number, then effects of changes in diesel emissions on particle number, BC, and climate-relevant properties such as absorption of sunlight, and finally the contribution of biomass burning emissions to OA concentrations.

In Chapter 2, the sources of atmospheric particle number concentrations are investigated with a focus on ultrafine particles, which compose 90% of particle number concentrations in urban settings (Seinfeld and Pandis, 2006). Source-

specific size distributions from the literature are used to develop a new number emissions inventory for July 2001 in the Eastern U.S. that includes biomass burning, dust, gasoline automobiles, industrial sources, non-road diesel, and on-road diesel. A new number-focused zero-out method is developed and implemented in the three-dimensional number-focused CTM PMCAMx-UF, and the contribution to particle number concentrations of each emission source, as well as long-range transport and nucleation is quantified separately for several particle size ranges.

Chapter 3 uses PMCAMx-UF to investigate the effects of reduced and increased diesel emissions, which are the largest source of BC emissions in North America. Two diesel emission scenarios are developed based on the source-resolved emissions inventory from Chapter 2: (1) half diesel particulate emissions and (2) double diesel particulate emissions. The effects of these changes to diesel emissions on particle number, BC, and climate-relevant aerosol properties such as absorption coefficients and aerosol optical depth are investigated.

In Chapter 4, the three-dimensional mass-focused CTM PMCAMx is used to investigate the contribution of bbOA to OA concentrations in the continental U.S. for three representative months of the 2008 modeling year. PMCAMx simulates the emission, secondary formation, and evolution of organic aerosol concentrations using the volatility basis set (Donahue et al., 2006). The model separately tracks both semi-volatile primary OA (POA, emitted directly in the particle phase) and secondary OA (SOA, oxidized organic vapors that have condensed) from several pathways: fresh POA, SOA from anthropogenic vapors,

SOA from biogenic vapors, SOA from intermediate- and semi-volatile precursors, and long-range transport OA. The bbOA concentrations are calculated as the difference between PMCAMx simulations with and without biomass burning emissions. The results of PMCAMx are then compared to the results of a version of the three-dimensional CTM CAMx that considers primary bbOA nonvolatile and secondary bbOA negligible.

Laboratory and field studies show mixed results regarding the changes in OA concentrations downwind of biomass burning plumes (Heilman et al., 2014). Chapter 5 investigates the evolution of OA from a biomass burning plume using a plume-scale Lagrangian trajectory model. A base case is developed from the parameters of real fires, and sensitivity studies of OA concentrations to OH concentrations, the aging rate constant, vertical dispersion, horizontal dilution, and initial and background concentrations are performed. The results are analyzed to determine which conditions lead to net production, loss, or no significant changes in OA concentrations.

Chapter 6 summarizes the results and conclusions of this work and offers ideas for future modeling studies. It includes recommendations for future field and laboratory measurements that could better inform modeling work.

References

Bond, T.C., Doherty, S.J., Fahey, D.W., Forster, P.M., Bernsten, T., DeAngelo, B.J., Flanner, M.G., Ghan, S., Kärcher, B., Koch, D., Kinne, S., Kondo, Y., Quinn, P.K., Sarofim, M.C., Schultz, M.G., Schulz, M., Venkataraman, C., Zhang, H., Zhang, S., Bellouin, N., Guttikunda, S.K., Hopke, P.K., Jacobson, M.Z., Kaiser, J.W., Klimont, Z., Lohmann, U., Schwarz, J.P., Shindell, D., Storelvmo, T., Warren, S.G., Zender, C.S., 2013. Bounding the role of black carbon in the climate system: a scientific assessment. J. Geophys. Res. 118, 5380-5552.

Delfino, R.J., Sioutas, C., Malik, S., 2005. Potential role of ultrafine particles in associations between airborne particle mass and cardiovascular health. Environ. Health Persp. 113, 934-946.

Donahue, N.M., Robinson, A.L., Stanier, C.O., Pandis, S.N., 2006. Coupled partitioning, dilution, and chemical aging of semivolatile organics, Environ. Sci. Technol. 40, 2635-2643.

Gaydos, T.M., Pinder, R., Koo, B., Fahey, K.M., Yarwood, G., Pandis, S.N., 2007. Development and application of a three-dimensional aerosol chemical transport model, PMCAMx. Atmos. Environ. 41, 2594-2611.

Janssen, N.A., Gerlofs-Nijland, M.E., Lanki, T., Salonen, R.O., Cassee, F., Hoek, G., Fischer, P., Brunekreef, B., Krzyzanowski, 2012. Health effects of black carbon. Report prepared by the World Health Organization. Copenhagen, Denmark.

Jung, J., Fountoukis, C., Adams, P.J., Pandis, S.N., 2010. Simulation of in situ ultrafine particle formation in the eastern United States using PMCAMx-UF. J. Geophys. Res. 115, D03203.

Heilman, W.E., Liu, Y., Urbanski, S., Kovalev, V., Mickler, R., 2014. Wildland fire emissions, carbon, and climate: plume rise, atmospheric transport, and chemistry processes. Forest Ecol. Manag. 31, 70-79.

IPCC, 2013. Climate change 2013: the physical science basis. Contribution of Working Group I to the Fifth Assessment Report of the Intergovernmental Panel on Climate Change. Cambridge University Press, New York, NY.

Lelieveld, J., Barlas, C., Giannadaki, D., Pozzer, A., 2013. Model calculated global, regional and megacity premature mortality due to air pollution. Atmos. Chem. Phys. 13, 7023-7037.

Pierce, J.R., Adams, P.J., 2009. Uncertainty in global CCN concentrations from uncertain aerosol nucleation and primary emission rates. Atmos. Chem. Phys. 9, 1339-1356.

Pope III, C.A., Burnett, R.T., Krewski, D., Jerrett, M., Shi,Y., Calle, E.E., Thun, M.J., 2009. Cardiovascular mortality and exposure to airborne fine particulate matter and cigarette smoke: shape of the exposure-response relationship. Circulation 120, 941-948.

Seinfeld, J.H., Pandis, S.N., 2006. Atmospheric chemistry and physics: from air pollution to climate change, second ed. John Wiley and Sons, Hoboken, NJ.

Zhang, Q., Jimenez, J.L., Canagaratna, M.R., Allan, J.D., Coe, H., Ulbrich, I., Alfarra, M.R., Takami, A., Middlebrook, A.M., Sun, Y.L., Dzepina, K., Dunlea, E., Docherty, K., De-Carlo, P.F., Salcedo, D., Onasch, T., Jayne, J.T., Miyoshi, T., Shimono, A., Hatakeyama, S., Takegawa, N., Kondo, Y., Schneider, J., Drewnick, F., Borrmann, S., Weimer, S., Demerjian, K., Williams, P., Bower, K., Bahreini, R., Cottrell, L., Griffin, R.J., Rautiainen, J., Sun, J.Y., Zhang, Y.M., Worsnop, D.R., 2007. Ubiquity and dominance of oxygenated species in organic aerosols in anthropogenically-influenced Northern Hemisphere midlatitudes. Geophys. Res. Lett. 34, L13801.

Chapter 2. Sources of ultrafine particles in the Eastern United States[1]

2.1 Introduction

Ultrafine particles (less than 100 nm in diameter) play a role in climate change and may be relevant to human health. Since these smaller particles typically dominate aerosol number distributions, they can greatly contribute to the number of cloud condensation nuclei (CCN) through growth by condensation (Pierce and Adams, 2009). CCN affect the albedo (reflectance) of a cloud, with greater numbers increasing the cloud's albedo (Seinfeld and Pandis, 2006). The changes in cloud properties such as cloud lifetime due to aerosols is currently the most uncertain factor in the global radiative balance of the earth (IPCC, 2013). In addition, multiple studies highlighted in the review by Delfino et al. (2005) indicate a possible link between exposure to ultrafine particles and cardiovascular disease.

Most previous work on particle source apportionment has focused on mass concentrations, both using observations (Zhou et al., 2005; Aiken et al., 2009; Heo et al., 2009) and models (Marmur et al., 2006; Lane et al., 2007; Wang et al., 2009). Since ultrafine particles dominate number concentrations in polluted areas but contribute little to mass, mass-based source apportionment does not accurately describe the sources of particles in the ultrafine range. In this study, N_x denotes the

[1] Posner, L.N., Pandis, S.N., 2015. Sources of ultrafine particles in the Eastern United States. Atmos. Environ. 111, 103-112.

number concentration of particles with diameters greater than x nm, e.g. N_3 is the number concentration of particles with diameters larger than 3 nm. N_{x-y} denotes the number concentration of particles between x and y nm in diameter, e.g. $N_{0.8-3}$ is the number concentration of particles with diameters between 0.8 and 3 nm. There has been some observation-based work that has focused on particle number source apportionment of N_{13} in Spain (Pey et al., 2009) and N_3 in Pittsburgh (Zhou et al., 2004). For July 2001, Zhou et al. (2004) used advanced factor analysis and size distribution measurements to estimate that 58% of primary N_3 came from local traffic, 29% from stationary combustion, and 13% was related to remote combustion sources and secondary PM.

Study of the sources of ultrafine particles using a chemical transport model (CTM) requires accurate simulation of the two main pathways through which these particles enter the atmosphere: nucleation and direct emissions. The contribution of nucleation to particle number concentrations has been explored in several studies (Spracklen et al., 2006; Elleman and Covert, 2009; Jung et al., 2010). Other studies have broadly investigated the accurate representation of number emissions and their contribution to particle number concentrations. Spracklen et al. (2006) considered the contribution of primary emissions to global particle number concentrations. Elleman and Covert (2010) applied source-specific number distributions to three general sources in order to improve model-measurement agreement for number concentrations. In this study, we both develop a detailed number emissions inventory for six source types, each with a source-specific number size distribution

derived from the literature, and then investigate the contribution of each source to particle number concentrations in several size ranges.

Previous work using PMCAMx-UF for Pittsburgh (Jung et al., 2008) and the Eastern U.S. (Jung et al., 2010) focused on nucleation as a source of particle number concentrations. The authors compared the results of using several nucleation rate parameterizations in a box model to observations in Pittsburgh for July 2001, and the ternary sulfuric acid-water-ammonia nucleation rate parameterization of Napari et al. (2002) was found to correctly reproduce the lack or occurrence of nucleation on all days tested (Jung et al., 2008). Since this nucleation rate parameterization tended to overpredict particle number concentrations in Pittsburgh, however, the authors scaled the rate parameterization using a 10^{-5} nucleation tuner and implemented it in the nucleation routine of PMCAMx-UF (Jung et al., 2010). Since this previous application of PMCAMx-UF was focused on nucleation, the authors did not develop a source-resolved number emissions inventory; instead, they assumed a single source number distribution for each particulate species. For all primary carbonaceous emissions, the authors used a traffic number distribution based on the measurements of Stanier et al. (2004) taken during the Pittsburgh Air Quality Study (PAQS). All other emitted species were given size distributions recommended by AeroCom (Dentener et al., 2006). In order to perform a detailed study of the sources of emitted particle number, it is necessary to develop a source-resolved number emissions inventory with careful attention to individual source number distributions.

We first describe the development of a new source-resolved number emissions inventory for a summertime period in the Eastern U.S. and then introduce a number-focused zero-out method for source apportionment of ultrafine particle number concentrations. We evaluate the performance of the model against measurements in Pittsburgh and then investigate the source contributions to ultrafine particle number concentrations over the Eastern U.S. Finally, the sensitivity of our results to the nucleation rate parameterization is investigated.

2.2 PMCAMx-UF description

PMCAMx-UF (Jung et al., 2010) is a three-dimensional number-focused CTM based on the mass-focused three-dimensional CTM PMCAMx (Gaydos et al., 2007). In PMCAMx-UF, the aerosol module of PMCAMx is replaced by the Dynamic Model for Aerosol Nucleation (DMAN) (Jung et al., 2006). DMAN incorporates the TwO-Moment Aerosol Sectional Algorithm (TOMAS) (Adams and Seinfeld, 2002) to track particle number and mass simultaneously and accurately for each size section of a multi-component aerosol population. DMAN simulates gas-phase chemistry, nucleation, coagulation, condensation and evaporation.

The chemical mechanism used in PMCAMx-UF is based on Carbon Bond 5 (CB05) (Yarwood et al., 2005). The PMCAMx-UF mechanism includes 100 reactions of 59 species (34 gas species, 12 radical species, and 13 aerosol species) and utilizes the CMC chemistry fast solver (ENVIRON, 2003). TOMAS in PMCAMx-UF simulates the aerosol size distribution using a 41 size bin sectional

approach to track particles with diameters ranging from 0.8 nm to 10 μm. Each size section contains twice as much mass per particle as the previous size section, the smallest of which contains 3.75×10^{-25} kg dry aerosol mass per particle. In addition, there are two size sections with largest diameters at 20 and 40 μm that are used to describe cloud chemistry. The model tracks particulate elemental carbon, crustal material (including other species considered by the model as inert), water, chloride, sodium, ammonium, nitrate, sulfate, primary organic aerosol, and four secondary organic aerosol surrogate species. Primary organic aerosol is assumed to be non-volatile. The scaled (10^{-5} nucleation tuner) sulfuric acid-ammonia-water parameterization of Napari et al. (2002) is used in the base case simulation. For ammonia concentrations below 0.01 ppt, which is outside of the range of the original parameterization, the binary nucleation parameterization of Vehkamäki et al. (2002) is used.

Though the nucleation mechanism used in this application of PMCAMx-UF does not include organics, their direct contribution to the growth of fresh nucleated particles is very small. The latter is due to the fact that only semi-volatile organics are simulated and therefore, due to the Kelvin effect, their condensation rate on particles that are only a few nm is negligible. Patoulias et al. (2014) have recently addressed the second weakness by extending the model to simulate extremely low volatility organics.

Table 2.1. Mass boundary conditions for July 2001 in PMCAMx-UF.

Modeled chemical species	Boundary concentration ($\mu g\ m^{-3}$)
Side boundary conditions	
Organic aerosol	0.80
Primary elemental carbon	0.10
Ammonium	0.37
Nitrate	0.10
Sulfate	0.90
Sodium ion [eastern boundary, only]	0.50
Chloride [eastern boundary, only]	0.50
Top boundary conditions	
Organic aerosol	0.50
Ammonium	0.14
Nitrate	0.36

2.2.1 Boundary and initial conditions

In this study, PMCAMx-UF is used to simulate a 3492 x 3240 km area over the Eastern U.S. The domain is gridded into 97 (east-west) by 90 (north-south) cells that are each 36 x 36 km. 14 vertical layers above the surface up to 6 km are also simulated, but values reported in this study are the average output for the first simulation layer (30 m elevation), only. The mass boundary conditions of Karydis et al. (2007) are used with the following additions: 1 $\mu g\ m^{-3}$ of sea salt is added to the eastern boundary to more accurately represent above-ocean conditions. In addition, boundary conditions are made altitude-dependent: boundary concentrations above 3 km are represented by the top boundary conditions (Table 2.1).

Table 2.2. Number size distributions for the boundary and initial conditions in PMCAMx-UF.

	Aitken mode			Accumulation mode			Coarse mode		
	Number (cm^{-3})	Mean diameter (μm)	σ	Number (cm^{-3})	Mean diameter (μm)	σ	Number (cm^{-3})	Mean diameter (μm)	σ
Initial, northern, southern, and western	1600	0.020	1.45	580	0.12	1.65	0.10	1.80	2.40
Eastern	133	0.008	4.54	66.6	0.27	1.62	1.55	0.58	2.49
All above 3 km	129	0.007	4.42	59.7	0.25	1.79	-	-	-

Lognormal number size distributions from Jaenicke (1993) are used for the boundary and initial conditions (Table 2.2). The coarse mode is used only for crustal species and sea salt. The top boundary conditions follow the free tropospheric distribution. Initial and boundary conditions (except for the eastern boundary) are remote continental conditions, whereas the marine distribution is used for the eastern boundary. Below 3 km, the number concentration for the northern, western, and southern boundaries is 1900 cm^{-3}, and the eastern boundary is 100 cm^{-3}. Above 3 km, the boundary concentration is 30 cm^{-3}.

2.3 Development of number emissions inventory

2.3.1 Mass emissions inventory for the Eastern U.S.

The LADCO 2001 BaseE source-resolved mass emissions inventory (LADCO, 2003) is used in this study. The available sources include open biomass burning, dust, gasoline automobiles, industrial emissions, natural gas, non-road diesel, on-road diesel, and wood combustion. Further description of this inventory

can be found in Lane et al. (2007). In this study, we use the recommendations of Lane et al. (2007) to reduce elemental carbon mass emission rates from on-road and non-road diesel to approximately half their original mass emission rate uniformly across the modeling domain. In addition, biomass and wood burning emissions are lumped into a single biomass burning source, and natural gas combustion particulate emissions are assumed to be negligible. The composition of PM_{10} emitted by the different source types considered in this work is given in Table 2.3 (LADCO, 2013).

Table 2.3. Average source emissions composition over the Eastern U.S. for July 2001.

	PM_{10} composition (% mass)					
	Biomass	Dust	Gasoline	Industrial	Non-road diesel	On-road diesel
Elemental carbon	20	0	9	9	31	18
Organic aerosol	44	6	45	30	33	11
Crustal	36	94	46	5	36	71
Nitrate	0	0	0	0	0	0
Sulfate	0	0	0	56	0	0

Table 2.4. Number size distributions for each source.

	Aitken mode			Accumulation mode			Coarse mode		
	Number[a] (# μg^{-1})	Mean diameter (μm)	σ	Number (# μg^{-1})	Mean diameter (μm)	σ	Number (# μg^{-1})	Mean diameter (μm)	σ
Biomass	-	-	-	1.6×10^8	0.123	1.71	-	-	-
Dust	-	-	-	-	-	-	6.8×10^4	1.3	2.0
Gasoline	4.8×10^9	0.021	2.11	3.0×10^8	0.092	1.52	-	-	-
Industrial, non- and on-road diesel	8.7×10^8	0.017	1.48	7.7×10^8	0.055	1.98	-	-	-
Industrial power plant	1.7×10^9	0.025	1.90	-	-	-	1.3×10^8	0.15	1.5

[a] The number emissions are normalized with respect to the total PM_{10} mass from the source.

2.3.2 Number emissions inventory for the Eastern U.S.

Source-specific lognormal number size distributions are assumed for all source emission types (Table 2.4). Biomass is distributed using number emissions data from FLAME III (Hennigan et al., 2011). The dust size distribution recommended by AeroCom (Dentener et al., 2006) is used for dust emissions. Gasoline emissions have the light-duty vehicle number distribution of Ban-Weiss et al. (2010), and industrial (except power plant), non-road and on-road diesel emissions have the heavy-duty vehicle number distribution of Ban-Weiss et al. (2010). Power plant emissions follow the number distribution recommended by Elleman and Covert (2010).

According to this July 2001 number emissions inventory, gasoline automobiles are estimated to be responsible for 40% of the ultrafine particle emissions, followed by industrial sources (33%), non-road diesel (16%), on-road diesel (10%), and 1% from biomass burning (Table 2.5). Maps of the particle number emission rates for each source for this summertime period are shown in Figure 2.1. The large contribution of the industrial source category in Canada to particle number emissions is due to the inclusion of diesel sources, while farming activity is responsible for non-road diesel emissions in the Midwest. For this summertime period, biomass burning was not a significant contributor to particle number emissions, and, though dust particles are large and significantly contribute to mass emissions, dust contributes much less than 1% of the number of emitted particles.

Table 2.5. Source contributions to number emissions in the Eastern U.S. for July 2001.

Emission source	Percentage in size range						
	$N_{0.8\text{-}3}$	$N_{3\text{-}10}$	$N_{10\text{-}50}$	$N_{50\text{-}100}$	N_{100}	$N_{<100}$	N_{TOT}
Biomass	0	0	0	4	15	1	2
Dust	0	0	0	0	0	0	0
Gasoline	94	66	37	32	20	40	38
Industrial	6	18	36	32	35	33	33
Non-road diesel	0	9	16	19	18	16	16
On-road diesel	0	7	11	13	12	10	11
Total (# d^{-1})	7.3×10^{21}	2.8×10^{23}	2.2×10^{24}	4.7×10^{23}	2.4×10^{23}	3.1×10^{24}	3.3×10^{24}

Figure A1 in the Supplementary Information shows average diurnal number emissions profiles from our number emissions inventory in Pittsburgh, Pennsylvania. Gasoline dominates the ultrafine particle number emissions in Pittsburgh for all size ranges, whereas dust and biomass burning contribute the least. Increases in gasoline and on-road diesel emissions during morning and evening rush hour can be seen in the diurnal profiles of number emissions in each size range. Overall, emissions in Pittsburgh are similar to the average of the Eastern U.S. domain; gasoline is estimated to be responsible for 40% of the emitted ultrafine particles, followed by 27% from industrial sources, 20% from non-road diesel, and 13% from on-road diesel.

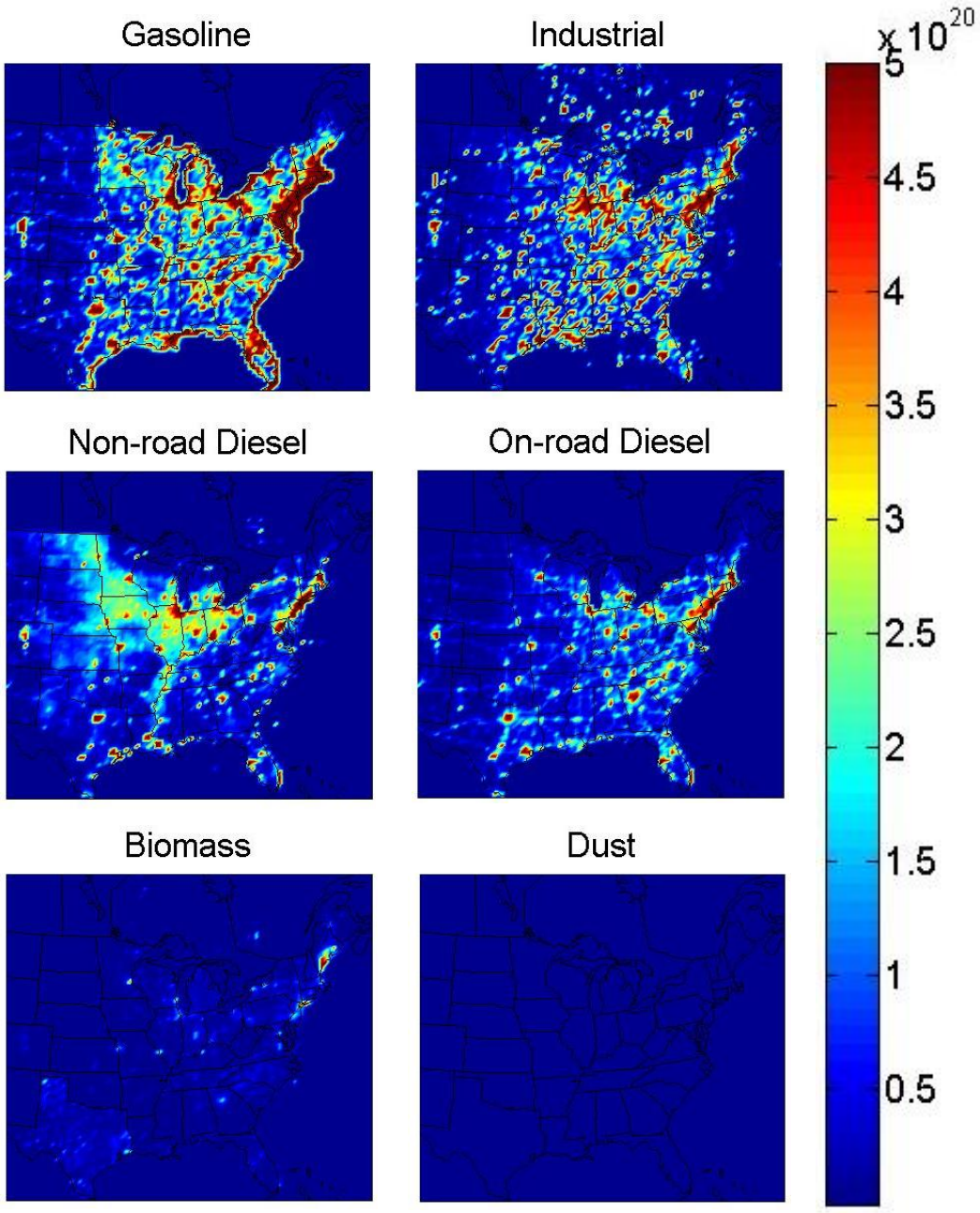

Figure 2.1. Source-resolved total particle number emission rates (particles day^{-1} km^{-2}) for July 2001.

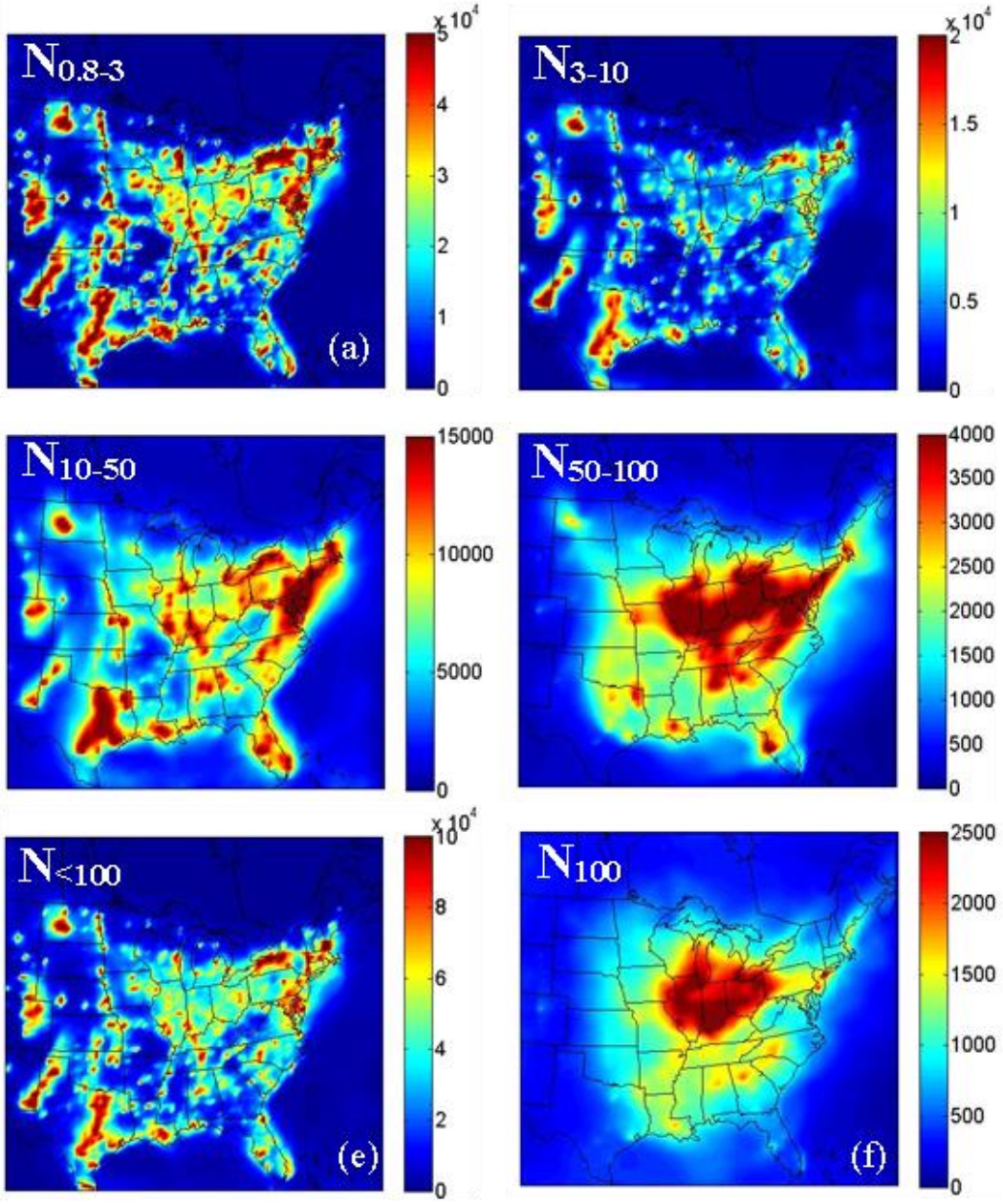

Figure 2.2. Predicted number concentrations (cm^{-3}) at ground level for particles with diameters in the size ranges (a) 0.8-3 nm, (b) 3-10 nm, (c) 10-50 nm, (d) 50-100 nm, (e) less than 100 nm and (f) greater than 100 nm for July 2001.

2.4 Simulated particle number concentrations in the Eastern U.S.

For the base case simulation, emissions from all sources were included in PMCAMx-UF to simulate the atmosphere over the Eastern U.S. during July 2001. The first two simulation days were ignored as model spin-up. The spatial distributions of N_{TOT} (equivalent to $N_{0.8}$), N_3, $N_{10,}$ and N_{100} over the Eastern U.S. are similar to the spatial distributions of Jung et al. (2010), but absolute number concentrations differ between the two studies due to the updated emissions in our study. Figure 2.2 depicts maps of the particle number concentrations over the Eastern U.S. in several size ranges. The average predicted number concentrations at ground level over the modeling domain are $N_{0.8\text{-}3}$ = 9900 cm^{-3}, $N_{3\text{-}10}$ = 2800 cm^{-3}, $N_{10\text{-}50}$ = 4000 cm^{-3}, $N_{50\text{-}100}$ = 1200 cm^{-3}, and N_{100} = 650 cm^{-3}. Ultrafine particle concentrations are affected by nucleation, primary sources, and also the availability of condensable vapors that allow them to grow to larger sizes. The spatial distributions of particles smaller than 10 nm are affected significantly by nucleation frequency and intensity resulting in high concentrations in the corresponding areas of the domain. The concentrations of larger particles are determined both by primary emissions but also by the growth of the smaller particles to the corresponding sizes and have as a result a more regional character.

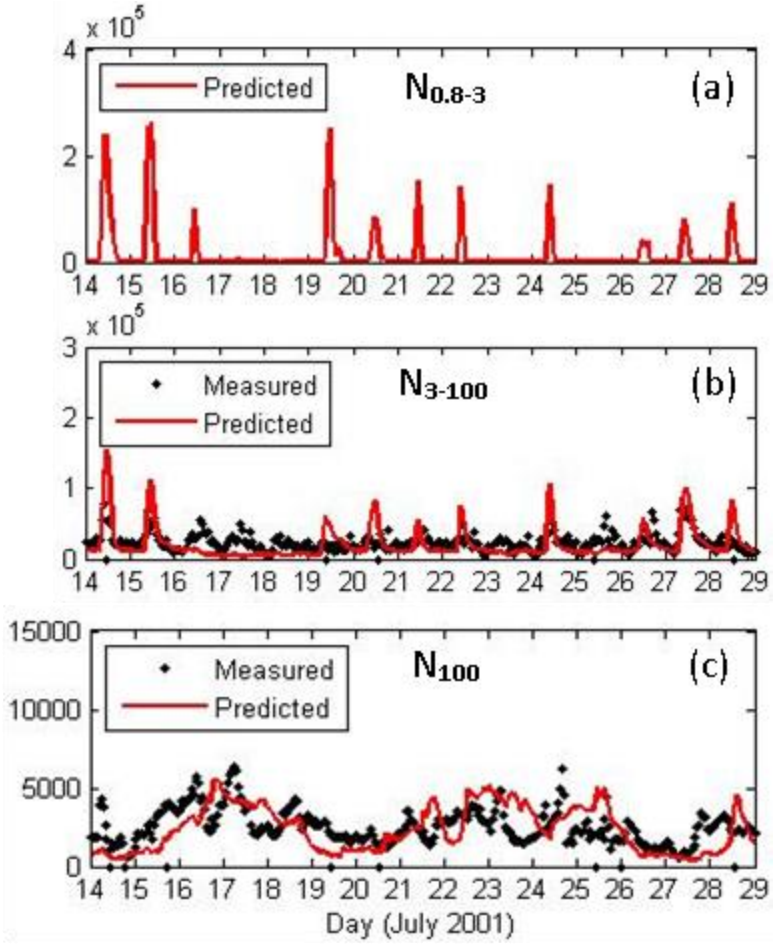

Figure 2.3. Comparison of PMCAMx-UF predictions to hourly measurements taken during the Pittsburgh Air Quality Study (PAQS) for July 14-28, 2001 for (a) $N_{0.8\text{-}3}$, (b) $N_{3\text{-}100}$, and (c) N_{100} (cm^{-3}).

2.4.1 Model evaluation

Figure 2.3 shows comparisons of PMCAMx-UF predictions to the results of the Pittsburgh Air Quality Study (Stanier et al., 2004). The predicted and observed average number concentrations (cm^{-3}) at ground level over Pittsburgh for July 14-28, 2001 are, for $N_{3\text{-}10}$ (predicted: 3500 cm^{-3}, observed: 8400 cm^{-3}), $N_{10\text{-}50}$ (predicted: 11100 cm^{-3}, observed: 10300 cm^{-3}), $N_{50\text{-}100}$ (predicted: 5200 cm^{-3}, observed: 3500 cm^{-3}), and N_{100} (predicted: 2400 cm^{-3}, observed: 2500 cm^{-3}).

Overall, in the measureable ultrafine range (N_{3-100}) PMCAMx-UF underpredicts the number concentration of particles by 12%. The model underpredicts N_{3-10} by 63%, which could be due to errors in the nucleation predictions or emissions in this range, but overpredicts N_{10-50} by only 8%. Modeled N_{50-100} is overpredicted by 50%. Finally, the model underpredicts N_{100} by only 5%. Jung et al. (2010) noted an error of 22% and 49% for N_3 and N_{10}, respectively. In this work we find an error of only -10% and 15%, respectively, for these size ranges. This improvement in model-measurement agreement indicates that some of the error in Jung et al. (2010)'s work may have been due to errors in the previous representation of number emissions, which were updated in this study.

2.5 Sources of particle number in the Eastern U.S.

2.5.1 Source apportionment approach

Performing number source apportionment in an atmospheric model is challenging. Zeroing all but one source's number emissions would result in changing the condensation and coagulation sinks, to which the model responds non-linearly for particle number concentrations. Such major nonlinearities should be avoided or else the zero-out simulations could be rendered incomparable to the base case. Thus, a modified zero-out method is used in this study to source apportion particle number concentrations.

A zero-out inventory for each emissions source (biomass burning, gasoline, industrial, non-road diesel, and on-road diesel) except dust, which is explained later, was developed and used in a separate zero-out simulation. In a mass-based

zero-out technique, all particle emissions of a source are assumed to be zero. Here we zero the number emissions of the specific source up to a threshold diameter, keeping the larger particles mostly intact. This modification to the zero-out method is designed to preserve most of the surface area and mass of emitted particles while capturing the source's contribution to number emissions. The source-specific zero-out threshold diameters (shown in Table 2.6) were determined by the point at which approximately 90% of the source's number emissions are eliminated. This approach is not applicable to dust emissions due to the elimination of too much mass and surface area in order to remove 90% of the particle number; thus the small source contribution of dust to particle number concentrations is not evaluated in this study. The changes in mass emissions due to these perturbations are less than 6% for each zero-out simulation. The removal of more than 90% of the corresponding number emissions suggests that the error in our approach should be of the order of 10% or less. This was confirmed by a number balance of the corresponding source contributions.

Table 2.6. Zero-out diameters used for source apportionment simulations.

	Zero-out diameter[1] (μm)	Mass removed (%) of total emissions	Number removed (%) of source emissions
Industrial [non power plant]	0.102	1	92
Industrial [power plant]	0.081	1	90
Non-road diesel	0.102	2	92
On-road diesel	0.102	3	92
Biomass	0.258	5	92
Gasoline	0.081	2	93

[1]For each zero-out simulation, a source's emissions are zeroed below its zero-out diameter.

The contribution of each source to ultrafine particle number concentrations was determined by subtracting the predicted number concentrations of the source's zero-out simulation from the respective predicted number concentration of the base simulation with the nucleation routine turned off. Zero-out simulations were performed with the nucleation routine turned off in order to avoid additional particles nucleating in the zero-out cases due to the decrease in the condensation sink from unavoidable removal of some emitted particle surface area in the zero-out inventories. The source contribution of nucleation to all size ranges was determined by a separate simulation including non-zeroed emissions from all sources and the nucleation routine turned on.

Since the condensation sink at and near the boundaries of the model domain is dominated by the boundary conditions, the same zero-out method that was used for ultrafine particle number emissions could not be used to quantify the contribution of long-range transport (represented by the boundary conditions) to modeled particle number concentrations. Instead a modified perturbation approach was used for the initial and boundary conditions so as to not greatly disturb condensation sinks and thus to minimize non-linear effects when compared to the base case simulation. For these zero-out simulations, the original mass and number concentrations of the initial and boundary conditions were divided by a factor of two uniformly across all size bins in two separate simulations.

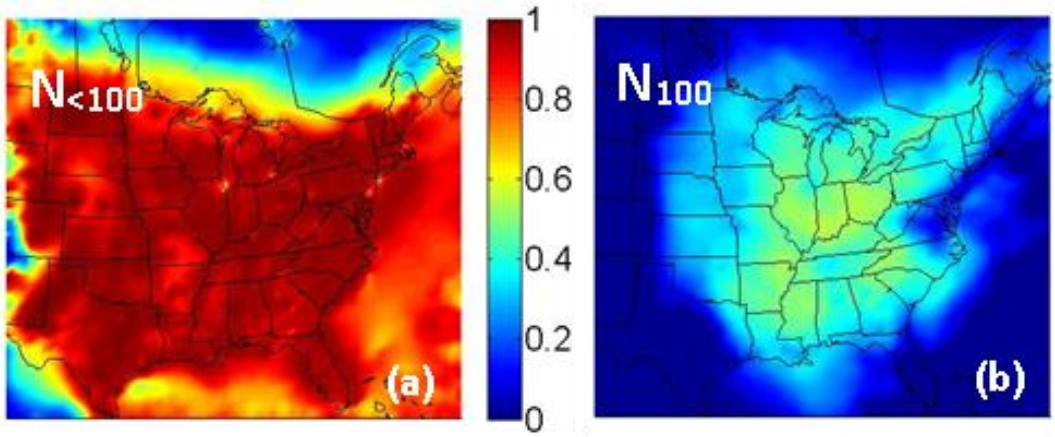

Figure 2.4. Predicted fractional contribution of nucleation to total particle number concentrations (cm^{-3}) at the ground level for particles with diameters (a) less than 100 nm and (b) greater than 100 nm for July 2001.

Table 2.7. Eastern U.S.-averaged model source apportionment predictions.

Source	Percentage of primary particles, only, in size range				
	N_{3-10}	N_{10-50}	N_{50-100}	N_{100}*	$N_{<100}$
Biomass	< 1	< 1	< 1	14	1
Gasoline	67	38	33	19	36
Industrial	15	31	33	33	31
Long-range transport	2	3	3	5	4
Non-road diesel	11	18	19	17	18
On-road diesel	5	10	12	12	10
	Percentage of total particles in size range				
Nucleation	99	89	77	36	96

*N_{100} is estimated based on emissions source contributions.

Given that most of our zero-out diameters eliminate particles below 100 nm, we use the following assumption to source apportion larger particles: a primary source's contribution to N_{100} in a specific grid cell and time period is approximately equal to the source's contribution to number emissions of particles larger than 100 nm in diameter in the same grid cell and time period. We use this zeroth order assumption since the focus of this work is ultrafine particles. The accuracy of our source apportionment approach can be evaluated by particle number concentration

number balances in each size range. This evaluation is described in a subsequent section.

2.5.2 Model source apportionment predictions in the Eastern U.S.

In order to reduce the influence of long-range transport (represented by the boundary conditions), we focus on the Eastern U.S. sub-domain proposed by Murphy et al. (2010). The authors found the average impact of the boundary conditions to organic aerosol concentrations in this sub-domain to be below 20% for most of the Eastern U.S. In this work, nucleation was found to be the major contributor to ultrafine particle number concentrations on average over the Eastern U.S. sub-domain (>90%) and in most parts of the domain individually (Figure 2.4). This is due to the high nucleation frequency during this time period. Given the variability of nucleation frequency, we will focus on primary particles (instead of total particles) in the rest of this discussion. On average over the Eastern U.S. sub-domain, gasoline was predicted to contribute 36% of the primary ultrafine particles, industrial sources (31%), non-road diesel (18%), on-road diesel (10%), biomass burning (1%), and long-range transport (4%). The domain-averaged error in this calculation, referred to as unaccounted particles, is approximately 1% of the domain-average ultrafine particle number concentration. Fractional and absolute source contributions to primary ultrafine particle number concentrations in the Eastern U.S. can be found in Figures 2.5 and 2.6, respectively. Gasoline was found to be the largest source of primary ultrafine particles in each size range, contributing the majority of $N_{3\text{-}10}$ and contributing almost equally with industrial sources and

diesel (on- and non-road combined) to $N_{10\text{-}50}$ and $N_{50\text{-}100}$. Biomass burning was not found to be a significant contributor to ultrafine particle concentrations during this summertime period. Domain-averaged source contributions to particle number concentrations are given in Table 2.7.

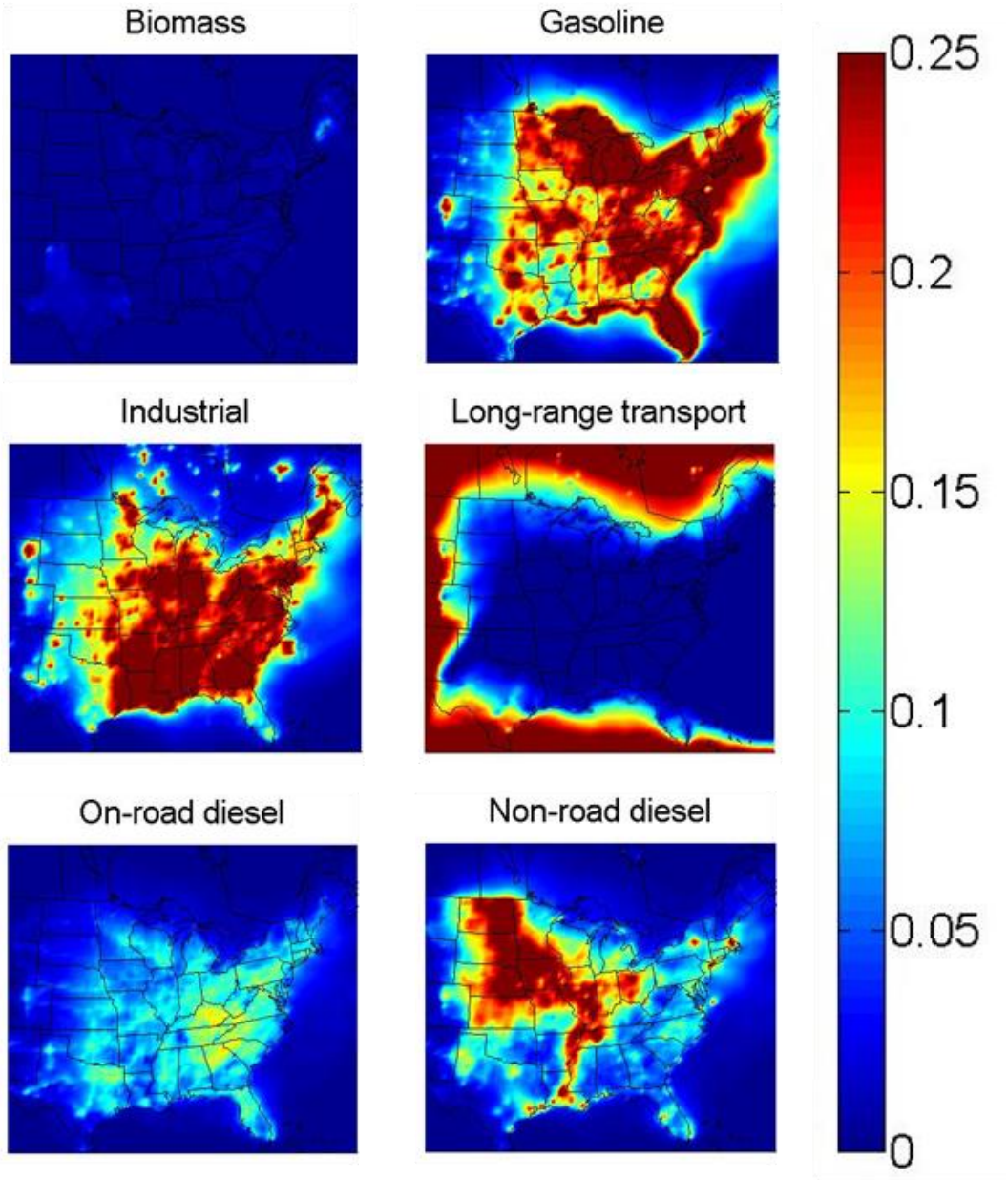

Figure 2.5. Predicted fractional source contributions to primary ultrafine particle number concentrations (cm^{-3}) at the ground level for July 2001.

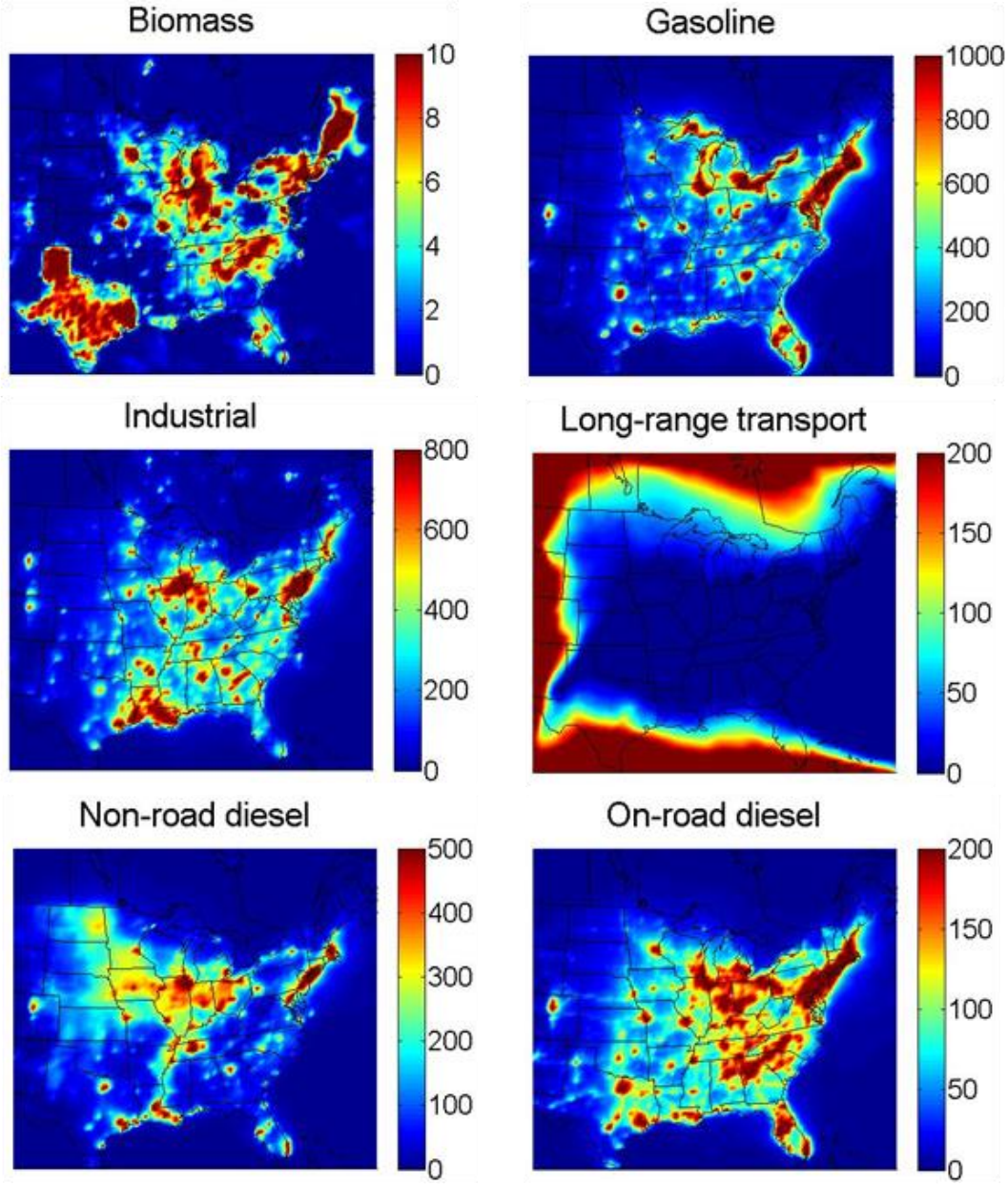

Figure 2.6. Predicted absolute source contributions to ultrafine particle number concentrations (cm^{-3}) at the ground level for July 2001 (scales are different for each source).

Though transport processes affect the geographic distribution of source contributions to ultrafine particle number concentrations, there is much similarity between the spatial distribution of source contributions to modeled particle number concentrations and input emissions in the Eastern U.S. In the Midwest, the prominent non-road diesel emissions associated with farming (Lane et al., 2007) were found to contribute significantly to particle number concentrations. Gasoline and industrial sources were the largest contributors to particle number concentrations over much of the Eastern U.S. due to significant emissions scattered throughout the domain, whereas on-road diesel is a smaller contributor to particle number concentrations. Long-range transport contributes to ultrafine particle number concentrations along the boundaries of our domain, with a smaller absolute contribution at the eastern boundary due to a much smaller number concentration over the Atlantic Ocean.

2.5.3 Model source apportionment predictions in Pittsburgh

In Pittsburgh, 88% of the ultrafine particles are estimated to come from nucleation during this photochemically-active period. Of the remaining 12%, 35% can be attributed to industrial sources, followed by gasoline (32%), non-road diesel (20%), on-road diesel (11%), and long-range transport (2%). Source contributions to $N_{3\text{-}10}$, $N_{10\text{-}50}$, $N_{50\text{-}100}$, and N_{100} in Pittsburgh for this time period are shown in Figure A2. These predictions can be compared to observation-based July 2001 particle number source apportionment from the Pittsburgh Air Quality Study (Zhou et al., 2004). The authors estimated that gasoline and on- and non-road diesel were

responsible for 60% of observed N_3, while industrial and other combustion sources, both local and regional, were responsible for 40%. These estimates agree well with the predictions of PMCAMx-UF from this study: gasoline and diesel sources (65%) and industrial sources and long-range transport (35%).

2.5.4 Model source apportionment predictions in other Eastern U.S. cities

Source apportionment of ultrafine particle number concentrations was also calculated for other Eastern U.S. cities (Figure A3). Gasoline and on-road diesel were found to be significant contributors to particle number concentrations in these urban areas. In addition, the industrial source contribution to ultrafine particle number concentrations was found to be large in Philadelphia, Chicago, and Pittsburgh due to significant industrial activities in these areas.

2.6 Sensitivity test to the nucleation rate parameterization

In order to test the sensitivity of the model predictions to the nucleation rate, the nucleation rate tuner in PMCAMx-UF was reduced from the default 10^{-5} to 10^{-7} in a separate simulation for sensitivity analysis. Using the 10^{-7} tuner, the model shows increased bias in predictions of N_3 and N_{10} (50% and -32%, respectively) in Pittsburgh with respect to observations (PAQS) as compared to Jung et al. (2010)'s work (-12% and 15%, respectively) and our work using the 10^{-5} tuner (-11% and 6%, respectively). The 10^{-5} tuner also shows better model-measurement agreement in the measurable ultrafine range ($N_{3\text{-}100}$, 10^{-5}: -11%, 10^{-7}: -14%). The 10^{-7} tuner does, however, reduce the $N_{50\text{-}100}$ error from 49% using the base 10^{-5} default

nucleation rate tuner to 7%, indicating that some of the error in this size range may be attributed to the nucleation rate. The estimated source apportionment of primary particles in this study was not affected by changes to the nucleation rate.

2.7 Conclusions

Using source-specific size distributions, a number emissions inventory for the Eastern U.S. (including biomass burning, dust, gasoline automobiles, industrial sources, and non- and on-road diesel) was developed for July 2001 to study the sources of ultrafine particle number concentrations. The number emissions inventory was then input into the three-dimensional CTM PMCAMx-UF to simulate the atmosphere over the Eastern U.S. during July 2001. Simulated number concentration results in Pittsburgh were found to reproduce average observed number concentrations in the measureable ultrafine range ($N_{3\text{-}100}$) within 12%. However, larger errors could be found in specific size ranges, which could either be due to the size distributions used or errors in the growth rates of ultrafine particles due to condensation of secondary organics.

A modified zero-out method for number source apportionment was then introduced that minimizes non-linear responses to the imposed perturbations. The results of zero-out simulations for each source were used to source apportion particle number concentrations in the Eastern U.S. for July 2001. Nucleation was found to be the dominant source of ultrafine particles, followed by gasoline, industrial sources, on-road and non-road diesel, and long-range transport. Gasoline was predicted to be the dominant source of the smaller ultrafine particle

concentrations ($N_{0.8\text{-}50}$) followed by comparable contributions from industrial sources and diesel (both non-road and on-road). Industrial sources, diesel and gasoline were found to contribute approximately equally to larger ultrafine particle concentrations ($N_{50\text{-}100}$). Biomass burning was not found to be a significant source of particle number during the summertime period investigated.

2.8 References

Adams, P.J., Seinfeld, J.H., 2002. Predicting global aerosol size distributions in general circulation models. J. Geophys. Res. 107, 4370-4392.

Aiken, A.C., Salcedo, D., Cubison, M J., Huffman, J.A., DeCarlo, P.F., Ulbrich, I.M., Docherty, K.S., Sueper, D., Kimmel, J.R., Worsnop, D.R., Trimborn, A., Northway, M., Stone, E.A., Schauer, J.J., Volkamer, R.M., Fortner, E., de Foy, B., Wang, J., Laskin, A., Shutthanandan, V., Zheng, J., Zhang, R., Gaffney, J., Marley, N.A., Paredes-Miranda, G., Arnott, W.P., Molina, L.T., Sosa, G., and Jimenez, J.L., 2009. Mexico City aerosol analysis during MILAGRO using high resolution aerosol mass spectrometry at the urban supersite (T0) – Part 1: Fine particle composition and organic source apportionment. Atmos. Chem. Phys. 9, 6633-6653.

Ban-Weiss, G.A., Lunden, M.M., Kirchstetter, T.W., Harley, R.A., 2010. Size-resolved particle number and volume emission factors for on-road gasoline and diesel motor vehicles. J. Aerosol Sci. 41, 5-12.

Delfino, R.J., Sioutas, C., Malik, S., 2005. Potential role of ultrafine particles in associations between airborne particle mass and cardiovascular health. Environ. Health Persp. 113, 934-946.

Dentener, F., Kinne, S., Bond, T., Boucher, O., Cofala, J., Generoso, S., Ginoux, P., Gong, S., Hoelzemann, J.J., Ito, A., Marelli, L., Penner, J.E., Putaud, J.-P., Textor, C., Schulz, M., van der Werf, G.R., Wilson, J., 2006. Emissions of primary aerosol and precursor gases in the years 2000 and 1750, prescribed data-sets for AeroCom. Atmos. Chem. Phys. 6, 4321-4344.

Elleman, R.A., Covert, D.S., 2009. Aerosol size distribution modeling with the Community Multiscale Air Quality modeling system in the Pacific Northwest: 2. Parameterizations for ternary nucleation and nucleation mode processes. J. Geophys. Res. 114, D012187.

Elleman, R.A., Covert, D.S., 2010. Aerosol size distribution modeling with the Community Multiscale Air Quality modeling system in the Pacific Northwest: 3. Size distribution of particles emitted into a mesoscale model. J. Geophys. Res. 115, D03204.

ENVIRON, 2003. User's guide to the comprehensive air quality model with extensions (CAMx), version 4.20. Prepared by ENVIRON International Corporation, Novato, California.

Gaydos, T.M., Pinder, R., Koo, B., Fahey, K.M., Yarwood, G., Pandis, S.N., 2007. Development and application of a three-dimensional aerosol chemical transport model, PMCAMx. Atmos. Environ. 41, 2594-2611.

Hennigan, C.J., Miracolo, M.A., Engelhart, G.J., May, A.A., Presto, A.A., Lee, T., Sullivan, A.P., McMeeking, G.R., Coe, H., Wold, C.E., Hao, W.-M., Gilman, J.B., Kuster, W.C., de Gouw, J., Schichtel, B.A., Collet Jr., J.L., Kreidenweis, S.M., Robinson, A.L., 2011. Chemical and physical transformations of organic aerosol from the photo-oxidation of open biomass burning emissions in an environmental chamber. Atmos. Chem. Phys. 11, 7669-7686.

Heo, J.-B., Hopke, P.K., Yi, S.-M., 2009. Source apportionment of $PM_{2.5}$ in Seoul, Korea, Atmos. Chem. Phys. 14, 4957-4971.

IPCC, 2013. Climate change 2013: the physical science basis. Contribution of Working Group I to the Fifth Assessment Report of the Intergovernmental Panel on Climate Change. Cambridge University Press, New York, NY.

Jaenicke, R., 1993. Aerosol-Cloud-Climate Interactions. P.V. Hobbs, ed., Academic Press, San Diego, CA.

Jung, J., Adams, P.J., Pandis, S.N., 2006. Simulating the size distribution and chemical composition of ultrafine particles during nucleation events. Atmos. Environ. 40, 2248-2259.

Jung, J., Pandis, S.N., Adams, P.J., 2008. Evaluation of nucleation theories in a sulfur-rich environment. Aerosol Sci. Tech. 42, 495-504.

Jung, J., Fountoukis, C., Adams, P.J., Pandis, S.N., 2010. Simulation of in situ ultrafine particle formation in the eastern United States using PMCAMx-UF. J. Geophys. Res. 115, D03203.

Karydis, V.A., Tsimpidi, A.P., Pandis, S.N., 2007. Evaluation of a three-dimensional chemical transport model (PMCAMx) in the eastern United States for all four seasons. J. Geophys. Res. 112, D14211.

LADCO, 2003. Midwest Regional Planning Organization: Base E modeling inventory. Prepared by the Lake Michigan Air Directors Consortium, Rosemont, IL.

LADCO, 2013. Midwest Regional Planning Organization: Base C modeling inventory. Prepared by the Lake Michigan Air Directors Consortium, Rosemont, IL.

Lane, T.E., Pinder, R.W., Shrivastava, M., Robinson, A.L., Pandis, S.N., 2007. Source contributions to primary organic aerosol: comparison of the results of a source-resolved model and the chemical mass balance approach. Atmos. Environ. 41, 3758-3776.

Marmur, A., Park., S.K., Mulholland, J.A., Toldbert, P.E., Russell, A.G., 2006. Source apportionment of $PM_{2.5}$ in the southeastern United States using receptor and emissions-based models: Conceptual differences and implications for time-series health studies. Atmos. Environ. 40, 2533-2551.

Murphy, B.N., Pandis, S.N., 2010. Exploring summertime organic aerosol formation in the Eastern United States using a regional-scale budget approach and ambient measurements. J. Geophys. Res. 115, D24216.

Napari, I., Noppel, M., Vehkamäki, H., Kulmala, M., 2002. Parameterization of ternary nucleation rates for H_2SO_4-NH_3-H_2O vapors. J. Geophys. Res. 107, 4381-4386.

Patoulias, D., Fountoukis, C., Riipinen, I., Pandis, S.N., 2014. The role of organic condensation on ultrafine particle growth during nucleation events. Atmos. Chem. Phys. Discuss. 14, 30761-30798.

Pey, J., Querol, X., Alastuey, A., Rodríguez, S., Putaud, J.P., Van Dingenen, R., 2009. Source apportionment of urban fine and ultra-fine particle number concentration in a Western Mediterranean city. Atmos. Environ. 43, 4407-4415.

Pierce, J.R., Adams, P.J., 2009. Uncertainty in global CCN concentrations from uncertain aerosol nucleation and primary emission rates. Atmos. Chem. Phys. 9, 1339–1356.

Seinfeld, J.H., Pandis, S.N., 2006. Atmospheric chemistry and physics: from air pollution to climate change, second ed. John Wiley and Sons, Hoboken, NJ.

Spracklen, D.V., Carslaw, K.S., Kulmala, M., Kerminen, V.-M., Mann, G.W., Sihto, S.-L., 2006. The contribution of boundary layer nucleation events to total particle concentrations on regional and global scales. Atmos. Chem. Physics. 6, 5631-5648.

Stanier, C.O., Khlystov, A.Y., Pandis, S.N., 2004. Ambient aerosol size distributions and number concentrations measured during the Pittsburgh Air Quality Study (PAQS). Atmos. Environ. 38, 3275-3284.

Vehkamäki, H., Kulmala, M., Napari, I., Lehtinen, K.E.J., Timmreck, C., Noppel, M., Laaksonen, A., 2002. An improved parameterization for sulfuric acid–water nucleation rates for tropospheric and stratospheric conditions. J. Geophys. Res. 107, 4622-4632.

Wang, Z.S., Chien, C.-J., Tonnesen, G.S., 2009. Development of a tagged species source apportionment algorithm to characterize three-dimensional transport and transformation of precursors and secondary pollutants. J. Geophys. Res. 114, D010846.

Yarwood, G., Rao, S., Yocke, M., Whitten, G.Z., 2005. Updates to the Carbon bond chemical mechanism: CB05. Prepared by ENVIRON International Corporation, Novato, CA, Yocke & Company, Novato, CA, Smog Reyes, Point Reyes Station, CA.

Zhou, L., Kim, E., Hopke, P.K., Stanier, C.O., Pandis, S.N., 2004. Advanced factor analysis on Pittsburgh particle size-distribution data. Aerosol Sci. Tech. 38, 118-132.

Zhou, L., Kim, E., Hopke, P.K., Stanier, C.O., Pandis, S.N., 2005. Mining airborne particulate size distribution data by positive matrix factorization. J. Geophys. Res. 100, D07S19.

Chapter 3. Reduction of diesel emissions: effects on black carbon and number concentrations in the Eastern U.S.

3.1 Introduction

$PM_{2.5}$ (particulate matter less than 2.5 μm in diameter) has been linked to both negative health effects (Lelieveld et al., 2013) and significant climate effects (IPCC, 2013). Though black carbon (BC) makes up only 5-10% of the $PM_{2.5}$ mass on average in urban areas (U.S. EPA, 2009), its potential effects on climate and health are considerable. The direct absorption of sunlight by BC has a positive (warming) effect on the energy balance of the earth (Bond et al., 2013; IPCC, 2013). Black carbon's short atmospheric lifetime (days), as compared to greenhouse gases such as CO_2 (years), can make BC mitigation efforts more immediately beneficial to climate. In addition, exposure to BC in the short and long term may be associated with increased risk of cardiopulmonary disease (Janssen et al., 2012). BC may even have a stronger correlation to increased blood pressure than exposure to total $PM_{2.5}$ mass, most likely due to the toxicity of the combustion chemicals coating its surface (Janssen et al., 2012).

The overall absorption or reflectance of sunlight off aerosols and the secondary effects of aerosol size and composition changes on clouds remain the most uncertain factors in the global radiative balance (IPCC, 2013). Mitigation efforts must take into account that BC sources also co-emit considerable amounts of organic PM and other species as well as aerosol precursors (e.g., sulfur dioxide)

that have a cooling effect. This competition between the heating and cooling components of BC source emissions determines the magnitude and sign of their effects on the overall radiative balance of the earth. Mitigation of major BC sources that have low emission rates of co-emitted species has the most potential for both health benefits as well as significant cooling effects on climate forcing (Bond et al., 2013).

In North America, on-road and non-road diesel engines contribute about 70% of BC emissions (Bond et al., 2013). The use of low sulfur diesel fuels and catalyzed diesel particulate filters (DPFs) in the U.S. has reduced the emissions of sulfur-containing compounds and NO_x from diesel vehicles (Herner et al., 2011). The ratio of (cooling) organic PM to (warming) BC emissions from diesel sources is about 0.5 (Ban-Weiss et al., 2008), which is smaller than the 4:1 ratio of biomass burning sources (Schmidt, 2011). Since diesel sources have the smallest ratio of co-emitted aerosols and aerosol precursors to black carbon, they are promising candidates for mitigation efforts (Bond et al., 2013).

Previous studies in the laboratory (Herner et al., 2011) and near-road (Dallmann et al., 2011; Kozawa et al., 2014) have investigated the effects of stringent regulation of heavy-duty diesel (HDD) vehicle emissions. California's 2010 HDD regulations require the oldest diesel vehicles to be replaced or to be retrofitted with DPFs, and provide incentives for HDD vehicles to be replaced by new, cleaner vehicles (CARB, 2010). DPFs are designed to reduce nitrogen oxides (NO_x) and PM emissions including BC. Dallmann et al. (2011) measured the concentrations of BC and NO_x in the diesel-dominated Port of Oakland before and

after 2010 regulation of HDD vehicles in California. The authors found that the fleet-averaged diesel BC emissions per mass of fuel burned decreased by about 50% after regulation. Kozawa et al. (2014) measured the concentrations of NO_x, BC, and ultrafine particle (less than 100 nm in diameter) number concentrations on a diesel-dominated highway in California from 2009 to 2011. They reported that the fleet-averaged BC emissions from diesel vehicles decreased by about 70% between 2009 and 2011.

Though DPFs have been shown to be effective at reducing particle mass emissions from HDD, corresponding changes in the particle number emissions are less clear. Several studies suggest that HDD equipped with DPFs can sometimes emit greater numbers of particles than those without DPFs. Herner et al. (2011) tested four DPFs and reported that the corresponding HDD, under certain conditions, emitted high concentrations of nucleation mode particles (less than 20 nm in diameter). Seigneur (2009) also concluded that DPFs can sometimes increase particle number emissions, such as during regeneration (Mathis et al., 2004), but overall decrease particle number emissions. Kozawa et al. (2014) found no statistically significant difference in the fleet-averaged diesel ultrafine particle number emissions after regulation.

Larger diesel particles contain organic compounds and a solid BC core (Sakurai et al., 2009). Freshly nucleated ultrafine particle emissions from diesel vehicles equipped with aftertreatment, however, are composed of only volatile compounds and lack a solid BC core (Herner et al., 2011). Though previous field literature suggests that diesel ultrafine particle number emissions can either remain

constant or even increase after the vehicle emissions are treated (Herner et al., 2011; Kozawa et al., 2014), the reduced emissions can cause changes in the atmosphere (e.g. reduce aerosol surface area and increase nucleation intensity).

Previous studies have investigated the modeled climate effects of BC source mitigation strategies on the global scale. Bauer et al. (2010) found that reducing diesel emissions generally showed a decrease in radiative fluxes, whereas reducing BC sources with a larger percentage of organic matter (OM) did not always lead to a reduction in radiative flux. Chen et al. (2010) concluded that reducing fossil fuel BC, OM, and particle number emissions generally decreased global cloud radiative forcing. The authors noted that a reduction of particle mass emissions could result in an increase in number emissions. This could change the concentration of particles that grow to become cloud condensation nuclei (CCN). CCN can grow further to become cloud droplets, changing the reflectance of sunlight off clouds and therefore affecting the global radiative balance (IPCC, 2013). Shindell et al. (2012) investigated the radiative forcing, health and crop yield effects of reducing all BC source emissions through technical measures. The authors found that the climate effects of BC mitigation were largely uncertain but that the health and crop yield effects were beneficial. Unlike most greenhouse gases, black carbon is not well-mixed in the atmosphere due to its short lifetime, so its effects vary regionally based on factors such as the locations of BC emission sources (Bond et al., 2013). Our work focuses on regional-level effects due to changes in diesel source emissions.

In this study, we use the regional chemical transport model (CTM) PMCAMx-UF to simulate the atmosphere over the Eastern U.S. during the summer

for two simple diesel perturbation scenarios: (a) a simplified mitigation effort that reduces diesel particulate emissions by one half and (b) a diesel particulate emissions increase to double the base values. We then quantify the effects of these two scenarios on BC concentrations, particle number concentrations and climate-relevant aerosol properties: absorption, extinction, and aerosol optical depth (AOD).

3.2 PMCAMx-UF description

PMCAMx-UF simulates the aerosol size distribution using a 41 size bin sectional approach to track particles with diameters ranging from 0.8 nm to 10 μm. There are two additional size bins with diameters of 20 μm and 40 μm to represent cloud droplets. The model in this application calculates nucleation rates based on the scaled (10^{-5} nucleation tuner) sulfuric acid-ammonia-water nucleation rate parameterization of Napari et al. (2002), and for small ammonia concentrations (below 0.01 ppt), the binary nucleation parameterization of Vehkamäki et al. (2002).

In this study, we use the same inputs as in Posner and Pandis (2015). PMCAMx-UF is used to simulate a 3492 x 3240 km area over the Eastern U.S. for July 12-28, 2001. The domain is gridded into 97 (east-west) by 90 (north-south) cells that are each 36 x 36 km. 14 vertical layers above the surface up to 6 km are also simulated. BC and number concentrations reported in this study are the average output for the ground layer, only; however reported climate-relevant effects are calculated based on all simulated layers.

3.3 Emission scenarios

3.3.1 Base emissions

The base July 2001 number emissions inventory developed in Posner and Pandis (2015) is used as the base inventory for this study. The inventory includes biomass burning (combined with wood combustion), dust, gasoline automobiles, industrial emissions, non-road diesel, and on-road diesel emissions. The absolute and fractional contribution of diesel sources (on- and non-road diesel) to total $PM_{2.5}$ BC and total number (N_{TOT}) emissions in the base case are shown in Figures 3.1 and 3.2, respectively. According to this July 2001 base emissions inventory, non-road and on-road diesel sources are responsible for 58% of the total emitted $PM_{2.5}$ BC and 27% of total number emissions in the Eastern U.S. domain. The large contribution of diesel sources to N_{TOT} and $PM_{2.5}$ BC emissions in the Midwest is associated with non-road diesel farming activity. Diesel sources are responsible for most of the $PM_{2.5}$ BC emissions throughout the domain but do not contribute as much to N_{TOT} emissions outside of the Midwest due to the predominance of other sources, such as gasoline.

3.3.2 Diesel perturbation emissions

The reduced diesel emissions inventory was derived to represent a simple case of diesel mitigation in which the base non-road and on-road diesel particulate emissions are reduced by 50%. Dallmann et al. (2011) found that 2010 regulation in California of HDD emissions reduced BC emissions from HDD by approximately 50%, so the half diesel case can be seen as a simplified change in

emissions due to regulation. The reduction was applied uniformly across the modeling domain and across all particle size sections. Gaseous emissions were assumed to remain constant for all simulations in this study. The half diesel scenario results in a 29% decrease in total BC emissions and a 14% decrease in N_{TOT} emissions as compared to the base emissions.

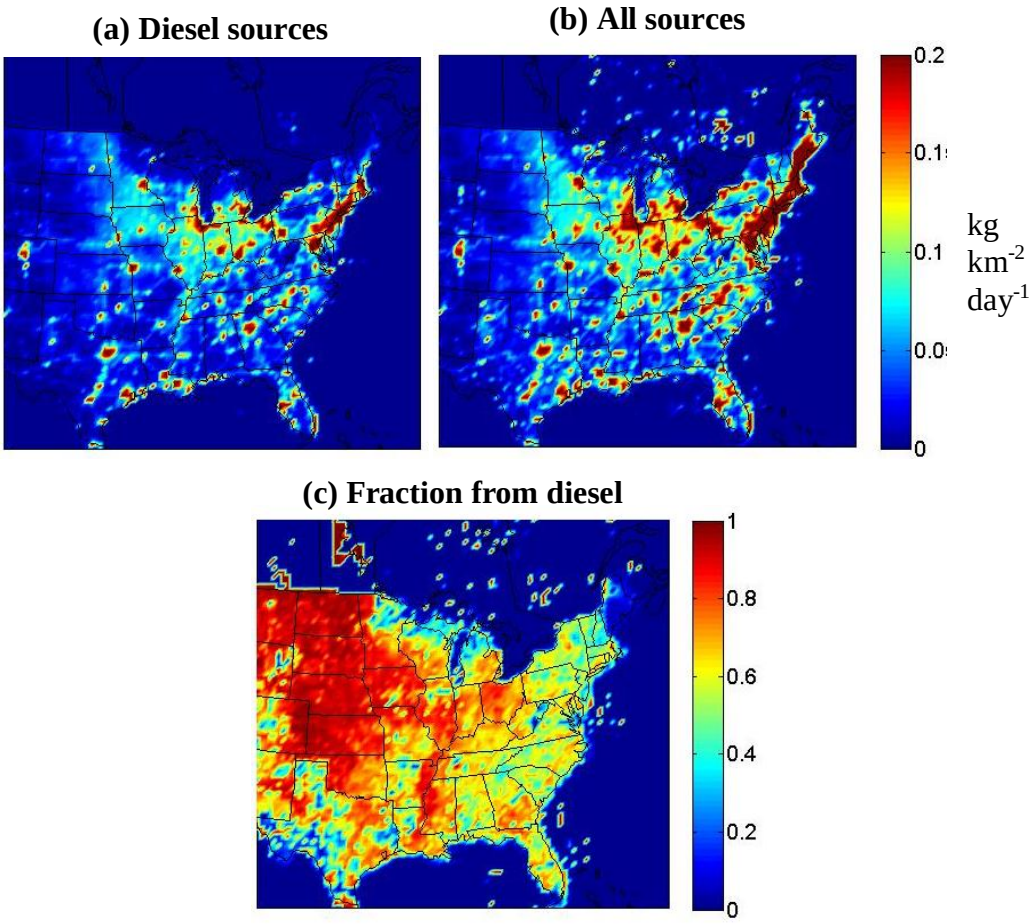

Figure 3.1. $PM_{2.5}$ BC emission rates (kg km^{-2} day^{-1}) from (a) diesel sources, (b) all sources, and (c) the fractional contribution of diesel sources for the July 2001 base simulation.

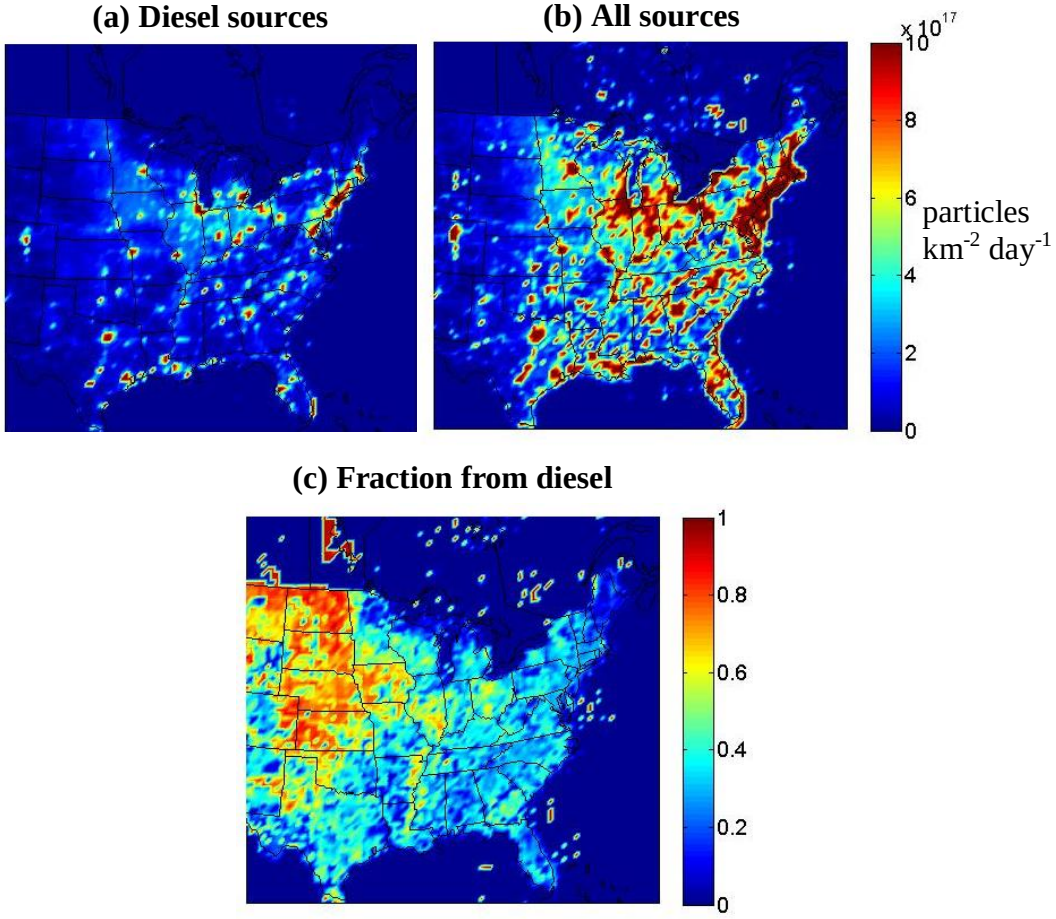

Figure 3.2. Total particle number (N_{TOT}) emission rates (particles km^{-2} day^{-1}) from (a) diesel sources, (b) all sources, and (c) the fractional contribution of diesel sources for the July 2001 base simulation**.**

The double diesel emissions scenario assumes a major future increase in the number of vehicles/machinery being used. Only the particulate emissions from diesel sources were doubled in this scenario. The increase in diesel emissions was applied uniformly across the modeling domain and across all particle size sections. The double diesel scenario results in a 58% increase in $PM_{2.5}$ BC and a 27% increase in N_{TOT} emissions as compared to the base emissions for the Eastern U.S. domain.

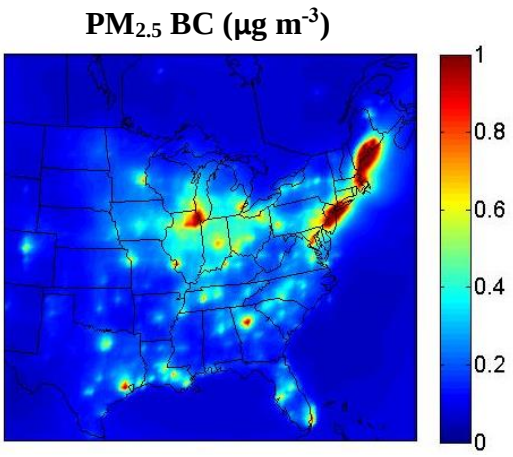

Figure 3.3. Predicted simulation-average concentrations of $PM_{2.5}$ BC (μg m^{-3}) at the ground level for the July 2001 base case.

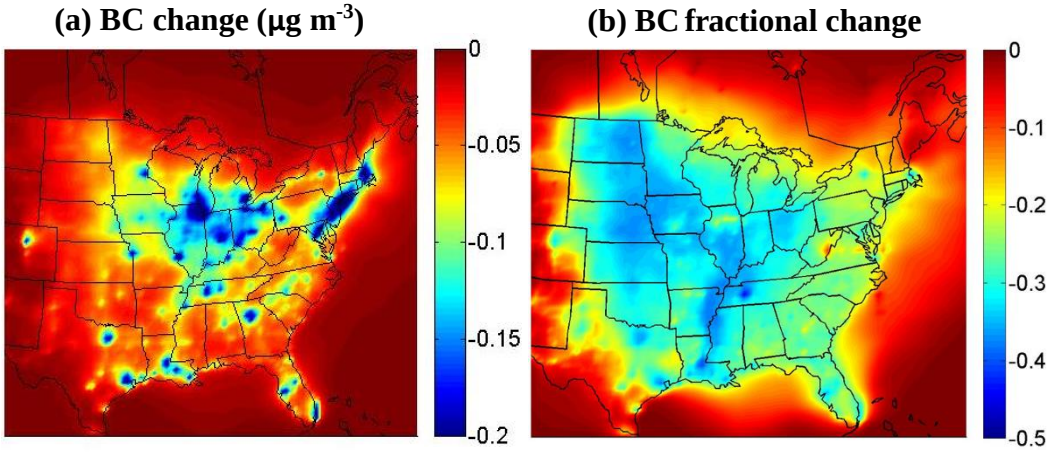

Figure 3.4. Predicted (a) absolute and (b) fractional changes to $PM_{2.5}$ BC (μg m^{-3}) at the ground level for the July 2001 half diesel simulation.

3.4 Simulated black carbon concentrations

BC in the real atmosphere is always coated with organic compounds. Since this version of PMCAMx-UF assumes that primary organic aerosol (POA) components are non-volatile, we focus on the differences between the base and perturbation simulations as opposed to absolute values.

3.4.1 Base case

The base case for this study is the same as the base case in Posner and Pandis (2015) for July 2001 in the Eastern U.S. Application of the Lane et al. (2007) recommended changes to BC mass emissions improved model-measurement agreement; these changes reduced the magnitude of the mean bias of predicted vs. observed concentrations at Speciation Trends Network (STN) (urban) sites (U.S. EPA, 2002) from 0.88 μg m^{-3} (Gaydos et al., 2007) to -0.17 μg m^{-3}. The model slightly underpredicts $PM_{2.5}$ BC concentrations in comparison to IMPROVE (rural) (U.S. EPA, 2002) observations: the mean bias changed from 0.17 (Gaydos et al., 2007) to -0.17 μg m^{-3} after the inventory changes. Predicted average ground concentrations of $PM_{2.5}$ BC are shown in Figure 3.3.

3.4.2 Scenario I: Reduction of diesel emissions by 50%

Since diesel is a major source of $PM_{2.5}$ BC emissions (58%) during this summer period in the Eastern U.S., the half diesel particulate emissions scenario results in a considerable decrease in $PM_{2.5}$ BC concentrations over most of the domain (Figure 3.4). In order to reduce the influence of the boundary conditions, we report domain averages for the Eastern U.S. subdomain proposed by Murphy et al. (2010) that does not include the areas around the boundaries. The Eastern U.S. subdomain-averaged $PM_{2.5}$ BC concentration reduction is 0.04 μg m^{-3} or 23% of the base values, which is smaller than what one would expect (29%) for a 50% reduction of 58% of the BC emissions. This is due to the influence of long-range transport simulated through the boundary conditions, which were kept constant for

all simulations. The largest absolute reductions are in the Northeast coast and the Chicago area, while the largest fractional reductions are in the Midwest where non-road diesel emissions are the dominant BC source.

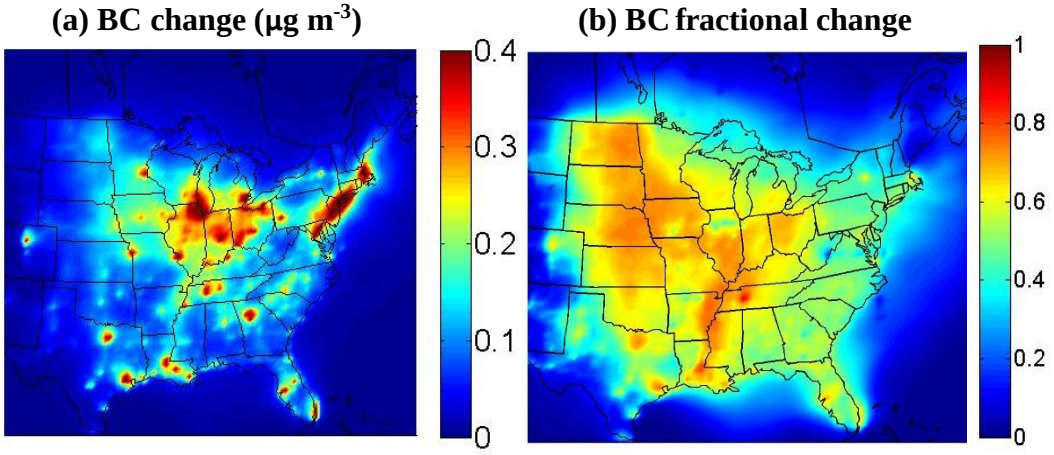

Figure 3.5. Predicted (a) absolute and (b) fractional changes to $PM_{2.5}$ black carbon concentrations (μg m^{-3}) at the ground level for the July 2001 double diesel simulation.

3.4.3 Scenario II: Double diesel emissions increase

The double diesel particulate emissions perturbation results in a considerable increase in $PM_{2.5}$ BC concentrations over most of the domain (Figure 3.5). The Eastern U.S. subdomain-averaged $PM_{2.5}$ BC concentration increase due to the double diesel perturbation is 0.08 μg m^{-3} or 46% of the average base value. This is lower than what one would expect (58%) for a proportional increase of the BC emissions because of the long-range transported BC that is assumed to remain constant. The spatial pattern of these increases is very similar to the spatial distribution of reductions due to the half diesel perturbation. The largest absolute increases in $PM_{2.5}$ BC concentrations are located where emissions from on-road diesel are largest (the Northeast coast and the Chicago area). Most of the largest

fractional reductions are where the non-road diesel emissions are largest and the main contributor to particle concentrations (the Midwest).

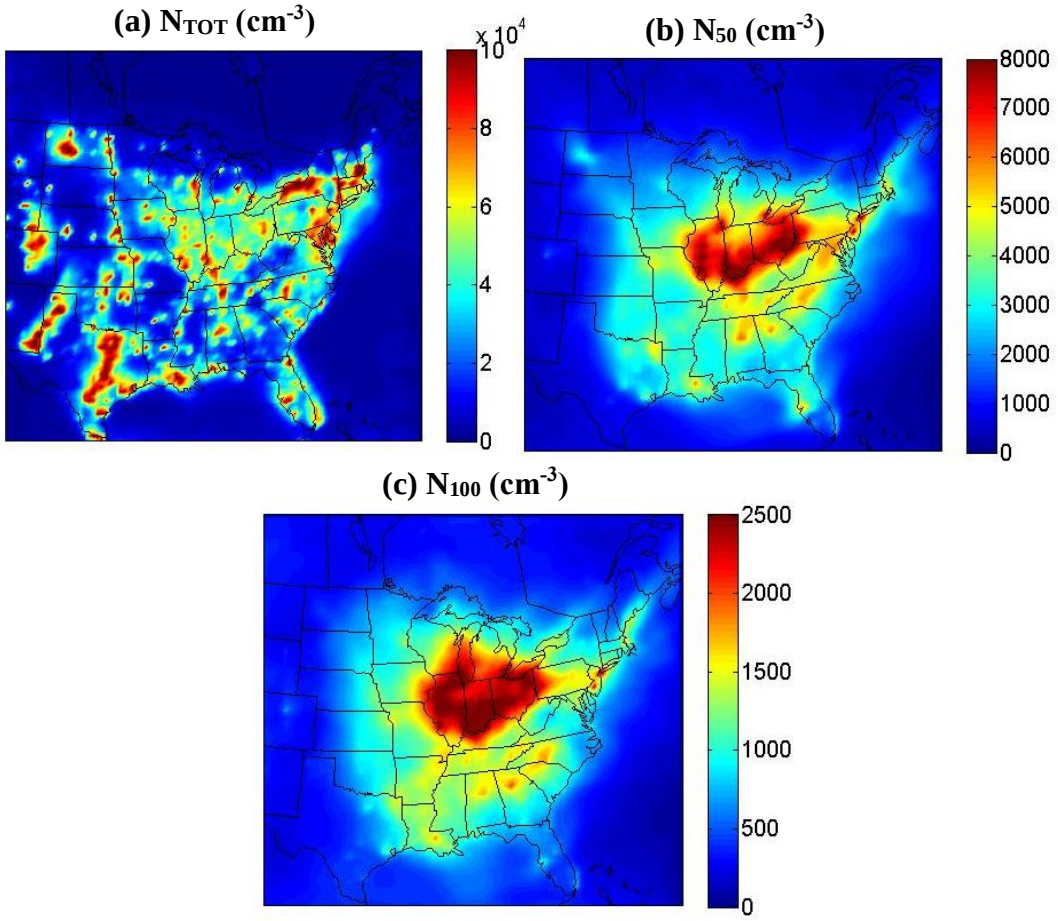

Figure 3.6. Predicted concentrations of (a) total particle number (cm^{-3}), (b) the number of particles greater than 50 nm in diameter (cm^{-3}), and (c) the number of particles greater than 100 nm in diameter (cm^{-3}) at the ground level for the July 2001 base case.

3.5 Simulated particle number concentrations

In this study we focus on total particle number concentrations (N_{TOT}), particles greater than 50 nm in diameter (N_{50}), and particles greater than 100 nm in diameter (N_{100}). Since ultrafine particles (less than 100 nm in diameter) form the

majority of N_{TOT}, they can greatly contribute to the number of particles that grow to become CCN (generally N_{100}) through condensation (Pierce and Adams, 2009).

3.5.1 Base case

Model predictions of particles greater than 3 nm in diameter (N_3), which is the range of measureable N_{TOT}, agree with observed Pittsburgh Air Quality Study (PAQS) (Stanier et al., 2004) measurements within 10% on average, and in the N_{100} range within 5%. Maps of the simulation-average ground N_{TOT}, N_{50}, and N_{100} concentration fields can be found in Figure 3.6. Using zero-out number but not mass simulations (Posner and Pandis, 2015), we calculated the contribution of diesel sources to ultrafine particle number concentrations for the July 2001 base case. Figure 3.7 shows the calculated absolute and fractional contribution of diesel sources to total particle number concentrations for the base case. The peaks in the number concentration contributions from diesel are seen where emissions from diesel sources are also large. Nucleation is the dominant source of particle number concentrations in the domain for this time period, so the domain-averaged fractional contribution of diesel to particle number concentrations is small. There are peaks in the Midwest due to the predominance of non-road diesel emissions in those areas with, according to the inventory, few other major emissions nearby. On average for July 2001 in the Eastern U.S., diesel particles were predicted to contribute 140 cm^{-3} or about 0.6% to total particle number concentrations.

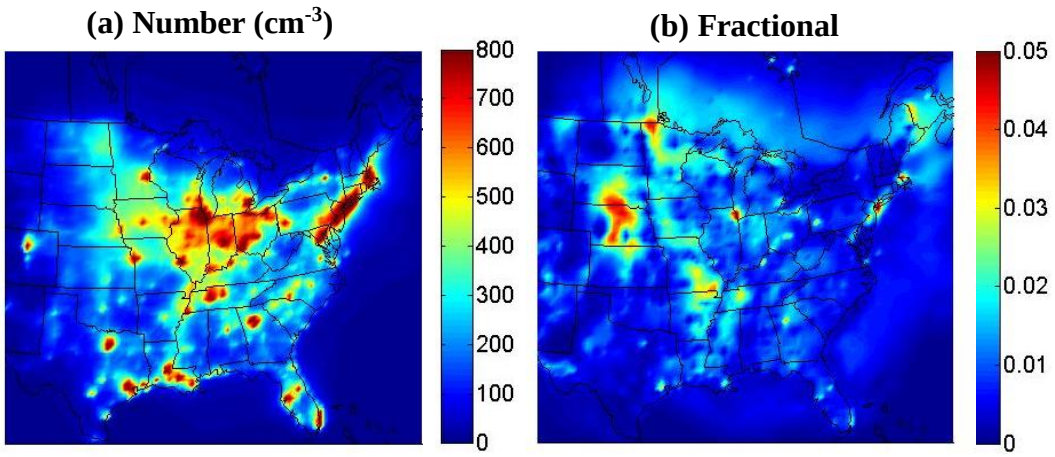

Figure 3.7. Predicted (a) absolute (cm^{-3}) and (b) fractional contributions of diesel sources to total particle number concentrations (cm^{-3}) at the ground level for the July 2001 base case.

3.5.2 Scenario I: Half diesel emissions reduction

If the effects of the half diesel emissions scenario on simulated particle number concentrations were linear, they would result in a 50% decrease of diesel particle number concentrations compared to the base case. Figure 3.8 shows the estimated linear changes as well as the actual simulated changes for this reduction scenario. A simple linear change would, on average for July 2001 in the Eastern U.S., result in a 70 cm^{-3} or 0.3% decrease in total particle number concentrations as compared to the base case. Instead PMCAMx-UF predicts an average increase of 350 cm^{-3} or 1.6% in total particle number concentrations. Domain-averaged N_{50} and N_{100}, however, decrease 0.9% and 1.6%, respectively. PMCAMx-UF also predicts a 1.4% decrease in $PM_{2.5}$ surface area.

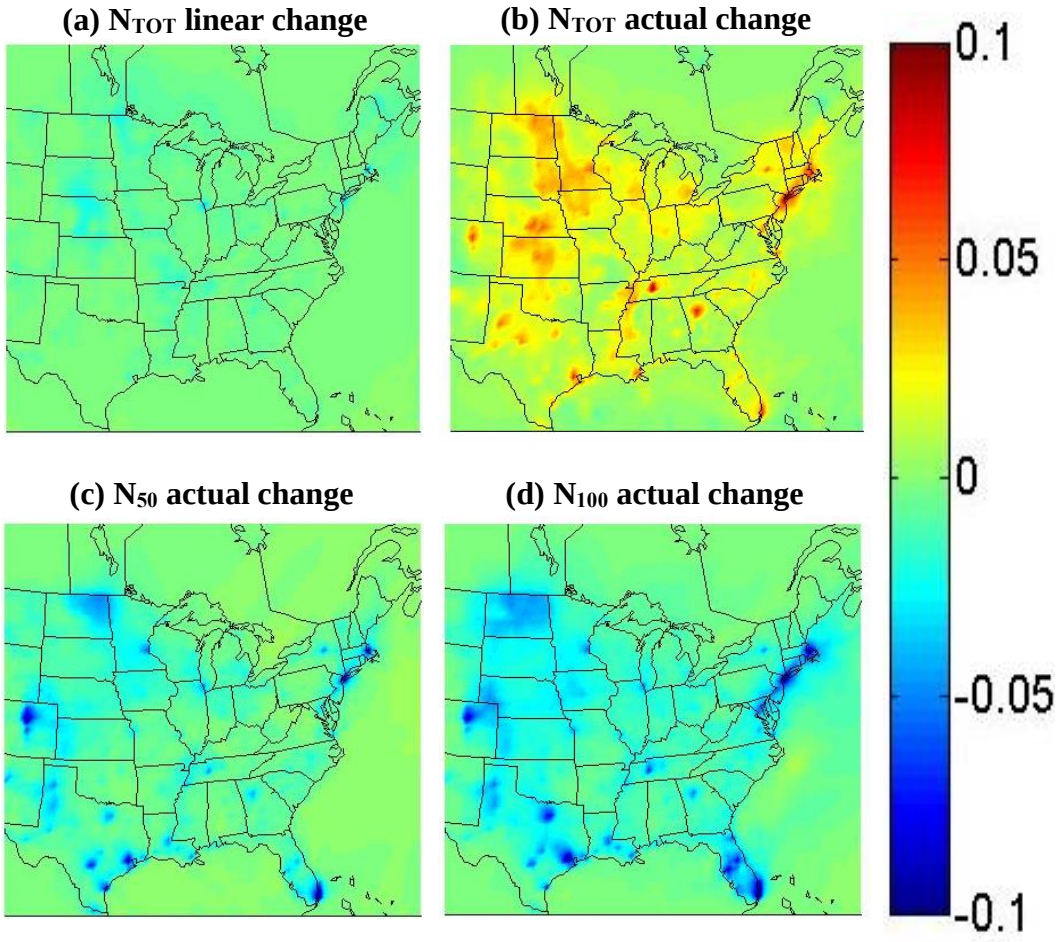

Figure 3.8. Predicted fractional changes to total particle number concentrations (cm^{-3}) at the ground level for July 2001 due to a 50% reduction of the base diesel particulate emissions calculated (a) assuming a linear change based on previous source apportionment results and (b) by the half diesel simulation and actual fractional changes to (c) N_{50} and (d) N_{100} determined by the half diesel simulation.

The reduction of particle emissions from diesel sources in this case changes not only the particle number emissions but also the corresponding condensation and coagulation sinks. There is less particle surface area for vapors to condense onto and fewer large particles with which smaller particles can coagulate. The results of this half diesel simulation suggest that reduction of the larger diesel particles can result in increased ultrafine particle number concentrations due to their increased

survival probability but also the increased nucleation rates. However, these effects do depend on the size range examined. The N_{100} concentration (used as a proxy of the CCN concentration) is predicted to decrease in this simulation despite the increase in total particle number. However, they decrease a lot less than what one would estimate assuming a proportional change.

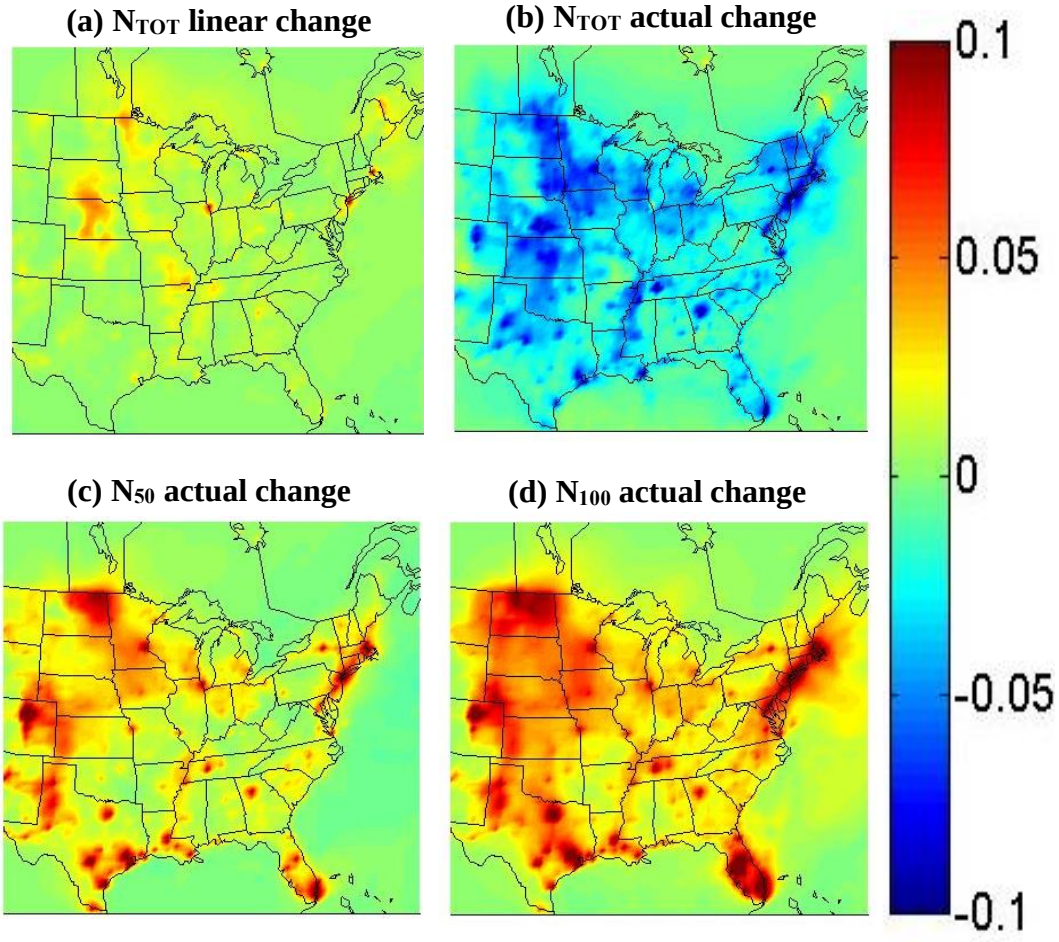

Figure 3.9. Predicted fractional changes to total particle number concentrations (cm^{-3}) at the ground level for July 2001 due to doubling the diesel particulate emissions calculated (a) assuming a linear change based on previous source apportionment results and (b) by the double diesel simulation and (c) actual fractional changes to N_{100} determined by the double diesel simulation.

3.5.3 Scenario II: Doubling of diesel emissions

Figure 3.9 shows the estimated (proportional) changes of the double diesel emissions scenario as well as the actual simulated changes. A simple linear change would result on average in a 140 cm^{-3} or 0.65% increase in total particle number as compared to the base case. Instead PMCAMx-UF predicts the opposite: an average 660 cm^{-3} or 3% decrease in total number concentrations. Domain-averaged N_{50} and N_{100}, however, are predicted to increase 1.9% and 3.3%, respectively. A 2.9% increase in $PM_{2.5}$ surface area is also predicted. This suggests that the increase in surface area caused by doubling the diesel emissions resulted in vapors that had previously condensed onto ultrafine particles or nucleated new particles instead condensing onto these larger particles. There was also an increase of the coagulation rates of smaller particles with the larger ones and a reduction of the nucleation rates.

The half and double diesel emissions simulations predict counterintuitive changes in the ultrafine particle number concentration results for the same reasons. The double diesel emissions scenario assumes doubling of the diesel particle number and mass emissions as compared to the base case, leading to an increase of the condensation and coagulation sinks. With the number of larger particles increased, there is more particle surface area for vapors to condense onto and more large particles with which smaller particles can coagulate, decreasing number concentrations.

3.6 Changes in aerosol optical properties

In this study, core-shell Mie theory is used assuming spherical particles (Bohren and Huffman, 1998) to compute climate-relevant properties of simulated aerosol concentrations at a wavelength of 550 nm. The assumed mixing state, simulated size distribution, mass and number concentrations of particles in the modeled atmosphere determine climate-relevant properties such as absorption and optical depth. BC in particular is important due to its strong absorption properties. PMCAMx-UF simulates aerosol concentrations assuming internal mixing of particles, i.e. that all particles in a given size section have the same chemical composition. The other extreme representation of particle composition is external mixing, i.e. each particle in a given size section is composed of a different chemical component, one chemical component per particle. Since particle mixing states in the real atmosphere vary between these two extremes, the optical properties of the aerosol have been calculated using model predicted size-composition distributions and both external and internal mixing assumptions. This gives a range of possible values for calculated climate relevant properties.

BC is a part of every particle in a given size section when internal mixing is assumed. The other extreme is external mixing for which pure BC particles are assumed with no additional chemical compounds that tend to scatter incoming solar radiation (such as sulfate). Since the internal mixing assumption calculates a greater number of BC-containing particles, its corresponding predictions for the absorption coefficient and absorption aerosol optical depth (AAOD) are higher than external

mixing. Extinction is the sum of absorption and scattering, so it depends on the relative magnitudes of both the absorption and scattering coefficients.

3.6.1 Base case

The absorption coefficient, extinction coefficient, and AAOD predictions for the base July 2001 simulation in the Eastern U.S. are shown in Figure 3.10. The average absorption coefficient during this July 2001 simulation period is, assuming external mixing, 0.91 Mm^{-1} and, assuming internal mixing, 2.01 Mm^{-1}. Spatially, the high absorption areas are those with considerable emissions from combustion sources (gasoline, diesel, and industrial sources along the Northeast coast and Chicago). The domain-averaged extinction coefficients are 18.95 Mm^{-1} and 19.35 Mm^{-1} for external and internal mixing, respectively. High values of the extinction coefficient, as well as the aerosol optical depth (AOD) can be found in areas with high sulfate concentrations. Domain-averaged AOD was determined to be 0.03 for both internal and external mixing. The domain-averaged calculated AAOD for this simulation are 9×10^{-4} and 2×10^{-3} for external and internal mixing, respectively. The spatial distribution of AAOD values is similar to that of the absorption coefficient.

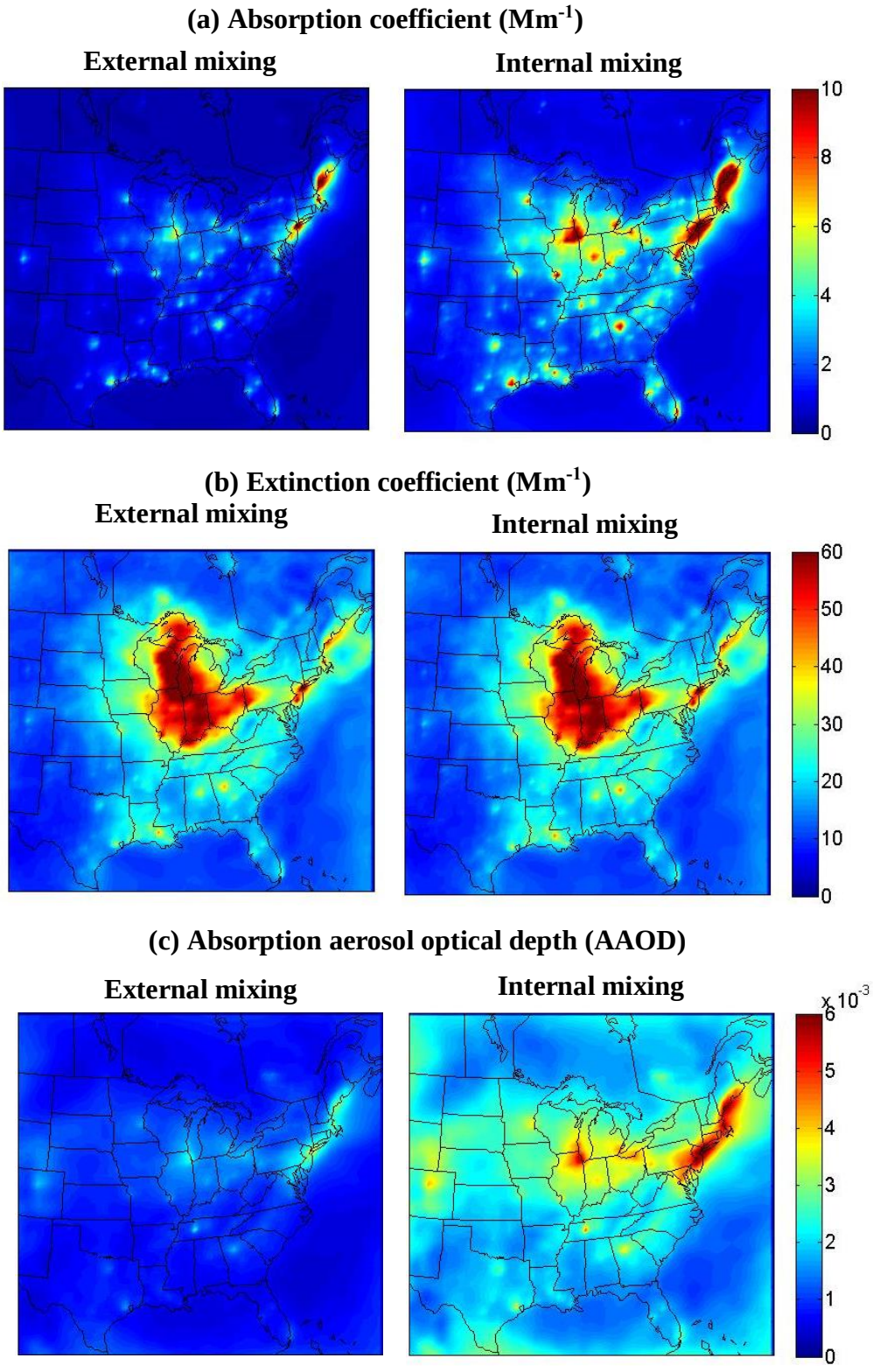

Figure 3.10. Predicted (a) absorption coefficients (Mm^{-1}), (b) extinction coefficients (Mm^{-1}), and (c) absorption aerosol optical depth (AAOD) for the July 2001 base simulation.

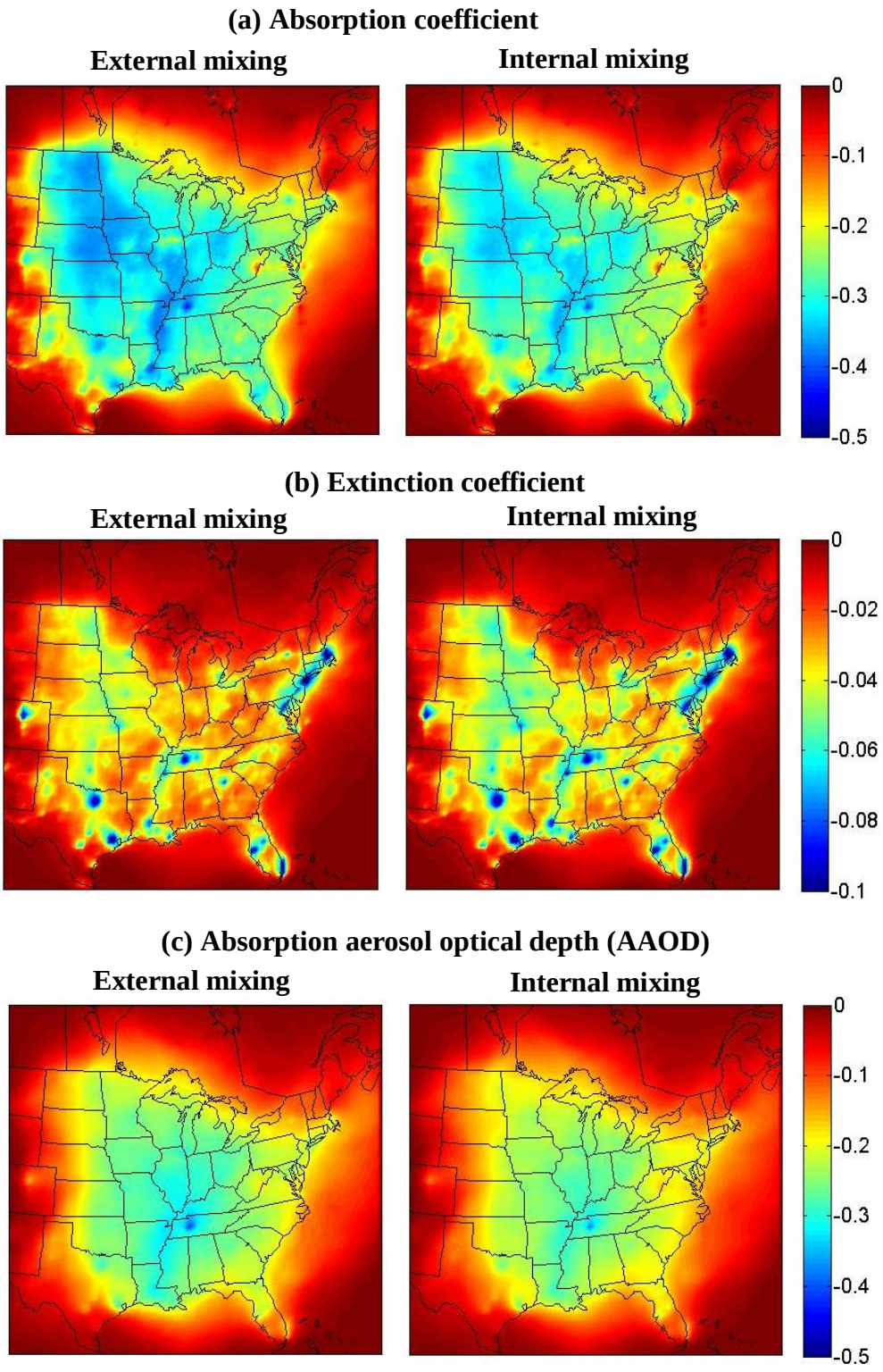

Figure 3.11. Predicted fractional changes to the (a) absorption coefficient, (b) extinction coefficient, and (c) absorption aerosol optical depth (AAOD) for the July 2001 half diesel simulation.

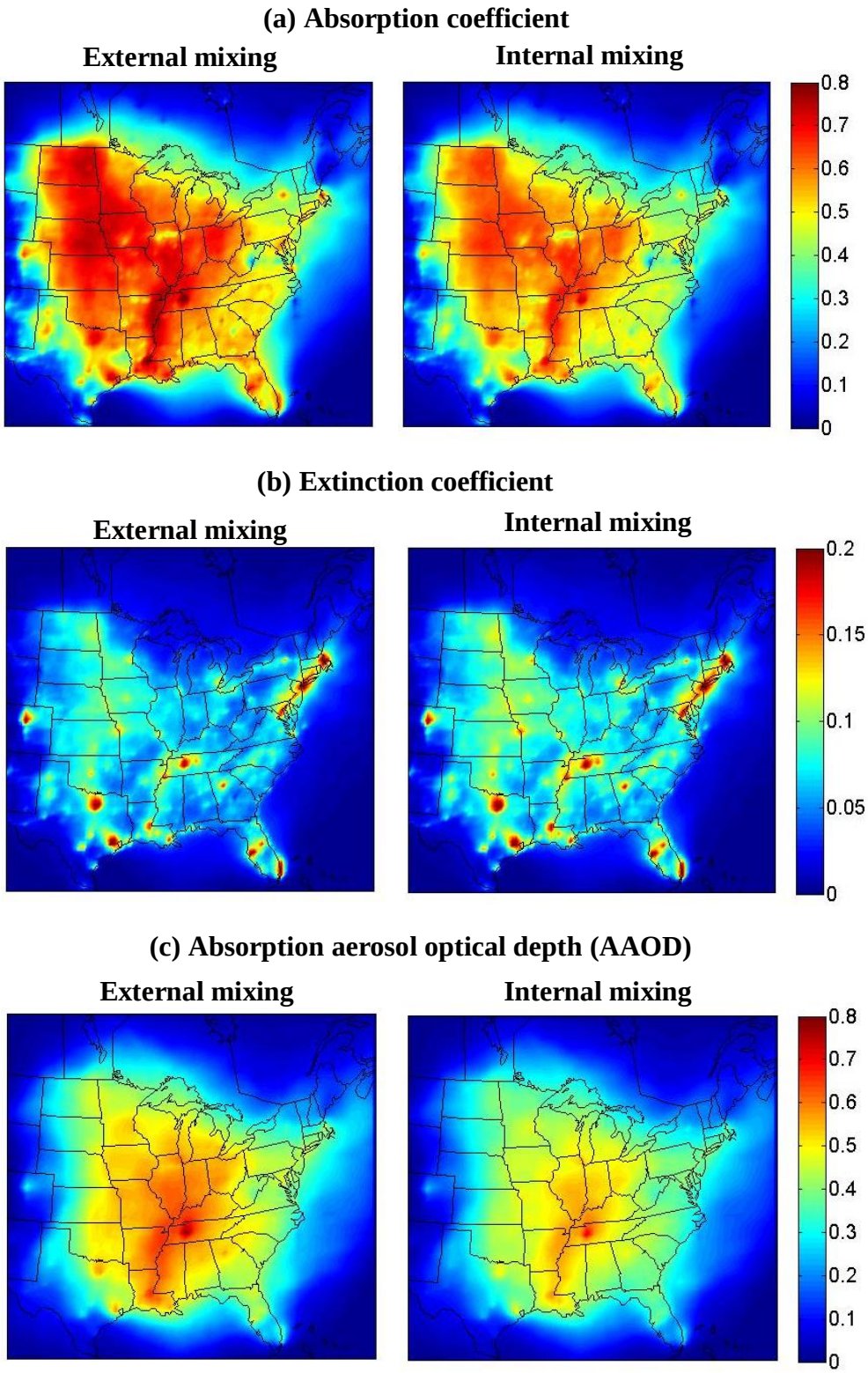

Figure 3.12. Predicted fractional changes to the (a) absorption coefficient, (b) extinction coefficient, and (c) absorption aerosol optical depth (AAOD) for the July 2001 double diesel simulation.

3.6.2 Scenario I: Half diesel emissions

The average fractional reduction of the absorption coefficient is, assuming external mixing, 30% and, assuming internal mixing, 27%. These changes correspond to the changes in $PM_{2.5}$ BC concentrations. The largest changes in absorption coefficient are in the Midwest where non-road diesel emissions are the dominant source (Figure 3.11). Since scattering aerosol dominates the overall extinction during this time period and there is little change in scattering when a major absorbing source is reduced, the average fractional reduction of the extinction coefficients for the half diesel simulation is only 2% for the external mixing assumption and 3% assuming internal mixing. The calculated change in AOD is only 1% for both external and internal mixing assumptions. The average AAOD reduction due to the half diesel perturbation is 16% and 15% for external and internal mixing assumptions, respectively.

3.6.3 Scenario II: Double diesel emissions

The average fractional increase of the calculated absorption coefficient due to the double diesel perturbation for the Eastern U.S. subdomain during this July 2001 simulation period is, assuming external mixing, 60% and, assuming internal mixing, 52%. The largest changes in absorption coefficient are also in the Midwest (Figure 3.12). The average fractional increase of the extinction coefficients is only 5% and 6% using external and internal mixing assumptions, respectively and 2% for AOD. The average AAOD increase due to the double diesel perturbation is 32% and 28% for the external and internal mixing assumptions, respectively. The

magnitudes of these domain-averaged fractional changes in the absorption coefficient, extinction coefficient, and AAOD for this period due to the doubled emissions are approximately twice as large (in absolute terms) as the changes due to the 50% reduction of the diesel emissions.

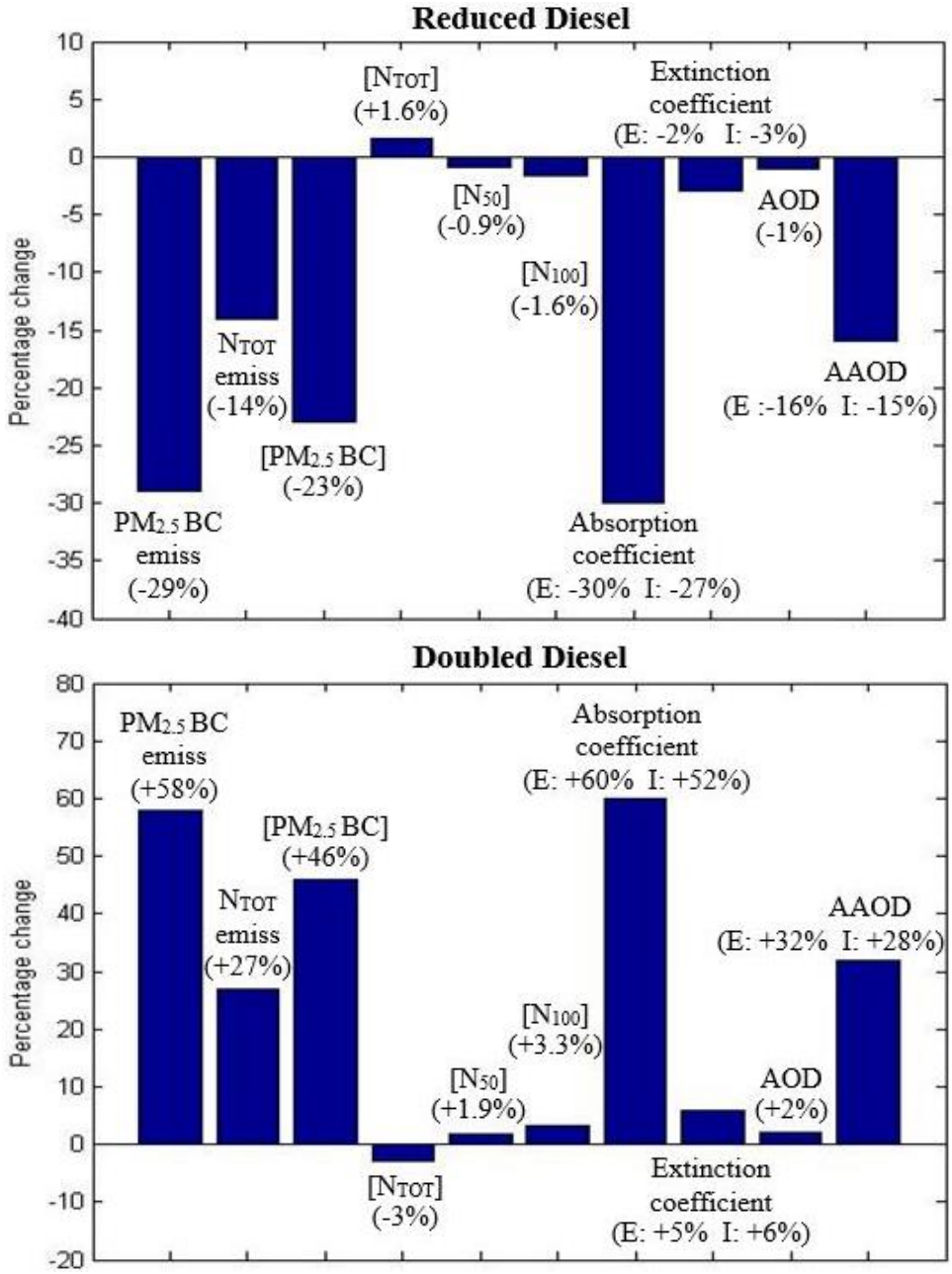

Figure 3.13. Summary of calculated changes to emissions, concentrations and aerosol optical properties for the reduced and doubled diesel cases.

3.7 Conclusions

The three-dimensional CTM PMCAMx-UF was used to simulate a summer period base case as well as two simple diesel emission change scenarios: (a) half and (b) double the diesel particulate emissions as compared to the base emissions. Simulation-averaged changes to aerosol emissions, concentrations, and optical properties are shown in Figure 3.13.

Reduction of the diesel PM emissions by 50% resulted in an increase of the total particle number concentrations on average by 1.6% due to a decrease in the coagulation and condensation sinks. At the same time a 1.6% decrease in N_{100} particle concentrations was predicted. Both changes are significantly different from those expected assuming a proportional change. The same scenario resulted in a 23% decrease in domain-averaged $PM_{2.5}$ BC concentrations and similar changes both in magnitude and spatial pattern for the absorption coefficient (27-30%) and AAOD (28-32%). These results suggest that mitigation of large diesel particles and/or particle mass emissions will reduce absorption climate-relevant properties related to black carbon and have health benefits; however the changes could also have the unintended effect of increased ultrafine particle number concentrations. The changes in CCN will be significantly less than expected assuming a proportional reduction during this photochemically active period.

The double diesel simulation resulted in a domain-average 3% decrease in total particle number concentrations and a 3.3% increase in N_{100} concentrations. The domain-averaged $PM_{2.5}$ BC concentration increased by 46%, and, similarly changes (52-60%) were predicted for the absorption coefficient. AAOD for the

double diesel perturbation increased by 28-32%. Extinction coefficients for both perturbation simulations changed by only a few percent due to the dominance of scattering aerosols in the Eastern U.S. These changes suggest that increased particle mass emissions from diesel sources increase climate-relevant effects related to black carbon and negatively affect health, but the changes may reduce ultrafine particle number concentrations.

3.8 References

Ban-Weiss, G.A., McLaughlin, J.P., Harley, R.A., Lunden, M.M., Kirchstetter, T.W., Kean, A.J., Strawa, A.W., Stevenson, E.D., Kendall, G.R., 2008. Long-term changes in emissions of nitrogen oxides and particulate matter from on-road gasoline and diesel vehicles. Atmos. Environ. 42, 220-232.

Bauer, S.E., Menon, S., Koch, D., Bond, T.C., Tsigaridis, K., 2010. A global modeling study on carbonaceous aerosol microphysical characteristics and radiative effects. Atmos. Chem. Phys. 10, 7439-7456.

Bohren, C.F., Huffman, D.R., 1998. Absorption and scattering of light by small particles. Wiley, New York, NY.

Bond, T.C., Doherty, S.J., Fahey, D.W., Forster, P.M., Bernsten, T., DeAngelo, B.J., Flanner, M.G., Ghan, S., Kärcher, B., Koch, D., Kinne, S., Kondo, Y., Quinn, P.K., Sarofim, M.C., Schultz, M.G., Schulz, M., Venkataraman, C., Zhang, H., Zhang, S., Bellouin, N., Guttikunda, S.K., Hopke, P.K., Jacobson, M.Z., Kaiser, J.W., Klimont, Z., Lohmann, U., Schwarz, J.P., Shindell, D., Storelvmo, T., Warren, S.G., Zender, C.S., 2013. Bounding the role of black carbon in the climate system: a scientific assessment. J. Geophys. Res. 118, 5380-5552.

California Air Resources Board (CARB), 2010. Drayage truck regulation. Sacramento, CA. http://www.arb.ca.gov/msprog/onroad/porttruck/finalregdrayage.pdf

Chen, W.-T., Lee, Y.H., Adams, P.J., Nenes, A., Seinfeld, J.H., 2010. Will black carbon mitigation dampen aerosol indirect forcing? Geophys. Res. Lett. 37, L09801.

Dallmann, T.R., Harley, R.A., Kirchstetter, T.W., 2011. Effects of diesel particle filter retrofits and accelerated fleet turnover on drayage truck emissions at the Port of Oakland. Environ. Sci. Technol. 45, 10773-10779.

Gaydos, T.M., Pinder, R., Koo, B., Fahey, K.M., Yarwood, G., Pandis, S.N., 2007. Development and application of a three-dimensional aerosol chemical transport model, PMCAMx. Atmos. Environ. 41, 2594-2611.

Herner, J.D., Hu, S., Robertson, W.H., Huai, T., Chang, M.-C.O., Rieger, P., Ayala, A., 2011. Effect of advanced aftertreatment for PM and NO_x reduction on heavy-duty diesel engine ultrafine particle emissions. Environ. Sci. Technol. 45, 2413-2419.

IPCC, 2013. Climate change 2013: the physical science basis. Contribution of Working Group I to the Fifth Assessment Report of the Intergovernmental Panel on Climate Change. Cambridge University Press, New York, NY.

Janssen, N.A., Gerlofs-Nijland, M.E., Lanki, T., Salonen, R.O., Cassee, F., Hoek, G., Fischer, P., Brunekreef, B., Krzyzanowski, 2012. Health effects of black carbon. Report prepared by the World Health Organization. Copenhagen, Denmark.

Kozawa, K.H., Park, S.S., Mara, S.L., Herner, J.D., 2014. Verifying emission reductions from heavy-duty diesel trucks operating on Southern California freeways. Environ. Sci. Technol. 48, 1475-1483.

Lane, T.E., Pinder, R.W., Shrivastava, M., Robinson, A.L., Pandis, S.N., 2007. Source contributions to primary organic aerosol: comparison of the results of a source-resolved model and the chemical mass balance approach. Atmos. Environ. 41, 3758-3776.

Lelieveld, J., Barlas, C., Giannadaki, D., Pozzer, A., 2013. Model calculated global, regional and megacity premature mortality due to air pollution. Atmos. Chem. Phys. 13, 7023-7037.

Mathis, U., Kaegi, R., Mohr, M., Zenobi, R., 2004. TEM Analysis of volatile nanoparticles from particle trap equipped diesel and direct-injection spark-ignition vehicles. Atmos. Environ. 38, 4347-4355.

Murphy, B.N., Pandis, S.N., 2010. Exploring summertime organic aerosol formation in the Eastern United States using a regional-scale budget approach and ambient measurements. J. Geophys. Res. 115, D24216.

Napari, I., Noppel, M., Vehkamäki, H., Kulmala, M., 2002. Parameterization of ternary nucleation rates for H_2SO_4-NH_3-H_2O vapors. J. Geophys. Res. 107, 4381-4386.

Pierce, J.R., Adams, P.J., 2009. Uncertainty in global CCN concentrations from uncertain aerosol nucleation and primary emission rates. Atmos. Chem. Phys. 9, 1339-1356.

Posner, L.N., Pandis, S.N., 2015. Sources of ultrafine particles in the Eastern United States. Atmos. Environ. 111, 103-112.

Sakurai, H., Tobias, H.J., Park, K., Zarling, D., Docherty, K.S., Kittelson, D.B., McMurry, P.H., Ziemann, P.J., 2003. On-line measurements of diesel nanoparticle composition and volatility. Atmos. Environ. 37, 1199-1210.

Schmidt, C.W., 2011. Black carbon: the dark horse of climate change drivers. Environ. Health Perspect. 119(4), A172-A175.

Seigneur, C., 2009. Current understanding of ultrafine particulate matter emitted from mobile sources. J. Air Waste Manag. Assoc. 59:1, 3-17.

Shindell, D., Kuylenstierna, J.C.I., Vignati, E., van Dingenen, R., Amann, M., Kilimont, Z., Ananeberg, S.C., Muller, N., Janssens-Maenhout, G., Raes, F., Schwartz, J., Faluvegi, G., Pozzoli, L., Kupianen, K., Höglund-Isaksson,

L., Embers, L., Streets, D., Ramanathan, V., Hicks, K., Kim Oanh, N.T., Milly, G., Williams, M., Demkine, V., Fowler, D., 2012. Simultaneously mitigating near-term climate change and improving human health and food security. Science 335, 183-189.

Stanier, C.O., Khlystov, A.Y., Pandis, S.N., 2004. Ambient aerosol size distributions and number concentrations measured during the Pittsburgh Air Quality Study (PAQS). Atmos. Environ. 38, 3275-3284.

U.S. EPA, 2002. User Guide: Air Quality System. Report prepared by the U.S. Environmental Protection Agency, Research Triangle Park, NC.

U.S. EPA, 2009. Integrated science assessment for particulate matter (final report). Report prepared by the U.S. Environmental Protection Agency, Washington, DC. EPA/600/R-08/139F.

Vehkamäki, H., Kulmala, M., Napari, I., Lehtinen, K.E.J., Timmreck, C., Noppel, M., Laaksonen, A., 2002. An improved parameterization for sulfuric acid–water nucleation rates for tropospheric and stratospheric conditions. J. Geophys. Res. 107, 4622-4632.

Chapter 4. Simulation of fresh and chemically-aged biomass burning organic aerosol

4.1 Introduction

Atmospheric particles less than 2.5 μm in diameter ($PM_{2.5}$) have been linked to increased risk of cardiovascular disease and mortality (Pope et al., 2009; Lelieveld et al., 2013). Organic aerosol (OA) is a major $PM_{2.5}$ component, forming 20-70% of $PM_{2.5}$ (Zhang et al., 2007). OA is usually grouped into two categories: primary OA (POA, organic aerosol directly emitted into the atmosphere in the particle phase) and secondary OA (SOA, organic vapor emissions that condense in the particle phase after chemical oxidation). Most chemical transport models (CTMs) have treated POA as nonvolatile and nonreactive, but most POA components are semivolatile; they can evaporate and oxidize, forming SOA as they dilute and are transported in the atmosphere (Robinson et al., 2007). POA vapors and SOA products of the first generation of OA chemistry can even further oxidize (chemical aging) to form additional SOA products (Donahue et al., 2006).

Globally, biomass burning is a major source of OA emissions (Bond et al., 2004; Akagi et al., 2011) and volatile organic compounds (Yokelson et al., 2008). Biomass burning organic aerosol (bbOA) can contribute significantly to OA concentrations both locally and far downwind (Heilman et al., 2014). Most previous source apportionment modeling using CTMs have assumed that biomass burning POA is non-volatile (Tian et al., 2009; Burr and Zhang, 2011; Hu et al., 2014) and

inert. As these emissions are diluted, however, a significant fraction of the semivolatile biomass burning POA evaporates and is then oxidized in the gas phase to form SOA (Hennigan et al., 2011; May et al., 2015). Another challenge is that a lot of the VOC emissions during biomass burning have not been speciated. Some of these compounds are likely of intermediate volatility and therefore are good precursors of SOA (Karl et al., 2007; Warneke et al., 2011; Jathar et al., 2014).

Since OA is composed of thousands of compounds, most of them unknown, the volatility basis set (VBS) framework was developed to efficiently simulate semi-volatile POA, the formation of SOA, and chemical aging of semivolatile SOA and POA (Donahue et al., 2006). The VBS modeling framework groups organic compounds by their effective saturation concentrations in logarithmically-spaced bins spanning the range of atmospherically-relevant saturation concentrations (0.01 to 10^6 μg m^{-3} at 298 K). In Donahue et al. (2009), these organic compounds are divided into subclasses: low volatility organic compounds (LVOCs, effective saturation concentration C^* = 0.01 to 0.1 μg m^{-3}), semivolatile organic compounds (SVOCs, C^* = 1 to 100 μg m^{-3}), intermediate volatility organic compounds (IVOCs, C^* = 10^3 to 10^6 μg m^{-3}), and outside of the range of the VBS, volatile organic compounds (VOCs, $C^* \geq 10^6$ μg m^{-3}). Murphy and Pandis (2009) implemented the VBS framework for semivolatile POA (Shrivastava et al., 2008) and SOA (Lane et al., 2008) with updated SOA product yields (Murphy and Pandis, 2010) into the three-dimensional CTM PMCAMx-2008. The authors found that using the updated

OA framework led to a statistically-significant improvement in model-measurement agreement (Murphy and Pandis, 2009).

In this study, the three-dimensional CTM PMCAMx was used to simulate the emission and evolution of bbOA to determine the relative importance of the primary and secondary production pathways as well as the predicted contribution of bbOA to total OA concentrations in the continental U.S. PMCAMx simulates the evolution of semivolatile POA and the formation of SOA using the VBS framework (Donahue et al., 2006). A source-resolved emission inventory for the continental U.S. was used as input for PMCAMx to simulate three seasonally-representative months with significant biomass burning during 2008. Corresponding zero-out simulations were then performed to determine the predicted bbOA concentrations. To investigate the effects of the VBS treatment of bbOA emissions, the PMCAMx zero-out results were then compared to the results of a version of the three-dimensional CTM CAMx that considers POA to be non-volatile and non-reactive (ENVIRON, 2015).

4.2 PMCAMx description

PMCAMx simulates changes in pollutant concentrations due to advection, dispersion, emission, wet and dry deposition, gas-phase and aqueous-phase chemistry, and aerosol processes (nucleation, coagulation, condensation, and evaporation). The model tracks gas concentrations as well as eight particle size sections ranging in diameter from 40 nm to 10 μm plus two additional size bins with largest diameters at 20 and 40 μm to represent cloud droplets.

The major difference between the version of the model used in this study and the one used by Murphy et al. (2010) is the gas-phase chemistry mechanism: Carbon Bond 5 (CB05) (Yarwood et al., 2005; ENVIRON, 2015) for this study and SAPRC-99 (Carter, 2000) for the previous work. This change was necessary due to the availability of the corresponding CB05-compatible inventories. CB05 includes 190 reactions of 135 species (79 gas phase species, 13 radical species, and 43 aerosol species).

In this study, PMCAMx is used to simulate the atmosphere over the continental U.S., southern Canada, and northern Mexico. This domain has an area of 5328 x 4032 km, split into 148 (north-south) and 112 (east-west) grid cells that are each 36 x 36 km. PMCAMx also simulates 25 vertical layers above the surface up to 19 km. Results reported in this study are for the surface level, only. Three month-long periods (April, July, and September 2008) are simulated in this study. The results of the first two days of each simulation (the first and second of each month) were discarded as model spin-up.

4.2.1 Updated plume rise algorithm

In the plume rise routine of previous versions of PMCAMx, a final plume rise height for a given point source was calculated internally based on the conditions of stability of the atmospheric layers above the stack and the larger of momentum and buoyancy fluxes (ENVIRON, 2015). All of the emissions were then injected into the single layer that contained the final plume rise height. In this version of PMCAMx, the plume is added to multiple cells depending on atmospheric

conditions. Each computational cell receives a fraction of the total emissions based on the layer's average pressure. Details of the algorithm can be found in ENVIRON (2010).

4.2.2 Representation of organic aerosol

Based on Murphy and Pandis (2010), the following OA components are simulated explicitly in PMCAMx: fresh POA, SOA originating from semivolatile and intermediate-volatility organic compounds (SOA-sv+SOA-iv), SOA from anthropogenic volatile organic compounds (aSOA-v), SOA from biogenic volatile organic compounds (bSOA-v), and long-range transport OA (lrtOA). The terminology used for the OA components is based on the naming framework of Murphy et al. (2014). The model distinguishes aSOA-v and bSOA-v by the typical nature of their volatile organic carbon (VOC) precursors: anthropogenic (e.g., toluene, high-volatility alkanes, and alkenes) and biogenic (e.g., isoprene, α-pinene, terpinene, and β-caryophyllene). As Murphy et al. (2014) notes, biomass burning includes natural wildfires, prescribed burning practices, and agricultural burning, so biomass burning SOA from VOC precursors is often difficult to classify as anthropogenic or biogenic. We refer to biomass burning SOA formed from anthropogenic VOCs as "anthropogenic" for the remainder of this study.

The fresh POA and the SOA-sv+SOA-iv are each represented by eight logarithmically-spaced volatility bins with effective saturation concentrations ranging from 0.1 to 10^6 μg m^{-3} at 298 K. aSOA-v and bSOA-v are represented by five logarithmically-spaced volatility bins with effective saturation concentrations

ranging from 0.1 to 10^3 μg m^{-3}. The lrtOA is assumed to be nonvolatile and nonreactive OA that has been heavily oxidized before transport into the model domain. As in Murphy and Pandis (2010), PMCAMx uses the yields of Hildebrandt et al. (2009) for SOA-v formation and ages only anthropogenic POA and SOA with an OH reaction rate of 10×10^{-12} cm^3 $molecule^{-1}$ s^{-1}. Biogenic SOA aging is assumed to have a small effect on absolute SOA concentration and is not explicitly simulated (Murphy and Pandis, 2010).

4.2.3 Boundary and initial conditions

The boundary conditions are based on the corresponding predictions of the MOZART global CTM (Emmons et al., 2010) and are updated daily. The MOZART data were interpolated to become compatible with the PMCAMx grid structure (ENVIRON, 2013). The initial conditions are based on output from an annual CAMx simulation for the same domain (ENVIRON, 2013). For the top of the domain, near-zero concentrations are assumed for all pollutants.

4.2.4 Meteorological and other related inputs

Meteorological inputs were generated using the Weather Research and Forecast Model (WRF) version 3.3.1 (NCAR, 2012). A detailed description and evaluation of the meteorological input data can be found in ENVIRON (2012). Land use data are based on the U.S. Geological Survey Geographic Information Retrieval and Analysis System (USGS GIRAS) database. The photolysis rate input

files were generated using NCAR's Tropospheric Ultraviolet and Visible (TUV) radiation model.

Table 4.1. Volatility distribution of PMCAMx OA emissions at 298 K.

C_i^* volatility bin (µg m^{-3})	Mass fraction of original non-volatile POA emission rate[a]	Volatility basis set organic compound group
10^{-1}	0.09	Low volatility (LVOC)
1	0.09	Semivolatile (SVOC)
10	0.14	
10^2	0.18	
10^3	0.3	Intermediate volatility (IVOC)
10^4	0.2	
	0.2	
10^5	0.5	
10^6	0.8	

[a] The mass fraction column sums to 2.5 times the original non-volatile POA emission rate due to the additional 1.5 times POA mass emissions added to represent IVOCs.

4.2.5 Volatility- and size-resolved emissions

The base case inventory includes emissions from biomass burning and all other sources (ENVIRON, 2013). Biomass burning emissions are source-resolved for agricultural burning, prescribed burning, and wildfires. The other emissions sources include on-road and off-road mobile sources, agricultural ammonia, biogenic sources, dust, lightning, oil and gas combustion, sea spray, marine vessel emissions, and emissions (area, mobile, and point sources) from Mexico and Canada.

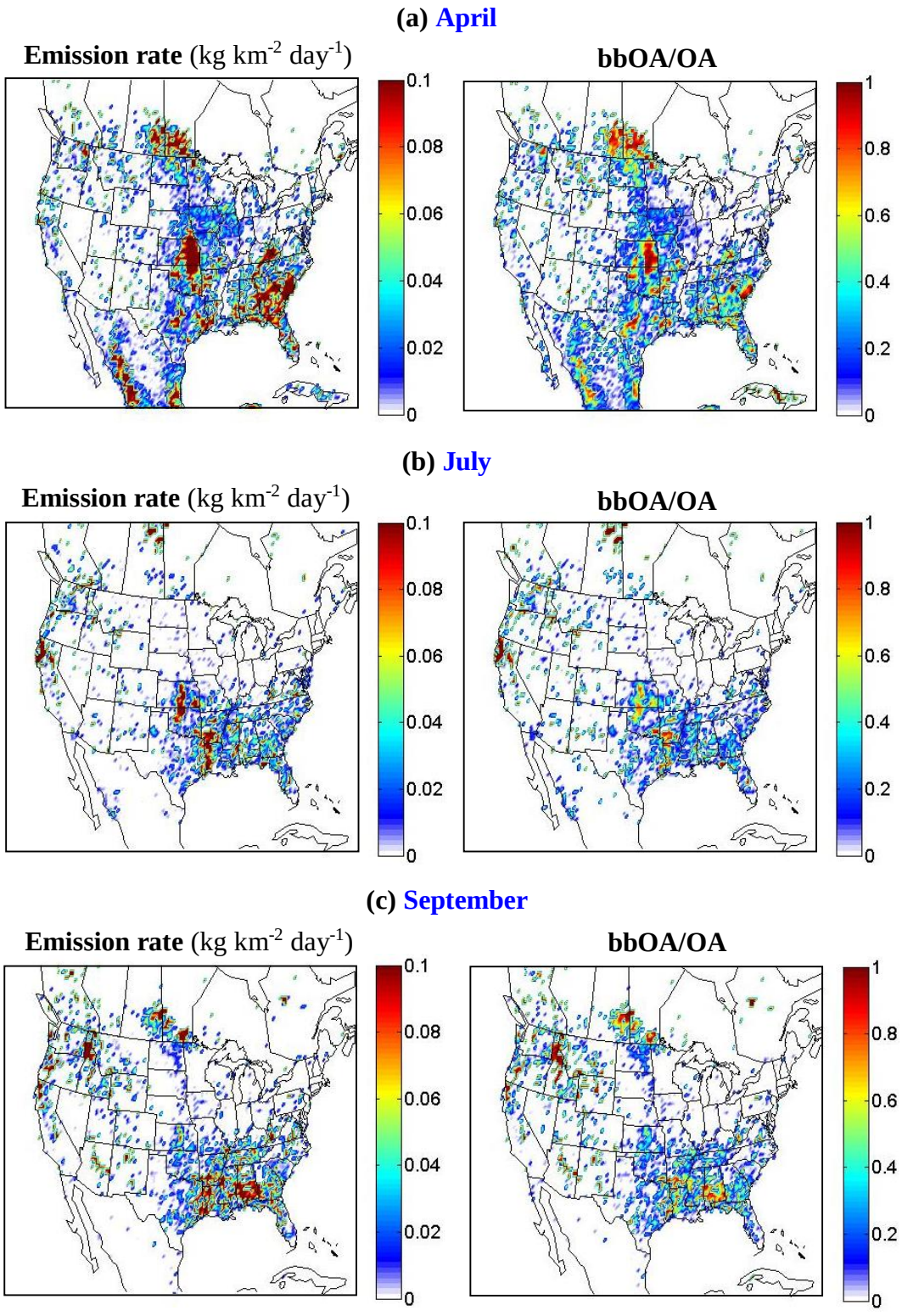

Figure 4.1. PMCAMx average $PM_{2.5}$ bbOA ($C^* \leq 100$ μg m^{-3}) emission rates (kg km^{-2} day^{-1}) and fractional contributions of bbOA to total OA emissions for (a) April, (b) July, and (c) September 2008.

We follow the approach of Murphy and Pandis (2010) to produce size- and volatility-resolved emissions from the original inventory. For each $PM_{2.5}$ aerosol species, we split the original inventory's $PM_{2.5}$ aerosol mass emission rates evenly between the six $PM_{2.5}$ size bins in PMCAMx. Though this is clearly a zeroth order approximation, the predicted $PM_{2.5}$ concentrations are not sensitive to this assumption. Coarse crustal material emission rates were split evenly between the two modeled $PM_{2.5\text{-}10}$ size bins.

The original POA emission rates are divided into volatility bins (C^* = 0.1 to 10^6 μg m^{-3}) based on the volatility distribution of Robinson et al. (2007) (Table 4.1). An additional 1.5 times the original non-volatile POA emission rate was added to represent IVOC (C^* = 10^4 to 10^6 μg m^{-3}) emissions. Maps of the average daily emission rates of fresh $PM_{2.5}$ bbOA ($C^* \leq 100$ μg m^{-3}) and bbOA contributions to OA emissions from all sources for the months of April, July, and September 2008 are shown in Figure 4.1.

The domain-averaged bbOA emission rate (0.03 kg km^{-2} day^{-1} for compounds with $C^* \leq 100$ μg m^{-3}) for *April* is 19% from agricultural burning (with high values located in the middle of the domain, including the Midwest farming region), 47% prescribed burning (mostly in the Southeast), and 34% wildfires (significant emissions in Mexico and Canada). In the summer months, hotter and drier conditions lead to more wildfires. The domain-averaged *July* bbOA emission rate (0.11 kg km^{-2} day^{-1}) is 1% agricultural burning (with highest emissions in Kansas and Oklahoma), 3% prescribed burning (over most of the Southeast with high values over Louisiana), and 96% wildfires (high emissions in Northern

California and Canada). The domain-averaged July emissions are dominated by wildfires in specific locations. The domain-averaged *September* (0.04 kg km^{-2} day^{-1}) bbOA emissions are composed of: 5% agricultural burning (mostly in Southwestern Canada, Northwestern Oregon, but also in California and the Southwest), 22% prescribed burning (highest values in the Southeast and the Northwest), and 73% wildfires (scattered throughout the domain).

Biomass burning emissions are important for all three periods examined. They represent 25% of the total OA emissions in April, 65% during July, and 37% in September. Though their relative importance to OA emissions varies from area to area (Figure 4.1), biomass burning emissions are an important OA source in the Southeast U.S. for all periods examined.

4.3 Predicted OA concentrations

4.3.1 Simulation-averaged OA concentrations

The base case simulation includes emissions from all sources. Maps of the average predicted total $PM_{2.5}$ OA concentrations for each simulation period are shown in Figure 4.2. Domain-averaged OA concentrations are: 0.98 μg m^{-3} in April, 2.36 μg m^{-3} in July, and 2.07 μg m^{-3} in September, 2008.

In *April*, the domain-averaged OA is composed of 32% SOA from SVOCs and IVOCs, 21% anthropogenic SOA, 20% biogenic SOA, 19% long-range transport OA, and 8% fresh POA. The importance of different OA sources locally varies throughout the domain. The OA concentration peaks in the Southeast U.S., Mexico, Cuba and Canada (Figure 4.2) mainly because of the higher biogenic SOA

levels in these areas. Some smaller peak concentrations of OA on the west coast are due to a combination of fresh POA and SOA from SVOCs and IVOCs. In general, most of the OA in this period is predicted to be secondary.

In *July*, the domain-averaged OA is 55% biogenic SOA, 22% SOA from SVOCs and IVOCs, 12% anthropogenic SOA, 7% fresh POA, and 4% long-range transport OA. Biogenic SOA is responsible for the high OA concentrations in the southeast US while fresh POA and SOA from SVOCs and IVOCs cause the high levels in Northern California.

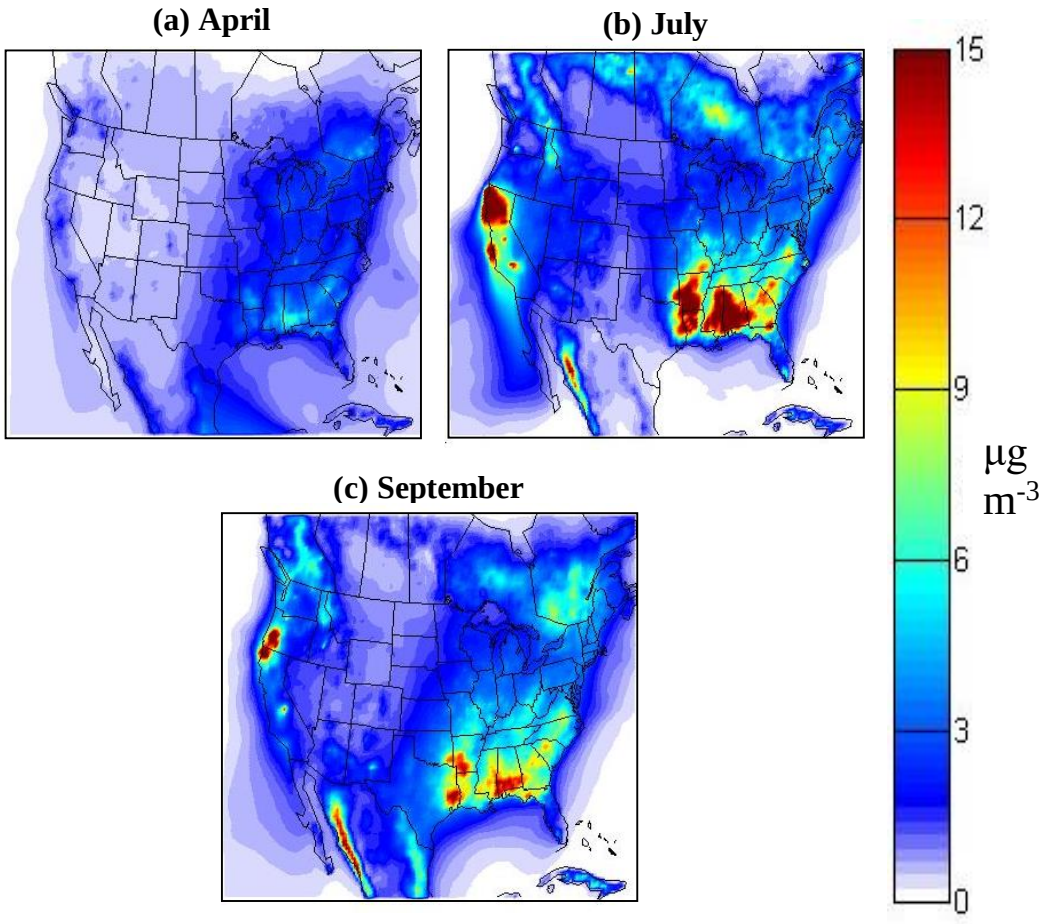

Figure 4.2. Predicted average PMCAMx $PM_{2.5}$ OA concentrations (μg m^{-3}) from all sources for (a) April, (b) July, and (c) September 2008.

In *September*, the domain-averaged OA is 53% biogenic SOA, 23% SOA from SVOCs and IVOCs, 16% anthropogenic SOA, 6% fresh POA, and 2% OA from long-range transport. The high OA concentrations on the west coast of the U.S. are due to fresh POA and SOA from SVOCs and IVOCs. As in other simulation months in this study, biogenic SOA dominates OA concentrations in the southeastern U.S.

4.3.2 Simulation-averaged biomass burning OA concentrations

The contribution of biomass burning to the total (primary and secondary) OA levels was calculated by performing additional simulations with zero biomass burning emissions and subtracting their results from the base case. All biomass burning emissions, gaseous and particulate, were zeroed. The difference of the two simulations is actually the change in concentrations if there was no biomass burning. Due to nonlinearities this is different from the actual current contribution of biomass burning to the OA concentrations.

Total bbOA is defined here as the sum of fresh biomass burning POA (bbPOA) and SOA originating from biomass burning emissions (bbSOA). This includes SOA from "anthropogenic" and biogenic VOCs, SOA from IVOCs (SOA-iv), and SOA from evaporated primary emissions (SOA-sv). Maps of bbOA concentrations and the fractional contributions of bbOA to total OA are shown in Figure 4.3.

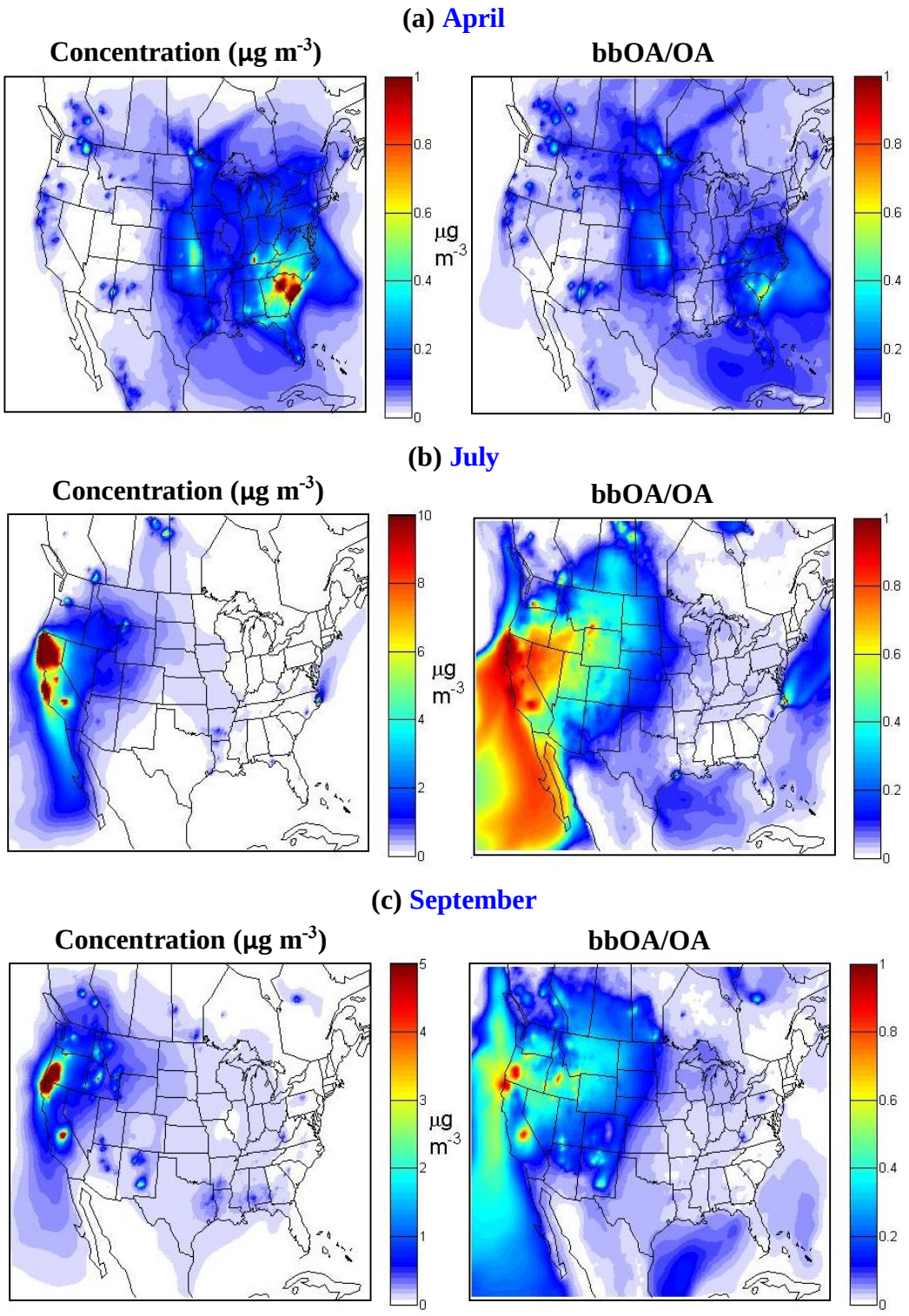

Figure 4.3. Predicted average PMCAMx $PM_{2.5}$ bbOA concentrations (μg m^{-3}) and fractional contributions of bbOA to total OA concentrations for (a) April, (b) July, and (c) September 2008. Different scales are used for each concentration plot.

The domain-averaged bbOA concentrations are: 0.07 μg m^{-3} during April, 0.49 μg m^{-3} in July, and 0.20 μg m^{-3} in September. Biomass burning is predicted to contribute 8% of the domain-averaged OA in April, 22% in July and 10% in September. Based on the emission inventories the high bbOA concentrations over the Carolinas and Georgia in *April* are dominated by prescribed burning emissions, while agricultural emissions contribute strongly to the bbOA concentrations over Topeka and Wichita, Kansas. The high bbOA concentrations over California and Saskatchewan in *July* are from major wildfires emissions in those areas. In *September*, wildfires and prescribed burning emissions contribute significantly to bbOA concentrations over Oregon and Northern California. Other moderately high bbOA concentrations for September in the Southwest and Southeast U.S. are mostly due to prescribed burning, while the moderately high values in Canada are due to agricultural burning and wildfires.

Maps of the contributions of fresh POA, SOA from SVOCs and IVOCs, SOA from "anthropogenic" VOCs, and SOA from biogenic VOCs to bbOA concentrations for April, July, and September, 2008 can be found in Figures 4.4, 4.5, and 4.6, respectively. Significant fresh POA is observed in areas immediately surrounding significant biomass burning locations for all simulated months, and the influence of SOA from SVOCs and IVOCs on bbOA concentrations extends out from the significant biomass burning sources even further than fresh POA.

In *April*, agricultural fires in the Midwest and southern Canada, prescribed burning in the Southeast and West coast, and wildfires in Mexico cause peaks in the fresh POA concentrations (Figure 4.4). In *July*, higher temperatures and drier

conditions lead to significant wildfire events in northern California and Canada with peaks in the fresh POA and SOA from SVOCs and IVOCs in those areas. In *September*, prescribed burning events in the west and Southeast contribute to peaks in fresh POA and SOA from SVOCs and IVOCs. There are also a few agricultural burning events in Canada that lead to peaks in fresh POA, but these do not contribute as greatly to SOA. Part of the biogenic and "anthropogenic" bbSOA predicted is due to increased partitioning of the corresponding SOA components from non-biomass burning sources to the particulate phase due to the increased OA concentrations.

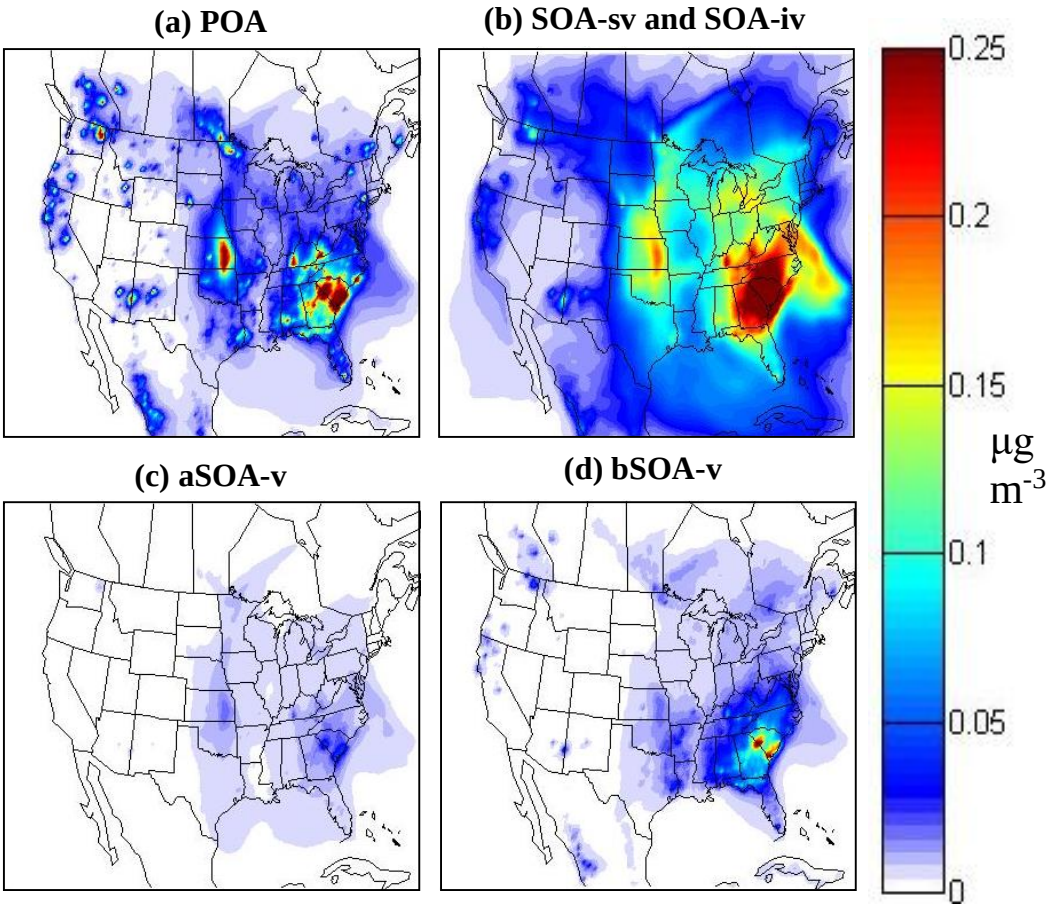

Figure 4.4. Predicted April 2008 bbOA concentrations (μg m^{-3}) from (a) fresh POA, (b) SOA from intermediate volatility and semivolatile precursors, (c) SOA from "anthropogenic" VOCs, and (d) SOA from biogenic VOCs.

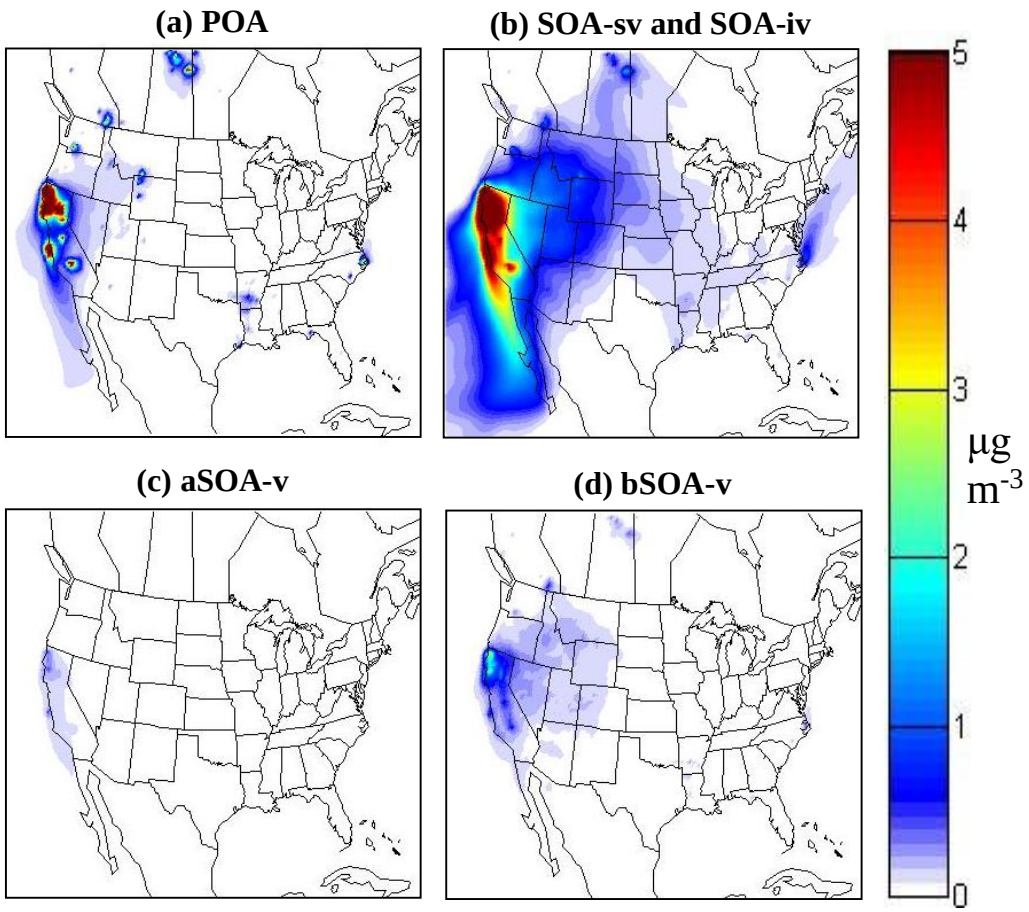

Figure 4.5. Predicted July 2008 bbOA concentrations (μg m^{-3}) from (a) fresh POA, (b) SOA from intermediate volatility and semivolatile precursors, (c) SOA from "anthropogenic" VOCs, and (d) SOA from biogenic VOCs.

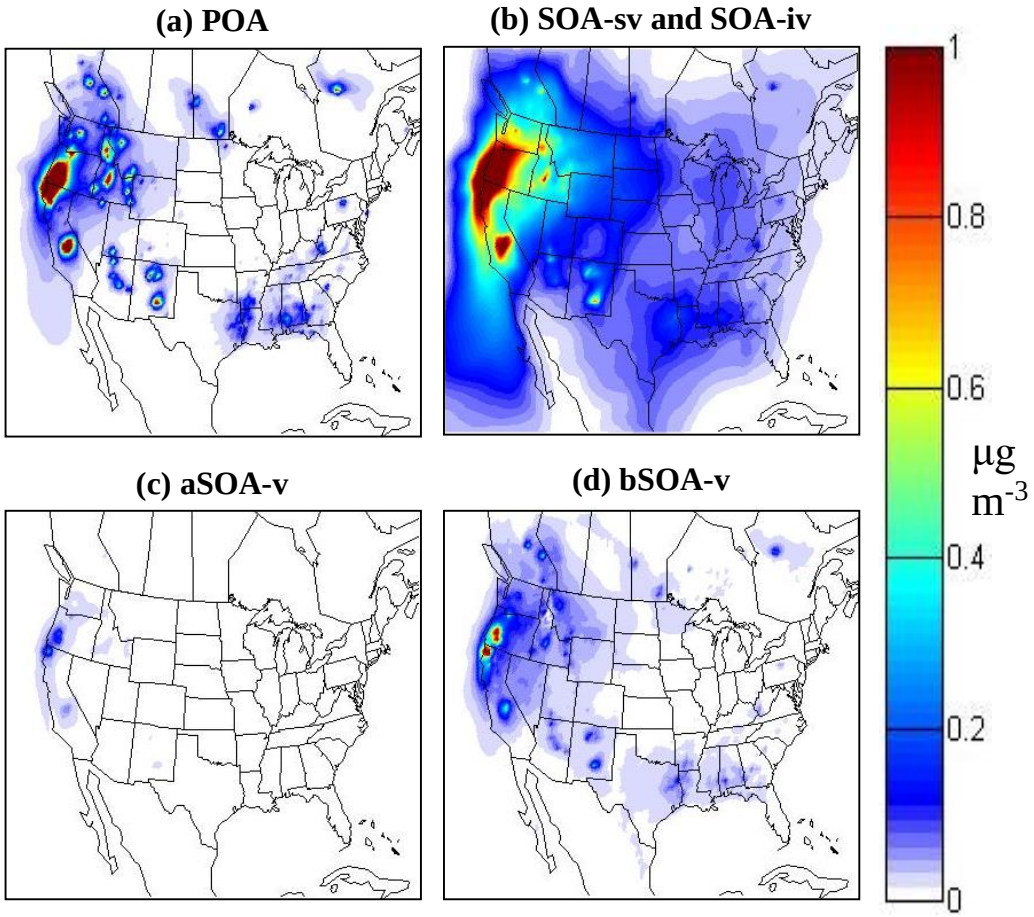

Figure 4.6. Predicted September 2008 bbOA concentrations (μg m^{-3}) from (a) fresh POA, (b) SOA from intermediate volatility and semivolatile precursors, (c) SOA from "anthropogenic" VOCs, and (d) SOA from biogenic VOCs.

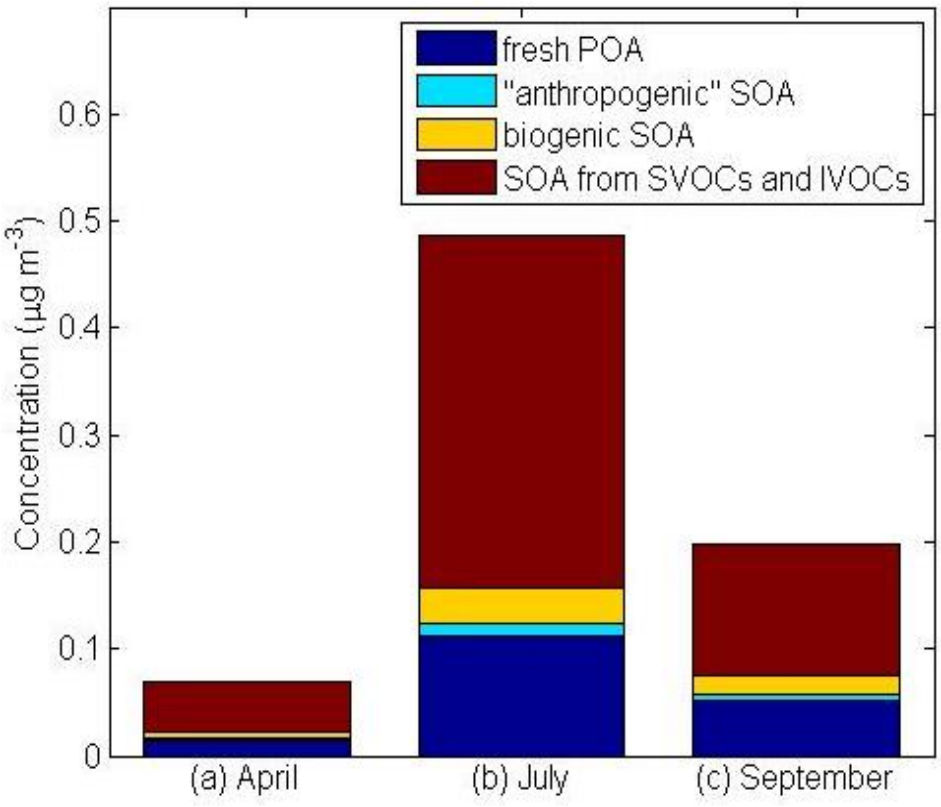

Figure 4.7. Domain-averaged contributions to $PM_{2.5}$ bbOA concentrations (μg m^{-3}) for (a) April, (b) July, and (c) September 2008.

Domain averages of the POA and SOA contributions to bbOA concentrations are shown in Figure 4.7. In April, 67% of bbOA is SOA from SVOCs and IVOCs, followed by 21% from fresh POA, 9% from biogenic SOA, and 4% from "anthropogenic" SOA. July has a very similar bbOA composition: 68% SOA from SVOCs and IVOCs, 23% from fresh POA, 7% biogenic SOA, and 2% "anthropogenic" SOA. In September, there is a slightly smaller contribution of SOA from SVOCs and IVOCs (62%), slightly more (27%) from fresh POA and biogenic SOA (9%), and 2% from anthropogenic SOA. Overall, SOA from SVOCs and IVOCs is predicted to be the largest contributor to bbOA concentrations for all months simulated, followed by fresh POA, biogenic SOA, and anthropogenic SOA.

4.3.3 Local and daily importance of bbOA concentrations

Though the domain-averaged bbOA contribution to OA concentrations is moderate, the influence of biomass burning on OA concentrations varies locally and is especially noticeable on days when there was significant biomass burning nearby. Time series of predicted bbOA and OA concentrations for Bartlesville, OK in April, Portland, OR in July, and Missoula, MO in September 2008 are shown in Figure 4.8. During *April* 2008 there was significant biomass burning near Bartlesville, OK and Winnipeg, Manitoba. Agricultural burning occurred near both cities during this time period, but Bartlesville was also near prescribed burning, and there was a wildfire near Winnipeg. The days with highest biomass burning impact had bbOA concentrations of 3.5 and 8.3 μg m^{-3}, respectively, composing 81% and 90% of OA concentrations at those times. In *July*, Portland, OR was near significant agricultural burning, and Redding, WA was near a wildfire. During the days of highest biomass burning impact, bbOA concentrations reached 4.8 and 58.1 μg m^{-3}, respectively, composing 52% and 96% of OA concentrations at those times. In *September*, Missoula, MO and Redding, WA were both affected by emissions from nearby wildfires and prescribed burning. Biomass burning emissions contribute 4.73 and 6.56 μg m^{-3}, respectively, which represented 64% and 76% of the OA at those times.

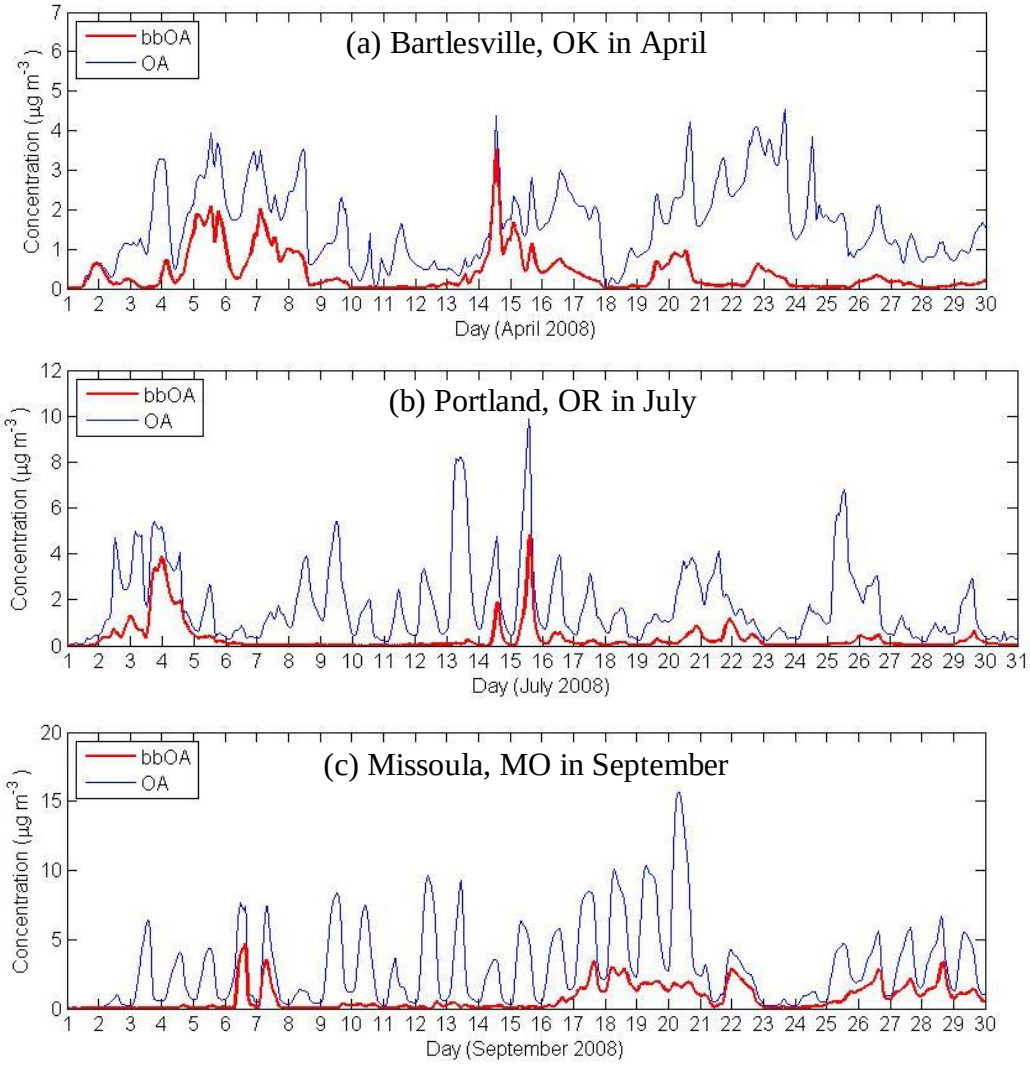

Figure 4.8. Time series of bbOA and OA concentrations (μg m^{-3}) for (a) Bartlesville, OK in April, (b) Portland, OR, in July, and (c), Missoula, MO in September 2008.

4.3.4 Sensitivity to the modeling treatment of bbOA

The above PMCAMx bbOA predictions were compared to those predicted by CAMx assuming that POA is nonvolatile and neglecting the formation of SOA from biomass burning. This comparison also serves as a study of the effects of using a VBS-based treatment of OA in a CTM compared to the traditional treatment of

the emissions of a combustion source like biomass burning. The bbOA predicted by CAMx was estimated using the Particulate Source Apportionment Technology (PSAT) algorithm (Yarwood et al., 2004). Maps of PMCAMx and CAMx predicted bbOA concentrations and the differences between these two models' predictions for the April 2008 simulation period are shown in Figure 4.9.

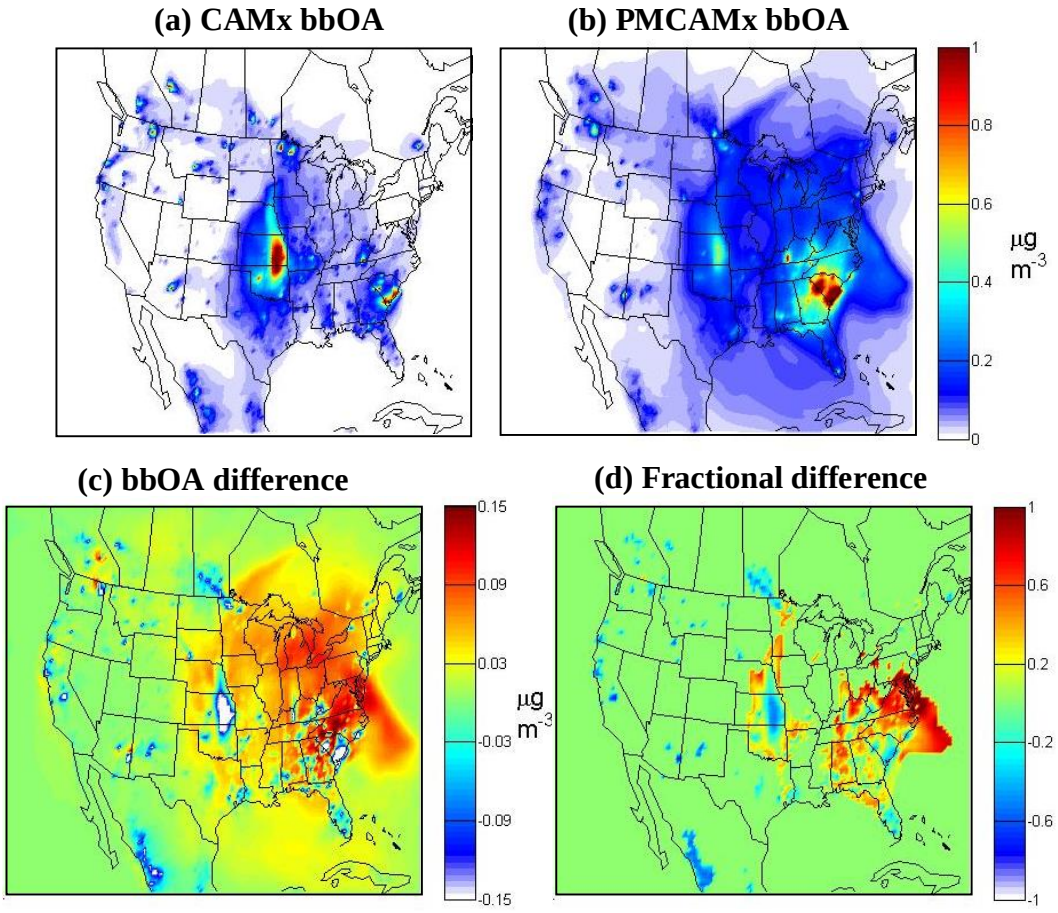

Figure 4.9. Predicted average April 2008 $PM_{2.5}$ bbOA concentrations (µg m^{-3}) (a) calculated by CAMx (non-volatile POA), (b) PMCAMx, (c) absolute difference between PMCAMx and CAMx bbOA (PMCAMx-CAMx), and (d) fractional difference between PMCAMx and CAMx bbOA ((PMCAMx-CAMx)/CAMx).

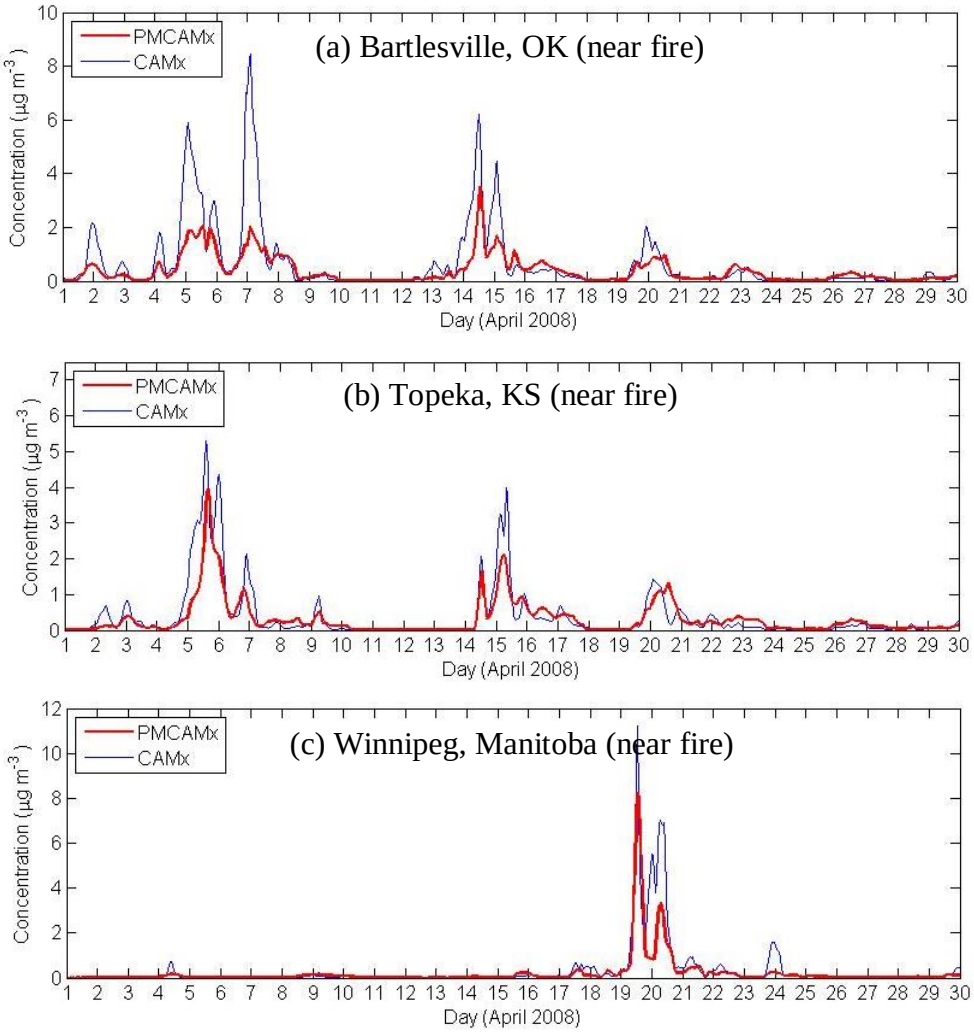

Figure 4.10. Time series of total (primary and secondary) bbOA concentrations calculated by PMCAMx and CAMx for (a) Bartlesville, OK, (b) Topeka, KS, and (c) Winnipeg, Manitoba. Fires were present very near these sites during the simulation period. Different scales are used in each graph.

PMCAMx bbOA concentration predictions are generally lower than CAMx predictions in areas close to significant biomass burning sources. Time series of the predicted concentrations of bbOA in three cities near significant fire activity during the April 2008 simulation period are shown in Figure 4.10. In these areas bbPOA evaporates due to dilution, and the time required for oxidation reactions to take

place causes the bbSOA concentrations to not increase quickly enough to balance the rate of evaporating bbPOA. On average, PMCAMx predicts 42% (0.27 μg m^{-3}) less bbOA than CAMx in Bartlesville, OK, 22% (0.08 μg m^{-3}) less in Topeka, KS, and 39% (0.12 μg m^{-3}) less in Winnipeg, Manitoba. PMCAMx predicts that 40-55% of the bbOA in these three cities is POA, whereas CAMx assumes 100% POA.

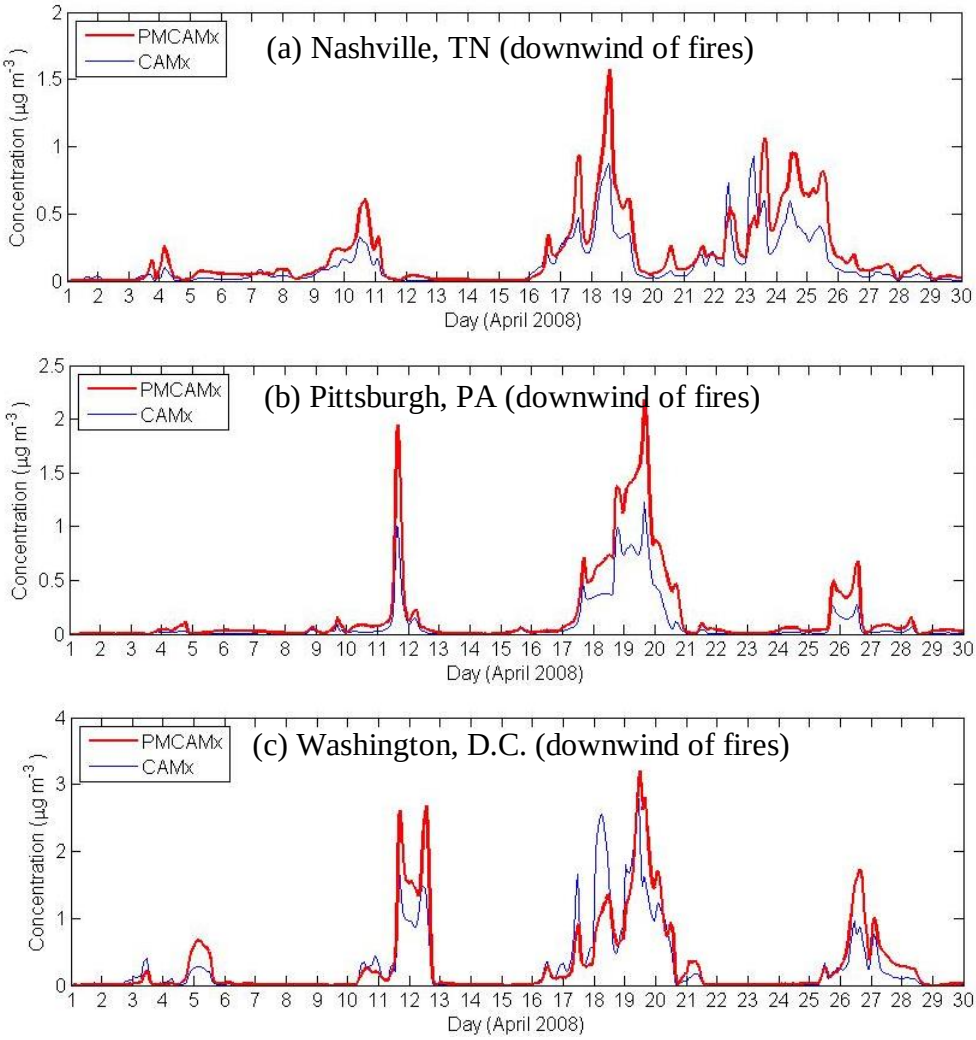

Figure 4.11. Time series of total (primary and secondary) bbOA concentrations calculated by PMCAMx and CAMx for (a) Nashville, TN, (b) Pittsburgh, PA, and (c) Washington, D.C. These sites were downwind of major fires during the simulation period. Different scales are used in each graph.

Downwind of the biomass burning sources, on the other hand, PMCAMx generally predicts higher bbOA concentrations than CAMx. Time series of the predicted concentrations of bbOA in three cities that were downwind of fires during the April 2008 simulation period are shown in Figure 4.11. In these areas, the bbSOA production overtakes the loss of bbPOA due to dilution/evaporation. On average, PMCAMx predicts 56% more bbOA than CAMx in Nashville, TN, 93% more in Pittsburgh, PA, and 17% more in Washington D.C. PMCAMx predicts that 12-20% of the bbOA in these three cities is POA, whereas CAMx assumes that 100% of the bbOA concentrations is POA.

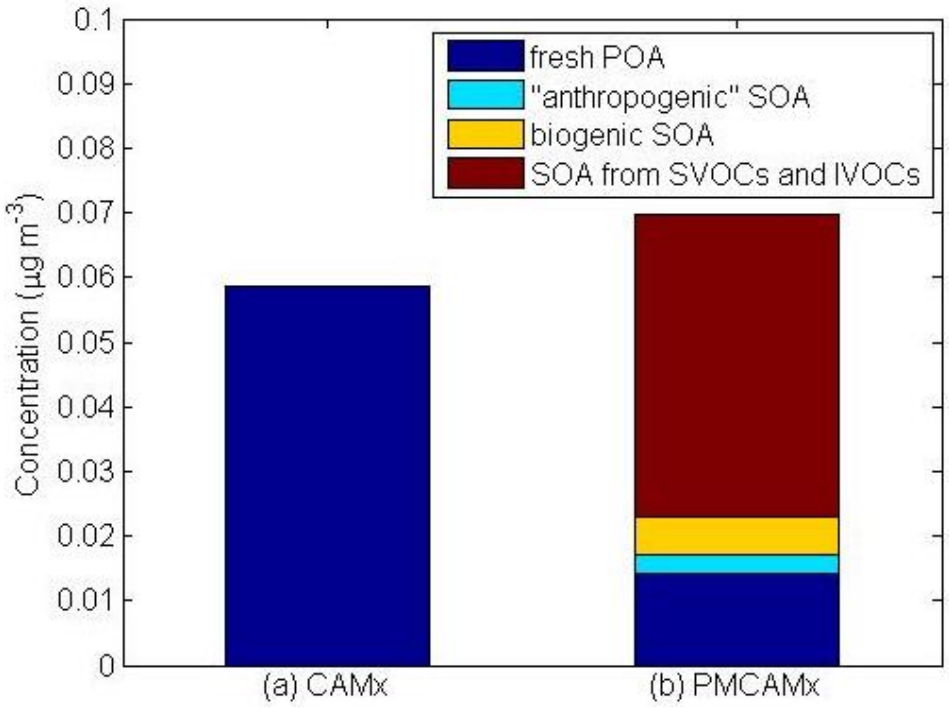

Figure 4.12. Comparison of domain-averaged contributions to April 2008 $PM_{2.5}$ bbOA concentrations (μg m^{-3}) determined by (a) CAMx (non-volatile POA) and (b) PMCAMx.

The domain-averaged bbOA concentration predictions (including the contributions of POA and SOA) of CAMx and PMCAMx are compared in Figure

4.12. The domain-averaged bbOA concentrations using the VBS treatment in PMCAMx are 20% higher than those using the traditional treatment in CAMx, and the predicted compositions are dramatically different. PMCAMx predicts that bbOA for this time period is composed of 21% fresh POA, 4% SOA from "anthropogenic" VOCs, 8% SOA from biogenic VOCs, and 67% SOA from SVOCs and IVOCs. On the other hand, CAMx assumes that all the bbOA is fresh primary.

4.4 Conclusions

The bbOA concentration results of three month-long simulation periods were investigated for the modeling year 2008 using the three-dimensional CTM PMCAMx. Domain-averaged bbOA contributions to OA concentrations from all sources are 8% for April, 22% for July, and 10% for September. The most significant bbOA contributions to OA concentrations for April over the domain are over the Eastern U.S. (with highest values over South Carolina) due to prescribed burning and Midwest (particularly Kansas) due to agricultural burning emissions. July 2008 bbOA concentrations are highest over the West Coast, with significant wildfire emissions during this time period coming from Northern California. Significant emissions from prescribed burning (mostly in Oregon) and wildfires (mostly in California) in September contribute largely to OA concentrations nearby.

The contribution of bbOA to OA concentrations varies locally throughout the domain. In April, the model predicts maximum bbOA concentrations at near-

fire locations (Bartlesville, OK and Winnipeg, Manitoba) of 3.5 and 8.3 μg m^{-3}, respectively. On the days of these maximum bbOA concentrations, bbOA composes a significant fraction (72-90%) of OA concentrations. In July, Portland, OR, and Redding, WA, experience days of maximum fire impact with bbOA concentrations of 4.8 and 58.1 μg m^{-3}, respectively, composing 52% and 96% of OA concentrations at those times. In September, Missoula, MO, and Redding, WA experience maximum bbOA concentrations of 4.7 and 6.6 μg m^{-3}, respectively, which composes 64% and 76% of the OA at those times.

The predicted domain-averaged bbOA concentration using the VBS approach (PMCAMx) is 20% higher than the prediction by the traditional approach assuming non-volatile POA and negligible SOA formation. The VBS approach predicts that 79% of this bbOA is secondary, whereas the traditional approach predicts that 100% of bbOA is primary. Near biomass burning emission sources, the VBS treatment predicts about 30% lower bbOA concentrations due to the evaporation of fresh POA and about 60% higher bbOA concentrations downwind of significant biomass burning emissions due to the production of secondary bbOA. Individual peak fire events can produce differences between the two model bbOA predictions of a factor of 3.

4.5 References

Akagi, S.K., Yokelson, R.J., Wiedinmyer, C., Alvarado, M.J., Reid, J.S., Karl, T., Crounse, J.D., Wennberg, W.O., 2011. Emission factors for open and domestic biomass burning for use in atmospheric models. Atmos. Chem. Phys. 11, 4039-4072.

Bond, T.C., Streets, D.G., Yarber, K.F., Nelson, S.M., Woo, J.-H., Klimont, Z., 2004. A technology-based global inventory of black and organic carbon emissions from combustion. J. Geophys. Res. 109, D14203.

Burr, M., Zhang, Y., 2011. Source apportionment of fine particulate matter over the Eastern U.S. Part I. Source sensitivity simulations using CMAQ with the brute force method. Atmos. Pollut. Res. 2, 300-317.

Carter, W.P.L., 2000. Programs and files implementing the SAPRC-99 mechanism and its associated emissions processing procedures for Models-3 and other regional models.

Donahue, N.M., Robison, A.L., Stanier, C.O., Pandis, S.N., 2006. Coupled partitioning, dilution, and chemical aging of semivolatile organics, Environ. Sci. Technol. 40, 2635-2643.

Donahue, N.M., Robinson, A.L., Pandis, S.N., 2009. Atmospheric organic particulate matter: from smoke to secondary organic aerosol. Atmos. Environ. 43, 94-106.

Emmons, L.K., Walter, S., Hess, P.G., Lamarque, J.-F., Pfister, G.G., Fillmore, D., Granier, C., Guenther, A., Kinnison, D., Laepple, T., Orlando, J., Tie, X., Tyndall, G., Wiedinmyer, C., Baughcum, S.L., Kloster, S., 2010. Description and evaluation of the Model for Ozone and Related Chemical Tracers, version 4 (MOZART-4). Geosci. Model Dev. 3, 43-67.

ENVIRON, 2010. Implementation of an alternative plume rise methodology in CAMx. Prepared by ENVIRON International Corporation, Novato, California.

ENVIRON, 2012. Western Regional Air Partnership (WRAP) West-wide Jump Start Air Quality Modeling Study (WestJumpAQMS) WRF application/evaluation. Prepared by ENVIRON International Corporation, Novato, California.

ENVIRON, 2013. Western Regional Air Partnership (WRAP) west-side jump start air quality modeling study (WestJumpAQMS) final modeling protocol. Prepared by ENVIRON International Corporation, Novato, California.

ENVIRON, 2015. User's guide to the comprehensive air quality model with extensions (CAMx), version 6.2. Prepared by ENVIRON International Corporation, Novato, California.

Heilman, W.E., Liu, Y., Urbanski, S., Kovalev, V., Mickler, R., 2014. Wildland fire emissions, carbon, and climate: plume rise, atmospheric transport, and chemistry processes. Forest Ecol. Manag. 31, 70-79.

Hennigan, C.J., Miracolo, M.A., Engelhart, G.J., May, A.A., Presto, AA., Lee, T., Sullivan, A.P., McMeeking, G.R., Coe, H., Wold, C.E., Hao, W.-M., Gilman, J.B., Kuster, W.C., de Gouw, J., Schichtel, B.A., Collet Jr., J.L., Kreidenweis, S.M., Robinson, A.L., 2011. Chemical and physical transformations of organic aerosol from the photo-oxidation of open biomass burning emissions in an environmental chamber. Atmos. Chem. Phys. 11, 7669-7686.

Jathar, S.H., Gordon, T.D., Hennigan, C.J., Pye, H.O.T., Pouliot, G., Adams, P.J., Donahue, N.M., Robinson, A.L., 2014. Unspeciated organic emissions from

combustion sources and their influence on the secondary organic aerosol budget in the United States. Proc. Natl. Acad. Sci. 111, 10473-10478.

Hildebrandt, L., Donahue, N.M., Pandis, S.N., 2009. High formation of secondary organic aerosol from the photo-oxidation of toluene. Atmos. Chem. Phys. 9, 2973-2986.

Hu, Y., Balachandran, S., Pachon, J.E., Baek, J., Ivey, C., Holmes, H., Odman, M.T., Mulholland, J.A., Russell, A.G., 2014. Fine particulate matter source apportionment using a hybrid chemical transport and receptor model approach. Atsmo. Chem. Phys. 14, 5415-5431.

Karl, T. G., Christian, T. J., Yokelson, R. J., Artaxo, P., Hao, W. M., and Guenther, A., 2007. The tropical forest and fire emissions experiment: method evaluation of volatile organic compound emissions measured by PTR-MS, FTIR, and GC from tropical biomass burning, Atmos. Chem. Phys. 7, 5883–5897.

Lane, T.E., Donahue, N.M., Pandis, S.N., 2008. Simulating secondary organic aerosol formation using the volatility basis-set approach in a chemical transport model. Atmos. Environ. 42, 7439-7451.

Lelieveld, J., Barlas, C., Giannadaki, D., Pozzer, A., 2013. Model calculated global, regional and megacity premature mortality due to air pollution. Atmos. Chem. Phys. 13, 7023-7037.

May, A.A., Lee, T., McMeeking, G.R., Akagi, S., Sullivan, A.P., Urbanski, S., Yokelson, R.J., Kreidenweis, S.M., 2015. Observations and analysis of organic aerosol evolution in some prescribed fire some plumes. Atmos. Chem. Phys. 15, 6323-6335.

Murphy B., Pandis S.N., 2009. Simulating the formation of semivolatile primary and secondary organic aerosol in a regional chemical transport model. Environ. Sci. Technol. 43, 4722–4728.

Murphy, B.N., Pandis, S.N., 2010. Exploring summertime organic aerosol formation in the Eastern United States using a regional-scale budget approach and ambient measurements. J. Geophys. Res. 115, D24216.

Murphy, B.N., Donahue, N.M., Robinson, A.L., Pandis, S.N., 2014. A naming convention for atmospheric organic aerosol. Atmos. Chem. Phys. 14, 5825-5839.

NCAR, 2012. ARW Version 3 modeling system user's guide. Prepared by the National Center for Atmospheric Research (NCAR), Boulder, Colorado.

Pope III, C. A., Burnett R.T., Krewski D., Jerrett M., Shi Y., Calle E. E., Thun M.J., 2009. Cardiovascular mortality and exposure to airborne fine particulate matter and cigarette smoke: Shape of the exposure-response relationship. Circulation 120, 941-948.

Robinson, A.L., Donahue, N.M., Shrivastava, M.K., Weitkamp, E.A., Sage, A.M., Grieshop, A.P., Lane, T.E., Pierce, J.R., Pandis, S.N., 2007. Rethinking organic aerosols: semivolatile emissions and photochemical aging. Science 315, 1259-1262.

Shrivastava, M.K., Lane, T.E., Donahue, N.M., Pandis, S.N., Robinson, A.L., 2008. Effects of gas particle partitioning and aging on primary emissions on urban and regional organic aerosol concentrations. J. Geophys. Res. 113, D18301.

Tian, D., Hu, Y., Wang, Y., Boylan, J.W., Zheng, M., Russell, A.G., 2009. Assessment of biomass burning emissions and their impacts on urban and regional $PM_{2.5}$: a Georgia case study. Environ. Sci. Technol. 43, 299-305.

Warneke, C., Roberts, J.M., Veres, P., Gilman, J., Kuster, W.C., Burling, I., Yokelson, R.J., and de Gouw, J.A., 2011. VOC identification and inter-comparison from laboratory biomass burning using PTR-MS and PIT-MS, Int. J. Mass Spectrom. Ion Proc. 303, 6–14.

Yarwood, G., R.E. Morris, G.M. Wilson., 2004. Particulate Matter Source Apportionment Technology (PSAT) in the CAMx Photochemical Grid Model. Proceedings of the 27th NATO/ CCMS International Technical Meeting on Air Pollution Modeling and Application. Springer Verlag.

Yarwood, G., Rao, S., Yocke, M., Whitten, G.Z., 2005. Updates to the Carbon bond chemical mechanism: CB05. Prepared by ENVIRON International Corporation, Novato, CA, Yocke & Company, Novato, CA, Smog Reyes, Point Reyes Station, CA.

Yokelson, R.J., Christian, T.J., Karl, T.G., Guenther, A., 2008. The tropical forest and fire emissions experiment: laboratory fire measurements and synthesis of campaign data. Atmos. Chem. Phys. 8, 3509-3527.

Zhang Q., Jimenez J.L., Canagaratna M.R., Allan J.D., Coe H., Ulbrich I., Alfarra M.R., Takami A., Middlebrook A.M., Sun Y.L., Dzepina K., Dunlea E., Docherty K., De-Carlo P.F., Salcedo D., Onasch T., Jayne J.T., Miyoshi T., Shimono A., Hatakeyama S., Takegawa N., Kondo Y., Schneider J., Drewnick F., Borrmann S., Weimer S., Demerjian K., Williams P., Bower K., Bahreini R., Cottrell L., Griffin R.J., Rautiainen J., Sun J.Y., Zhang Y.M., Worsnop D.R., 2007. Ubiquity and dominance of oxygenated species in organic aerosols in anthropogenically-influenced Northern Hemisphere midlatitudes. Geophys. Res. Lett. 34, L13801.

Chapter 5. Simulation of the plume-scale evolution of biomass burning organic aerosol

5.1 Introduction

Exposure to elevated levels of particulate matter less than 2.5 μm in diameter ($PM_{2.5}$) leads to increased risk of cardiovascular disease (Pope et al., 2009; Lelieveld et al., 2013). Particulate matter also reflects or absorbs sunlight, changing the energy balance of the earth (IPCC, 2013). Organic aerosol (OA) represents a significant portion of $PM_{2.5}$, averaging 20-70% (Zhang et al., 2007). OA is one of the most dynamic components of atmospheric PM: it evaporates, oxidizes, and condenses back to the particle phase with continuous changes in its concentration, chemical and physical properties. Investigation of the evolution of OA concentrations from major sources can improve our understanding of the role of the corresponding physical and chemical processes and inform mitigation efforts.

Globally, biomass burning is a major source of OA emissions (Akagi et al, 2011; Bond et al., 2013) and volatile organic compounds (VOCs) (Yokelson et al., 2008). Biomass burning organic aerosol (bbOA) can contribute significantly to OA concentrations at a local level both at the source and far downwind (Heilman et al., 2014). After emission, changes in bbOA concentrations depend on the relative balance between evaporation of fresh biomass burning primary organic aerosol (bbPOA) and the formation of biomass burning secondary organic aerosol (bbSOA) from the oxidation of semivolatile OA, intermediate volatility compounds (IVOCs)

and VOC precursors. Observed normalized (e.g., to CO) changes in the OA concentrations downwind of biomass burning emissions after several hours are highly variable (Cubison et al., 2011). In some biomass burning field studies, observed OA concentrations increase downwind of the fire (Yokelson et al., 2009; Singh et al., 2012), while in others, they decrease (Akagi et al., 2012; Jolleys et al., 2012, 2015) or do not change significantly (May et al., 2015). The evolution of bbOA is a significant gap in our understanding of the impact of biomass burning on both air quality and climate change (Heilman et al., 2014).

Several studies have investigated the theoretical plume-scale evolution of bbOA downwind of specific fires. May et al. (2015) modeled the OA measurements from several prescribed burns in South Carolina (May et al., 2014). The authors used the gas-particle partitioning equation (Donahue et al.., 2006; Robinson et al., 2010) to model the measured particulate bbOA emission factor (EF_{OA}) and total (gas plus particle) bbOA emission factor (EF_{TOT}) as a function of the concentration of OA (including background). For the specific biomass burning events studied, they found that there was no statistically-significant increase in OA concentrations downwind of the fire, suggesting that the evaporation of POA due to dilution dominated over the formation of SOA (May et al., 2015).

Alvarado et al. (2014) used a plume-scale Lagrangian transport model and the 1-D Volatility Basis Set (VBS) (Donahue et al., 2006) representation of OA to simulate a prescribed burn in California (Akagi et al., 2012). They varied a number of model parameters in order to reproduce the observed evolution of OA and ozone in the plume. From the results of these simulation cases, the authors developed a

set of reasonable revised parameters for the value of the OA aging rate (with OH), OH regeneration, split between fragmentation vs. functionalization, and ozone production.

In this study, we systematically investigate the conditions that could lead to variability of measured OA concentrations downwind of U.S. biomass burning emissions. The plume-scale model used is the 1-D Lagrangian transport model described in Murphy et al. (2011) that represents OA using the 1-D volatility basis set (VBS) (Donahue et al., 2006). This model is a one-dimensional version of PMCAMx, the CTM used in the previous chapters of this thesis. We develop a base case from real fire parameters and then perform a series of sensitivity tests of several parameters that affect OA concentrations: concentrations of OH, the aging rate constant, the dilution rate, and the volatility distribution of the initial plume OA. We then investigate these factors as to which could lead to a net increase, decrease, or little to no change in OA concentrations downwind of a biomass burning plume.

5.2 Lagrangian transport model

In this study, the one-dimensional Lagrangian transport model of Murphy et al. (2011) is used to track a parcel of air as it travels in space for a period of five simulation hours. This model is a 1-D version of the 3-D CTM PMCAMx. The modeled parcel is divided into 10 vertical layers up to a height of 2.5 km. Layer heights in this study are held constant for all simulations and are shown in Table 5.1. The model simulates gas-phase chemistry using the gas-phase SAPRC

chemical mechanism (Carter, 2000), dry and wet deposition, horizontal dilution, vertical dispersion, and primary gas and particulate emissions. Aerosol species with diameters from 40 nm to 10 μm are tracked using eight logarithmically-spaced size sections. Inorganic aerosol species include ammonium, sodium, nitrate, chloride, sulfuric acid, particulate water, black carbon, and crustal species.

Table 5.1. Constant plume conditions.

Layer number	Bottom height (m)	Top height (m)
1	0	55
2	55	135
3	135	240
4	240	370
5	370	540
6	540	750
7	750	1000
8	1000	1450
9	1450	1900
10	1900	2500

The model tracks four semivolatile OA components: (1) fresh POA (2) anthropogenic SOA from VOCs, (3) biogenic SOA from VOCs, (4) SOA from semivolatile and intermediate volatility organic compounds (SVOCs and IVOCs), and (5) long-range transport OA, which is considered nonvolatile due to the assumption that it has been heavily oxidized before entering the modeling domain. All semivolatile OA is represented by the 1-D Volatility Basis VBS framework (Donahue et al., 2006) with 12 logarithmically-spaced volatility bins of effective saturation concentrations (C^*) from 10^{-5} to 10^{6} μg m^{-3} (Murphy et al., 2011).

Table 5.2. Constant conditions for the base case and all scenarios.

Scenario	Condition	Value
Base case	OH concentration (molecule cm^{-3})	5.27×10^{6}
	Horizontal dilution rate (s^{-1})	0
	Aging rate (k_{OH}, cm^3 $molecule^{-1}$ s^{-1})	1×10^{-11}
	Vertical dispersion coefficient (K_{zz}, m/s)	5
	Plume injection layer	1
All scenarios	Relative humidity (%)	15.7
	Temperature (K)	298
	Pressure (mbar)	1013.25
	Wind speed (m/s)	2
	Photolysis rate (min^{-1})	0.42
	Emissions, cloud water, precipitable water, and cloud optical depth	0
	Land use code for surface roughness	Deciduous forest

5.3 Base case

5.3.1 Model inputs

The base case in this study is a simplified representation of a biomass burning plume in the U.S. Plume conditions that are assumed to remain constant are shown in Table 5.2. Standard temperature and pressure (298.15 K and 1013.25 hPa) are used in the base case. The relative humidity and background concentrations are from the reported values in Alvarado et al. (2014). A constant moderate OH level is assumed from average value given in Akagi et al. (2012). A low wind speed of 2 m s^{-1} is used, and horizontal dilution is neglected in the base case.

The initial plume concentration is injected only in the first layer of the model (up to a height of 55 m) in order to study vertical dispersion. Layers above

the surface height initially are at background concentrations. The initial plume OA concentration is taken from May et al. (2014) and adjusted to 298.15 K using the partitioning equation (Donahue et al., 2006) for this study to calculate the concentration of total (gas and particle) organic matter (C_{TOT} = 888 μg m^{-3}). C_{TOT} is then divided into volatility bins based on the volatility distribution of May et al. (2013). An additional 1.5 x C_{TOT} is added to the C^* = 10^4 to 10^6 μg m^{-3} volatility bins to represent IVOCs (Robinson et al., 2007). Initial plume concentrations of inorganic species from Alvarado et al. (2014) are divided evenly between the six modeled $PM_{2.5}$ size bins as in Murphy et al. (2011) and are shown in Table 5.3. Gas concentrations are shown in Table 5.4.

Table 5.3. Initial plume and background concentration of inorganic $PM_{2.5}$ (Alvarado et al., 2014).

Aerosol species	Initial plume concentration (μg m^{-3})	Background concentration (μg m^{-3})
Black carbon	187	0.357
Chloride	11.9	0
Ammonium	14.3	1.291
Nitrate	30.4	0.174
Sulfate	0.855	6.603

Table 5.4. Initial plume and background gas concentrations.

Gas species	Initial plume concentration (ppm)	Background concentration (ppm)
Carbon monoxide	$1.00 \times 10^{+1}$	1.29×10^{-1}
Carbon dioxide	1.00×10^{-6}	$3.90 \times 10^{+2}$
Nitric oxide	1.00×10^{-6}	1.50×10^{-5}
Nitrogen dioxide	1.00×10^{-6}	3.90×10^{-5}
Ozone	1.00×10^{-6}	5.00×10^{-2}
Hydrogen peroxide	1.00×10^{-6}	7.55×10^{-4}
Nitrous acid	1.00×10^{-6}	0
Sulfur dioxide	1.00×10^{-6}	1.20×10^{-4}
Nitric acid	1.00×10^{-6}	4.10×10^{-4}
Sulfuric acid (gaseous)	1.00×10^{-6}	0
Hydrochloric acid	1.00×10^{-6}	1.00×10^{-8}
Ammonia	1.00×10^{-6}	9.60×10^{-7}
Hydrogen gas	1.00×10^{-6}	1.00×10^{-8}
Methane	1.00×10^{-6}	1.90
Formaldehyde	1.00×10^{-6}	3.30×10^{-4}
Methanol	1.00×10^{-6}	0
Formic acid	1.00×10^{-6}	0
Ethene	1.00×10^{-6}	0
Acetaldehyde	1.00×10^{-6}	0
Ethanol	1.00×10^{-6}	0
Acetic acid	1.00×10^{-6}	0
Glyoxal	1.00×10^{-6}	0
Acetone	1.00×10^{-6}	0
Methyl glyoxal	1.00×10^{-6}	0
Methyl ethyl ketone	1.00×10^{-6}	0
Isoprene	1.00×10^{-6}	0
Benzaldehyde	1.00×10^{-6}	0
Limonene	1.00×10^{-6}	0
Phenol	1.00×10^{-6}	0
Biacetyl	1.00×10^{-6}	0
Peroxyacetyl nitrate	1.00×10^{-6}	3.00×10^{-5}

5.3.2 Simulated concentrations downwind of the initial plume

OA concentration measurements in the field are often normalized to a co-emitted species (e.g. CO) in order to account for dilution of the plume (May et al., 2015). We focus on the excess mixing ratio ΔOA/ΔCO in this study, which corrects for the background concentrations of both OA and CO. An increase in ΔOA/ΔCO implies net SOA production, whereas a decrease implies net evaporation of POA. We also use the POA and SOA results of our model to inform our understanding of the changes in the value of ΔOA/ΔCO over time. Unless otherwise noted, results shown in figures are for the ground level.

At ground level for the base case, the model predicts that the value of ΔOA/ΔCO initially decreases during the first simulation hour, suggesting the dominance of evaporation of POA during this time, and then increases beyond its starting value for the rest of the simulation period, indicating the production of SOA. The net change in ΔOA/ΔCO from the start of the simulation to the end is an increase of 120%. Figure 5.1 shows the time series for ΔOA/ΔCO, total OA, POA, and SOA for the base case. Since ΔOA/ΔCO increases over time, the base case results in a net increase of OA.

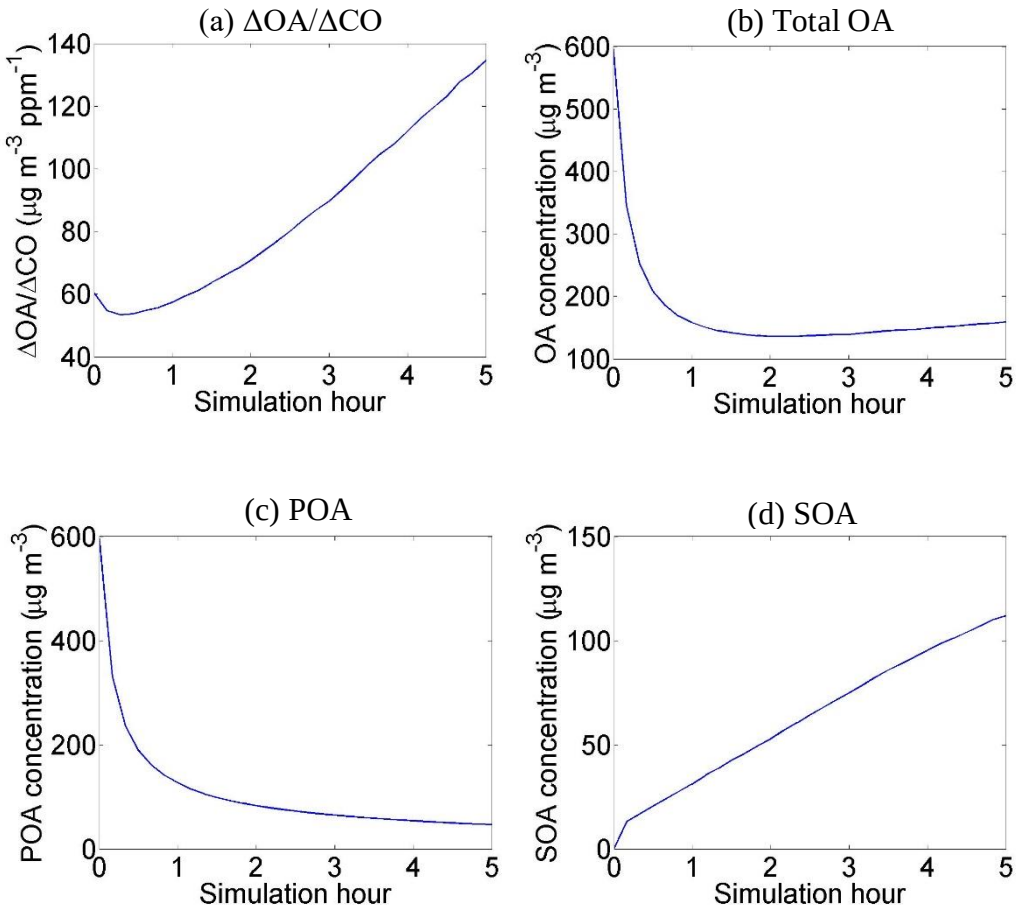

Figure 5.1. Time series of (a) ΔOA/ΔCO, (b) Total OA (SOA + POA), (c) POA, and (d) SOA for the base case.

5.4 Sensitivity cases

5.4.1 OH concentration and aging rate

The rates of OA oxidation reactions with OH depend on both OH concentrations and the aging rate constant. In this section, we investigate changes of OH concentrations and the aging rate constant. The ΔOA/ΔCO results of these sensitivity tests can be found in Figure 5.2. First we increase the OH concentration from its base value of 5.27 x 10^6 molecules cm^{-3} (Akagi et al., 2012) to approximately twice its base value (1.14 x 10^7 molecules cm^{-3}), which is the OH

concentration observed in a biomass burning event in Yokelson et al. (2009). This increase in OH concentration results in a net 310% increase in ΔOA/ΔCO (approximately twice as large as the base case net change) indicating an increase in SOA formation as expected. Next, we decrease the base OH concentration by a factor of two to 2.64 x 10^6 molecules cm^{-3}. This OH concentration reduction results in a net increase of ΔOA/ΔCO by 30% (only one-fourth of the base case net change) which indicates that SOA formation is reduced but still dominates over the evaporation of POA. In order to investigate the contribution of SOA chemistry, we then reduce the aging rate constant, k_{OH}, to zero. This results in a 30% decrease in the net change of ΔOA/ΔCO, which is due to POA evaporation in the absence of SOA formation.

Both of the OH concentration sensitivity cases still lead to a net increase in ΔOA/ΔCO indicating the dominance of SOA formation over POA evaporation for these cases. These results suggest that increased OH concentrations could significantly increase OA concentrations downwind of a fire, and decreased OH concentrations could decrease OA concentrations downwind of a fire. The no aging case indicates the importance of SOA chemistry to bbOA concentrations.

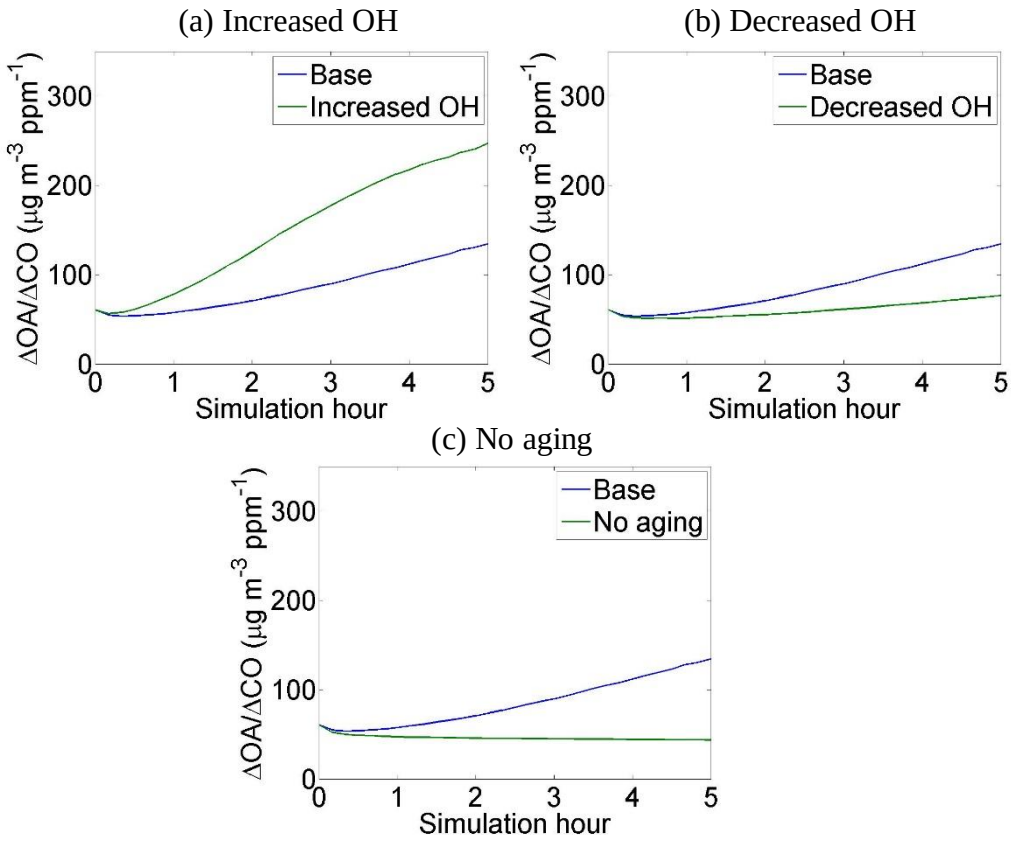

Figure 5.2. Time series of ΔOA/ΔCO of the base case in comparison to the (a) increased OH concentration, (b) decreased OH concentration, and (c) no aging cases.

5.4.2 Intermediate volatility precursors

To investigate the role of IVOCs in the evolution of bbOA from the plume, we zeroed the 1.5 x C_{OA} emissions that were added in the base case as IVOC emissions. IVOCs are mostly in the vapor phase at 298 K, but they can oxidize to form SOA. Zeroing these emissions results in only a 30% net increase of ΔOA/ΔCO, which is about 25% of the net increase predicted in the base case. Overall, however, this change still results in a small net increase in ΔOA/ΔCO (Figure 5.3).

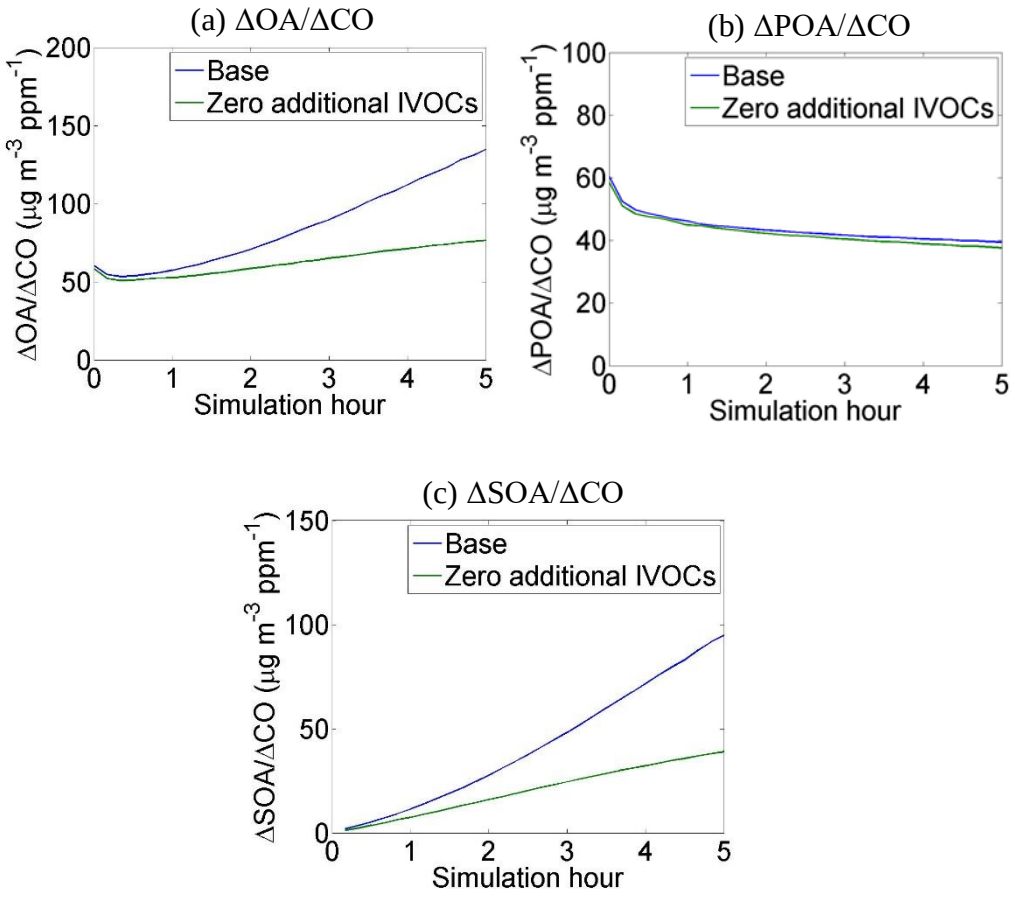

Figure 5.3. Time series of the base case versus the no additional IVOCs case values of (a) ΔOA/ΔCO, (b) ΔPOA/ΔCO, and (c) ΔSOA/ΔCO.

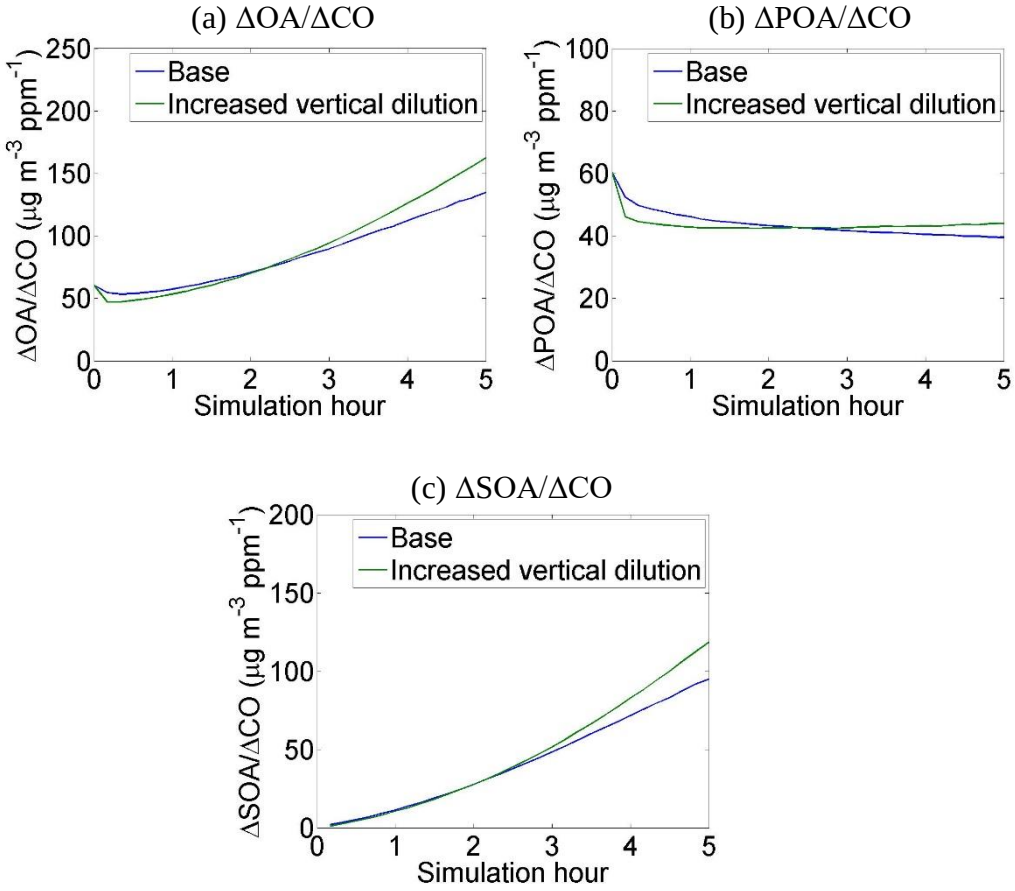

Figure 5.4. Time series of the base case versus the increased vertical dilution case values of (a) ΔOA/ΔCO, (b) ΔPOA/ΔCO, and (c) ΔSOA/ΔCO.

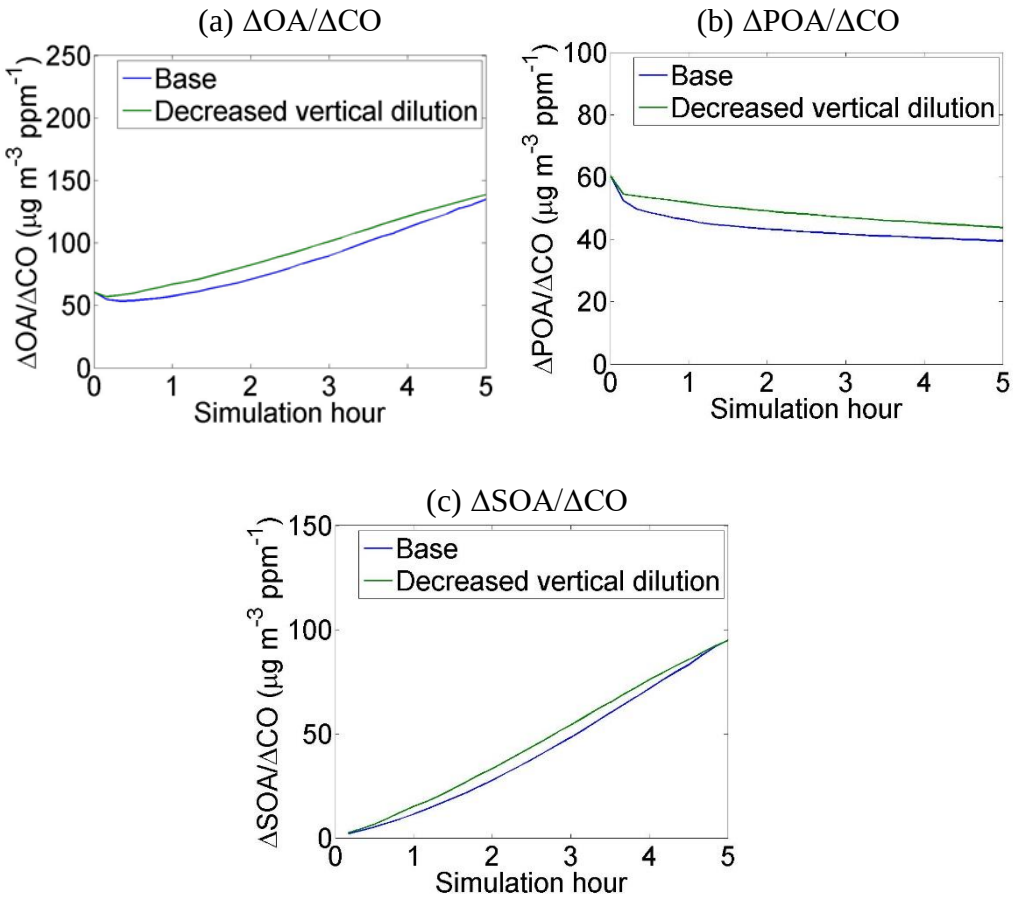

Figure 5.5. Time series of the base case versus the decreased vertical dilution case values of (a) ΔOA/ΔCO, (b) ΔPOA/ΔCO, and (c) ΔSOA/ΔCO.

5.4.3 Vertical dilution rate

The effects of an increased (50 m s^{-1}) and decreased (0.5 m s^{-1}) vertical dilution rate are investigated. These are each a factor of 10 from the base value (5 m s^{-1}). The increased vertical dilution rate results are shown in Figure 5.4. As plume concentrations dilute, absolute concentrations (not shown) of POA and SOA also decrease as compared to the base case, but the ΔOA/ΔCO (170% net increase) results suggest that the decrease in the concentration of organic aerosol due to evaporating POA may increase SOA formation in comparison to the dilution of

POA. The decreased vertical dilution case shows increases in POA and SOA concentrations in the first layer but results in a net 130% increase in ΔOA/ΔCO, which is similar to the base case (120%). The results of the decreased vertical dilution case are shown in Figure 5.5.

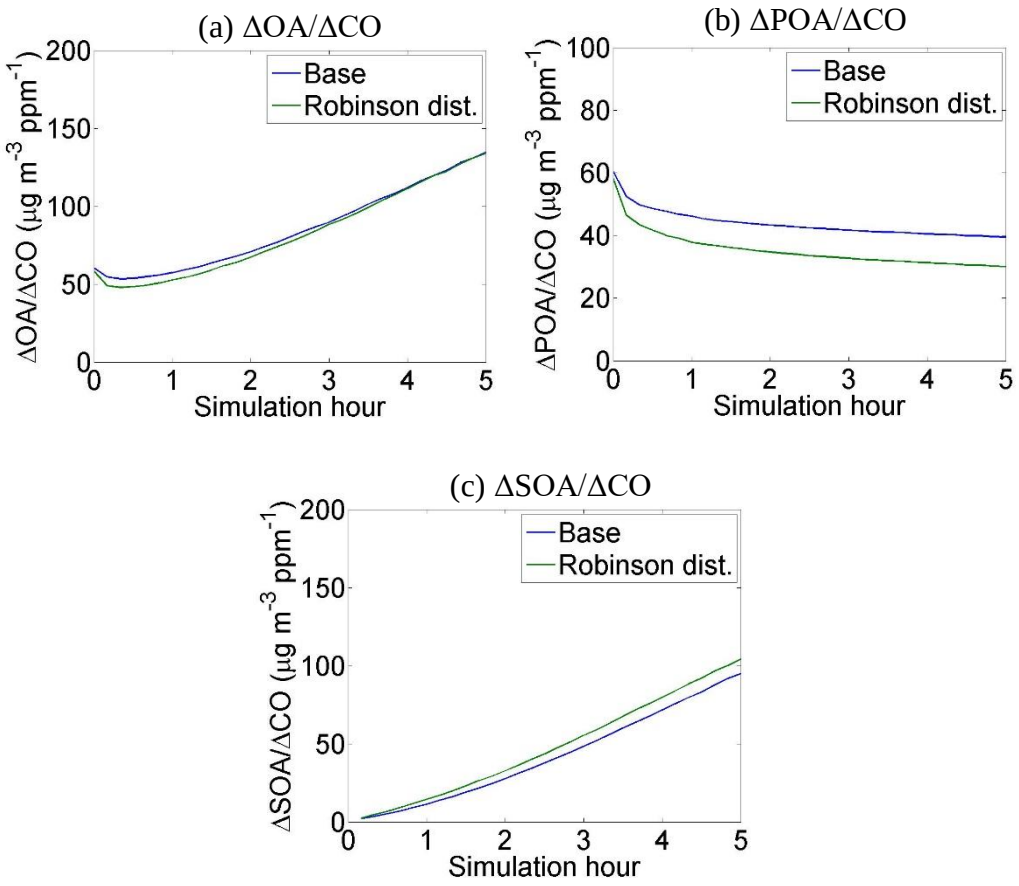

Figure 5.6. Time series of the base case vs. the initial bbOA distribution of Robinson et al. (2007) case values of (a) ΔOA/ΔCO, (b) ΔPOA/ΔCO, and (c) ΔSOA/ΔCO.

5.4.4 Initial plume distribution

The volatility distribution of Robinson et al. (2007) was used in this sensitivity test to see how the initial volatility distribution of the biomass burning plume would affect OA concentrations downwind of the plume. The results of this

sensitivity test are shown in Figure 5.6. Downwind of the plume, the Robinson et al. (2007) volatility distribution case predicts smaller ΔPOA/ΔCO and larger ΔSOA/ΔCO than the base case using the May et al. (2013) distribution. Overall the model does not predict that the change in ΔOA/ΔCO between the results of the two initial volatility distributions is large, and both cases predict a net increase in ΔOA/ΔCO.

5.5 Conclusions

A simple representation of a biomass burning plume in the U.S. was simulated using the 1-D Lagrangian transport model of Murphy et al. (2011). A systematic approach was taken to determine factors that could lead to variability in OA measurements downwind of a biomass burning plume. The role of SOA chemistry was investigated by increased and decreased OH concentration cases and a no aging case. As compared to the base case, doubled OH concentrations result in a net 50% increase in OA concentrations normalized to CO downwind of the plume, and a 50% reduction in OH concentrations results in a 75% decrease in ΔOA/ΔCO. Though there is still SOA production in the decreased OH concentration case, there is little predicted change to ΔOA/ΔCO. The no aging case resulted in a net 30% decrease in ΔOA/ΔCO, indicating that SOA chemistry can be an important contributor to downwind bbOA concentrations. Intermediate volatility emissions were zeroed in another sensitivity test. IVOCs were found to contribute about 75% of the OA downwind of the fire. Increased and decreased vertical diffusivity cases were also investigated. Increased vertical diffusivity resulted in decreased absolute

concentrations of OA at the surface level but increases in ΔOA/ΔCO as compared to the base case, suggesting that evaporated POA concentrations led to increased SOA production. The decreased vertical diffusivity case resulted in increased absolute concentrations of OA at the surface level and only a slight increase in ΔOA/ΔCO as compared to the base case. Finally, the Robinson et al. (2007) initial volatility distribution of the biomass burning OA was implemented in a sensitivity test and compared to the base case. The base case predicted more POA and less SOA than the Robinson et al. (2007) case, but there was little effect on the net changes to ΔOA/ΔCO between the two scenarios.

5.6 References

Akagi, S.K., Craven, J.S., Taylor, J.W., McMeeking, G.R., Yokelson, R.J., Burling, I.R., Urbanski, S.P., Wold, C.E., Seinfeld, J.H., Coe, H., Alvarado, M.J., Weise, D.R., 2012. Evolution of trace gases and particles emitted by a chaparral fire in California. Atmos. Chem. Phys. 12, 1397-1421.

Alvarado, M.J., Lonsdale, C.R., Yokelson, R.J., Akagi, S.K., Coe, H., Craven, J.S., Fischer, E.V., McMeeking, G.R., Seinfeld, J.H., Soni, T., Taylor, J.W., Weise, D.R., Wold, C.E., 2014. Investigating the links between ozone and organic aerosol chemistry in a biomass burning plume from a prescribed fire in California chaparral. Atmos. Chem. Phys. Discuss. 14, 32427-32489.

Carter, W.P.L., 2000. Programs and files implementing the SAPRC-99 mechanism and its associated emissions processing procedures for Models-3 and other regional models.

Cubison, M.J., Ortega, A.M., Hayes, P.L, Farmer, D.K., Day, D., Lechner, M.J., Brune, W.H., Apel, E., Diskin, G.S., Fisher, J.A., Fuelberg, H.E., Hecobian, A., Knapp, D.J., Mikoviny, T., Riemer, D., Sachse, G.W., Sessions, W., Weber, R.J., Weinheimer, A.J., Wisthaler, A., Jimenez, J.L., 2011. Effects of aging on organic aerosol from open biomass burning smoke in aircraft and laboratory studies. Atmos. Chem. Phys. 11, 12049-12064.

Donahue, N.M., Robison, A.L., Stanier, C.O., Pandis, S.N., 2006. Coupled partitioning, dilution, and chemical aging of semivolatile organics, Environ. Sci. Technol. 40, 2635-2643.

Heilman, W.E., Liu, Y., Urbanski, S., Kovalev, V., Mickler, R., 2014. Wildland fire emissions, carbon, and climate: plume rise, atmospheric transport, and chemistry processes. Forest Ecol. Manag. 31, 70-79.

Hennigan, C.J., Miracolo, M.A., Engelhart, G.J., May, A.A., Presto, A.A., Lee, T., Sullivan, A.P., McMeeking, G.R., Coe, H., Wold, C.E., Hao, W.-M., Gilman, J.B., Kuster, W.C., de Gouw, J., Schichtel, B.A., Collett Jr., J.L., Kreidenweis, S.M., Robinson, A.L., 2011. Chemical and physical transformations of organic aerosol photo-oxidation of open biomass burning emissions in an environmental chamber. Atmos. Chem. Phys. 11, 7669-7686.

Jolleys, M.D., Coe, H., McFiggans, G., Capes, G., Allan, James D., Crosier, J., Williams, P.I., Allen, G., Bower, K.N., Jimenez, J.L., Russell, L.M., Grutter, M., Baumgardner, D., 2012. Characterizing the aging of biomass burning organic aerosol by use of mixing ratios: a meta-analysis of four regions. Environ. Sci. Technol. 46, 13093-13102.

Jolleys, M.D., Coe, H., McFiggans, G., Taylor, J.W., O'Shea, S.J., Le Breton, M., Bauguitte, S. J.-B., Moller, S., Di Carlo, P., Aruffo, E., Palmer, P.I., Lee, J.D., Percival, C.J., Gallagher, M.W., 2015. Properties and evolution of biomass burning organic aerosol from Canadian boreal forest fires. Atmos. Chem. Phys. 15, 3077-3095.

May, A.A., Levin, E.J.T., Hennigan, C.J., Riipinen, I., Lee, T., Collett Jr., J.L., Jimenez, J.L., Kreidenweis, S.M., Robison, A.L., 2013. Gas-particle partitioning of primary organic aerosol emissions: 3. Biomass burning. J. Geophys. Res. Atmos. 118, 11327-11338.

May, A.A., McMeeking, G.R., Lee, T., Taylor, J.W., Craven, J.S., Burling, I., Sullivan, A.P., Akagi, S., Collet Jr., J.L., Flynn, M., Coe, H., Urbanski, S.P., Seinfeld, J.H., Yokelson, R.J., Kreidenweis, S.M., 2014. Aerosol emissions from prescribed fires in the United States: a synthesis of laboratory and aircraft measurements. J. Geophys. Res. Atmos. 119, 11826-11849.

May, A.A., Lee, T., McMeeking, G.R., Akagi, Sullivan, A.P., Urbanski, S., Yokelson, R.J., Kreidenweis, S.M., 2015. Observations and analysis of organic aerosol evolution in some prescribed fire smoke plumesAtmos. Chem. Phys. 15, 6323-6335.

Murphy, B.N., Donahue, N.M., Fountoukis, C., Pandis, S.N., 2011. Simulating the oxygen content of ambient organic aerosol with the 2D volatility basis set. Atmos. Chem. Phys. 11, 7859-7873.

Robinson, A.L., Donahue, N.M., Shrivastava, M.K., Weitkamp, E.A., Sage, A.M., Grieshop, A.P., Lane, T.E., Pierce, J.R., Pandis, S.N., 2007. Rethinking organic aerosols: semivolatile emissions and photochemical aging. Science 315, 1259-1262.

Robinson, A.L., Grieshop, A.P., Donahue, N.M., Hunt, S.W., 2010. Updating the conceptual model for fine particulate mass emissions from combustion systems. J. Air Waste Manage. 60, 1204-1222.

Singh, H.B., Anderson, B.E., Brune, W.H., Cai, C., Cohen, R.C., Crawford, J.H., Cubison, M.J., Czech, E.P., Emmons, L., Fuelberg, H.E., Huey, G., Jacob,

D.J., Jimenez, J.L., Kaduwela, A., Kondo, Y., Mao, J., Olson, J.R., Sachse, G.W., Vay, S.A., Weinheimer, A., Wennberg, P.O., Wisthaler, A., the ARCTAS science team, 2010. Pollution influences on atmospheric composition and chemistry at high northern latitudes: Boreal and California forest fire emissions. Atmos. Environ. 44, 4553-4564.

Yokelson, R.J., Christian, T.J., Karl, T.G., Guenther, A., 2008. The tropical forest and fire emissions experiment: laboratory fire measurements and synthesis of campaign data. Atmos. Chem. Phys. 8, 3509-3527.

Yokelson, R.J., Crounse, J.D., DeCarlo, P.F., Karl, T., Urbanski, S., Atlas, E., Campos, T., Shinozuka, Y., Kapustin, V., Clarke, A.D., Weinheimer, A., Knapp, D.J., Montzka, D.D., Holoway, J., Weibring, P., Flocke, F., Zheng, W., Toohey, D., Wennberg, P.O, Wiedinmyer, C., Mauldin, L., Fried, A., Richter, D., Walega, J., Jimenez, J.L., Adachi, K., Buseck, P.R., Hall, S.R., Shetter, R., 2009. Emissions from biomass burning in the Yucatan. Atmos. Chem. Phys. 9, 5785-5812.

Zhang Q., Jimenez J.L., Canagaratna M.R., Allan J.D., Coe H., Ulbrich I., Alfarra M.R., Takami A., Middlebrook A.M., Sun Y.L., Dzepina K., Dunlea E., Docherty K., De-Carlo P.F., Salcedo D., Onasch T., Jayne J.T., Miyoshi T., Shimono A., Hatakeyama S., Takegawa N., Kondo Y., Schneider J., Drewnick F., Borrmann S., Weimer S., Demerjian K., Williams P., Bower K., Bahreini R., Cottrell L., Griffin R.J., Rautiainen J., Sun J.Y., Zhang Y.M., Worsnop D.R., 2007. Ubiquity and dominance of oxygenated species in organic aerosols in anthropogenically-influenced Northern Hemisphere midlatitudes. Geophys. Res. Lett. 34, L13801.

Chapter 6. Conclusions and future work

6.1 Conclusions

The sources of atmospheric particles relevant to human health and climate changes were explored. A source-resolved number emissions inventory for a summertime period in the Eastern U.S. was developed. According to the inventory, gasoline automobiles are estimated to be responsible for 40% of the ultrafine particle emissions, followed by industrial sources (33%), non-road diesel (16%), on-road diesel (10%), and 1% from biomass burning. With the new emissions inventory as input, the three-dimensional number-focused CTM PMCAMx-UF reproduced average observed ultrafine particle number concentrations within 12%. A new number-focused zero-out method was developed and implemented, and on average over the Eastern U.S. sub-domain, gasoline was predicted to contribute 36% of the primary ultrafine particles, followed by industrial sources (31%), non-road diesel (18%), on-road diesel (10%), biomass burning (1%), and long-range transport (4%).

The source-resolved emissions inventory was then used to quantify the effects of reduced and increased diesel particulate emissions on particle number, black carbon, and aerosol optical properties. On average in the Eastern U.S. subdomain, a 50% reduction in diesel emissions resulted in a 23% reduction in $PM_{2.5}$ black carbon, 27-30% decrease in the absorption coefficient, and a 15-16% decrease in the absorption aerosol optical depth. Counterintuitively, the diesel reduction resulted in a 1.6% increase in total particle number concentrations due to

reductions of the condensation and coagulation sinks from the removal of particles. These results suggest that mitigation of large diesel particles and/or particle mass emissions will reduce absorption climate-relevant properties related to black carbon and have health benefits; however the changes could also have the unintended effect of increased ultrafine particle number concentrations. The doubled diesel emission case resulted in a 46% increase in $PM_{2.5}$ black carbon, a 52-60% increase in the absorption coefficient, and a 28-32% increase in aerosol optical depth. As with the diesel reduction case, the addition of particle surface area affected the coagulation and condensation sinks. The doubled diesel case led to a 3% decrease in total particle number concentrations over the domain. These changes suggest that increased particle mass emissions from diesel sources increase climate-relevant effects related to black carbon and negatively affect health, but the changes may reduce ultrafine particle number concentrations.

Next, the mass-focused CTM PMCAMx was used to simulate three representative months of the modeling year 2008. Domain-averaged biomass burning organic aerosol (bbOA) contributions to organic aerosol (OA) concentrations from all sources are 8% for April, 22% for July, and 10% for September, but the importance of bbOA on OA concentrations was greater than 90% for specific days in areas of the domain most affected by biomass burning events. The results of PMCAMx were then compared to the predictions from another CTM CAMx that assumes nonvolatile OA and negligible bbSOA formation. The predicted domain-averaged bbOA concentration using the VBS approach (PMCAMx) is 20% higher than the prediction by the traditional approach

assuming non-volatile POA and negligible SOA formation, however the VBS approach predicts that 79% of this bbOA is secondary, whereas the traditional approach predicts that 100% of bbOA is primary. Near biomass burning emission sources, the VBS treatment predicts about 30% lower bbOA concentrations due to the evaporation of fresh POA and about 60% higher bbOA concentrations downwind of significant biomass burning emissions due to the production of secondary bbOA.

Finally, the evolution of bbOA was explored using the 1D Lagrangian transport model described in Murphy et al. (2011) with the 1D volatility basis set (Donahue et al., 2006) representation of organic aerosol. A base case representative of a biomass burning plume in the U.S. was simulated, and several sensitivity tests to parameters that affect the evolution of bbOA concentrations downwind were performed and analyzed. Decreasing the OH concentration and zeroing the aging rate led to decreased SOA production and lower ΔOA/ΔCO values, while increasing the OH concentration increased SOA production. Changes to the vertical dispersion rate were found to affect absolute concentrations of POA, SOA, and the SOA/POA balance that determines the net change in ΔOA/ΔCO. In the final sensitivity test, the volatility distribution of Robinson et al. (2007) was applied to the biomass burning plume and found to predict less POA and more SOA than the original May et al. (2013) distribution but had little effect on the net change in ΔOA/ΔCO.

6.2 Future work

6.2.1 Suggested model improvements

PMCAMx-UF predictions would benefit from the formulation and implementation of an explicit source-tracking algorithm specifically for number, similar to the mass source-tracking algorithm PSAT (Yarwood et al., 2004). Extending the box model number source apportionment algorithm SANSA (Dan Westervelt, thesis) for use in a CTM such as PMCAMx-UF, for example, would enable calculation of particle number source apportionment from the results of one simulation versus several zero-out simulations. One major advantage to using a single simulation for source apportionment is that emissions from all sources can be included, eliminating the nonlinearities due to changes in the condensation and coagulation sinks by removal of particle surface area. In addition, this would enable source apportionment of larger particles ($N_{>100}$) relevant to CCN, whereas with zero out simulations it would likely not be accurate to source apportionment particles that contribute so much to particle surface area. The addition of a number-tracking algorithm to PMCAMx-UF would increase computational time but add accuracy and scientific value to the model predictions for particle number source apportionment.

Relatedly, it would improve the representation of emissions in PMCAMx-UF to add a subgrid number emissions processing parameterization (e.g. for sub-grid coagulation, Pierce et al., 2009). CTMs spread emissions over large grid cells (36 km x 36 km in PMCAMx-UF). For particle number emissions, this means that

many particles that are simulated to survive transport across the grid cell might in reality have succumbed to evaporation or coagulation instead.

6.2.2 Suggested model application

The source-resolved 2008 emissions inventory is an excellent tool for future source apportionment studies. Source-specific number distributions from the literature can be applied to each source, and the resulting number emissions inventory and simulated particle number concentrations can be used to investigate the sources of particle number emissions and concentrations. These inventories could also be used to investigate the effects of future mitigation scenarios on number and mass concentrations.

6.2.3 Suggested improvements for experimental emission studies to better inform models

The number size distributions and mass emission factors from laboratory/field studies in the literature are often difficult to confidently parameterize for use in a 3D chemical transport model without additional information. To model number size distributions in PMCAMx-UF, we typically fit the number size distribution of the data that is reported in figures to a bimodal logarithmic distribution (Seinfeld and Pandis, 2006), but emission factors of small particles are sensitive to the fit. It would be helpful if the authors of experimental studies could perform and report the parameters for a bimodal logarithmic fit to

their data and perhaps even a range of values that fit the data within the range of experimental uncertainty.

Studies that report bbOA emission factors do not often report the temperature and organic aerosol concentrations (C_{OA}, including background) at which the emissions data were measured. Primary organic aerosol was once assumed to be nonvolatile, but studies have shown that it is semivolatile instead (Robinson et al., 2007; Donahue et al., 2009; Jathar et al., 2014). Chemical transport models typically assume emissions are at 298 K and then partition organics based on the temperature of the modeled grid cell. Measurements taken at high temperatures and/or high concentrations of organic aerosol to derive organic aerosol emission factors, however, can be biased low for 298 K and atmospheric C_{OA} due to the evaporation of OA. One solution is to report EF_{TOT} values (May et al., 2015), which represent the emission factor of both gas and particle organic aerosol. Alternatively, if measurement temperature and C_{OA} are reported along with the emission factor (e.g. May et al., 2014), EF_{TOT} can be calculated assuming a volatility distribution (e.g. May et al., 2013) and the partitioning equation (Donahue et al., 2006; Robinson et al., 2010).

References

Donahue, N.M., Robinson, A.L., Pandis, S.N., 2009. Atmospheric organic particulate matter: from smoke to secondary organic aerosol. Atmos. Environ. 43, 94-106.

Jathar, S.H., Gordon, T.D., Hennigan, C.J., Pye, H.O.T., Pouliot, G., Adams, P.J., Donahue, N.M., Robinson, A.L., 2014. Unspeciated organic emissions from combustion sources and their influence on the secondary organic aerosol budget in the United States. Proc. Natl. Acad. Sci. 111, 10473-10478.

May, A.A., Levin, E.J.T., Hennigan, C.J., Riipinen, I., Lee, T., Collett Jr., J.L., Jimenez, J.L., Kreidenweis, S.M., Robison, A.L., 2013. Gas-particle partitioning of primary organic aerosol emissions: 3. Biomass burning. J. Geophys. Res. Atmos. 118, 11327-11338.

May, A.A., McMeeking, G.R., Lee, T., Taylor, J.W., Craven, J.S., Burling, I., Sullivan, A.P., Akagi, S., Collet Jr., J.L., Flynn, M., Coe, H., Urbanski, S.P., Seinfeld, J.H., Yokelson, R.J., Kreidenweis, S.M., 2014. Aerosol emissions from prescribed fires in the United States: a synthesis of laboratory and aircraft measurements. J. Geophys. Res. Atmos. 119, 11826-11849.

May, A.A., Lee, T., McMeeking, G.R., Akagi, S., Sullivan, A.P., Urbanski, S., Yokelson, R.J., Kreidenweis, S.M., 2015. Observations and analysis of organic aerosol evolution in some prescribed fire some plumes. Atmos. Chem. Phys. 15, 6323-6335.

Murphy, B.N., Donahue, N.M., Fountoukis, C., Pandis, S.N., 2011. Simulating the oxygen content of ambient organic aerosol with the 2D volatility basis set. Atmos. Chem. Phys. 11, 7859-7873.

Pierce, J.R., Theodoritsi, G., Adams, P.J., Pandis, S.N., 2009. Parameterization of the effect of sub-grid scale aerosol dynamics on aerosol number emission rates.

Robinson, A.L., Donahue, N.M., Shrivastava, M.K., Weitkamp, E.A., Sage, A.M., Grieshop, A.P., Lane, T.E., Pierce, J.R., Pandis, S.N., 2007. Rethinking organic aerosols: semivolatile emissions and photochemical aging. Science 315, 1259-1262.

Robinson, A.L., Grieshop, A.P., Donahue, N.M., Hunt, S.W., 2010. Updating the conceptual model for fine particulate mass emissions from combustion systems. J. Air Waste Manage. 60, 1204-1222

Westervelt, D., 2013. Characterizing the sources of cloud condensation nuclei using a global aerosol modeling approach. Thesis. Carnegie Mellon University, Pittsburgh, PA.

Yarwood, G., R.E. Morris, G.M. Wilson., 2004. Particulate Matter Source Apportionment Technology (PSAT) in the CAMx Photochemical Grid Model. Proceedings of the 27th NATO/ CCMS International Technical Meeting on Air Pollution Modeling and Application. Springer Verlag.

Appendix A. Additional results from Chapter 2.

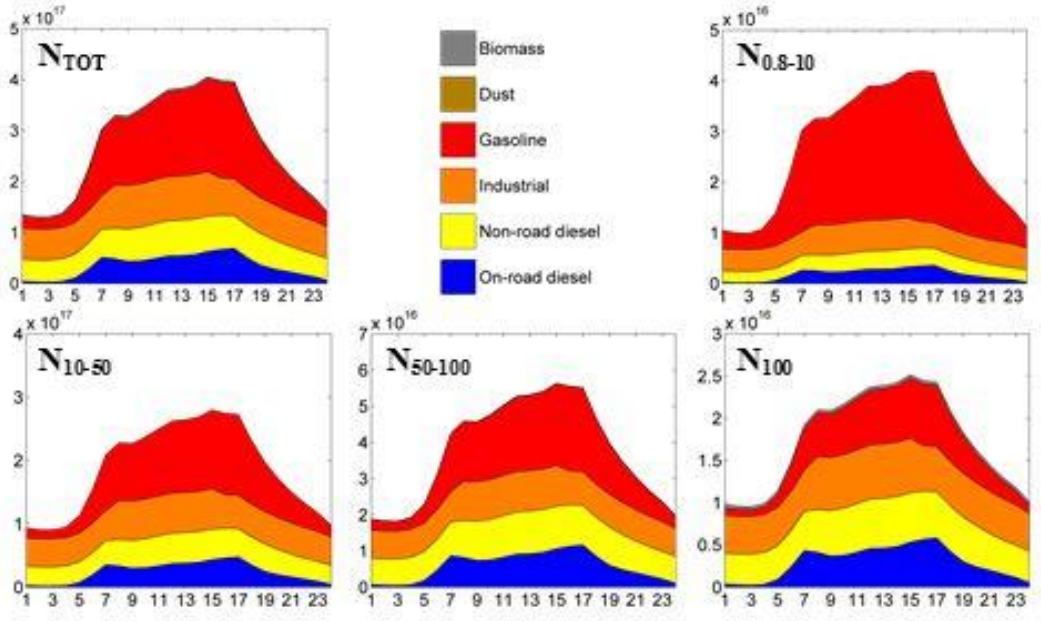

Figure A1. Diurnal number emissions profiles (# h^{-1} km^{-2}) by source for July 2001 in Pittsburgh.

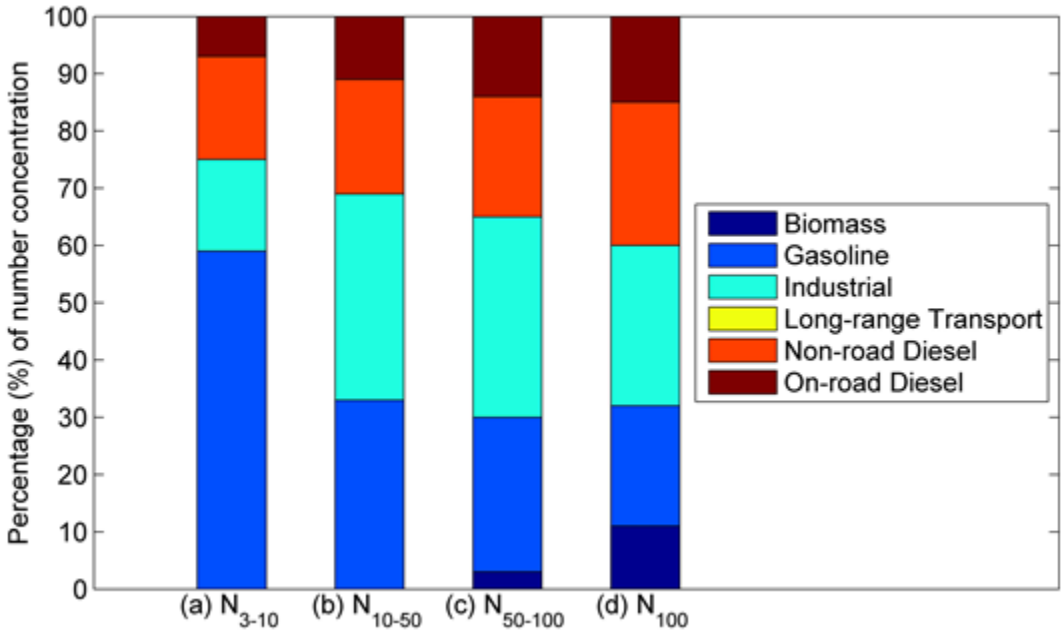

Figure A2. Predicted source apportionment in Pittsburgh for particle number concentrations with particle diameters in the size ranges (a) 3-10 nm, (b) 10-50 nm, (c) 50-100 nm, and (d) larger than 100 nm for July 2001.